Breast Cancer Detection and Classification Using New Fuzzy Level Set and Local Linear Radial Basis Function Neural Network

Ketema Bekere Abdisa

A Thesis Submitted to the

Department of Electronics and Communication Engineering Program
School of Electrical Engineering and Computing

Presented in Partial Fulfillment of the Requirement for the Degree of Master of Science in Electronics and Communication Engineering

Office of Graduate Studies
Adama Science and Technology University

Adama, Ethiopia

July 2019

Breast Cancer Detection and Classification Using New Fuzzy Level Set and Local Linear Radial Basis Function Neural Network

Ketema Bekere Abdisa

Advisor
Dr.Satyasis Mirshra (Ph.D)

A Thesis Submitted to the

Department of Electronics and Communication Engineering Program
School of Electrical Engineering and Computing

Presented in Partial Fulfillment of the Requirement for the Degree of Master of Science in Electronics and Communication Engineering

Office of Graduate Studies
Adama Science and Technology University

Adama, Ethiopia

July 2019

Approval sheet

As members of the Board of Examiners of the M.Sc. thesis open defense, by Ketema Bekere We have read and examined his thesis entitled on the breast cancer detection and classification using new fuzzy level set algorithm and local linear radial basis function neural network. This is, therefore, to certify that the thesis has been accepted in partial fulfillment of the requirement of the Degree.

Name of Student	Signature	Date
Advisor /Supervisor/	Signature	Date
Department Chair	Signature	Date
Internal Examiner	Signature	Date
External Examiner	Signature	Date

Declaration

I hereby assert that this thesis (MSc) is my original effort and has not been presented for a degree in any other university and all sources of material used for this thesis have been properly recognized.

Name: _____

Signature: _____

This thesis has been submitted for examination with my approval as thesis advisor.

Name: _____

Signature: _____

Date of submission: _____

ACKNOWLEDGEMENT

Above all, I would like to praise, honor and glorify the Almighty God for giving me the opportunity, strength, peace, and health to successfully complete this piece of work and for the inexorable support in my overall life.

I would like to give my unreservedly acknowledge to all my family, relatives and friends those who gave a lot of their contribution for my research works success.

I would like to express my deep hearted gratitude to my Advisor, Dr.Satyasis Mirshra (PhD) for providing me with their genuine guidance, constructive comments and encouragements to finalize the time-taking research work.

I would like to thanks to Dr. Feyisa Debbo (PhD) for providing me with their honest supervision and constructive comments.

At last but not least, I would like to thanks Adama Science and Technology University for giving me this coincidental to upgrade my skill with time.

CONTENTS

CHAPTER PAGE

LIST OF TABLES

TABLES PAGE

LIST OF FIGURES

FIGURES PAGE

LIST OF ACRONYM

AHE	Adaptive Histogram Equalization
ANFIS	Artificial Neural Fuzzy Inference System
ANN	Artificial Neural Network
BI-RADS	Breast Imaging Reporting and Data System
BPNN	Back Propagation Neural Network
CAD	Computer-Aided Diagnosis
CCL	Connected Component Labeling
CLAHE	Contrast-Limited Adaptive Histogram Equalization
CC	Cranialcaudal
DWCE	Density Weighted Contrast Enhancement
DNA	Deoxyribo-Nucleic Acid
DDSM	Digital MIAS db for Screening Mammography
FP	False Positive
FWT	Fast Wavelet Transform
FFWNN	Feed-Forward Neural Network
FFNN	Fitting Function Neural Network
GONN	Genetically Optimized Neural Network
GTSDM	Gray Tone Spatial Dependence Matrix
FCM	Fuzzy C-Mean
HM-LCE	Histogram Modified Local Contrast Enhancement
FIS	Fuzzy Inference System
IDM	Inverse Difference Moment
KNN	K-Nearest Neighbor
LDA	Linear Discriminant Analysis
LRBFNN	Linear Radial Basis Function Neural Network
LLRBFNN	Local Linear Radial Basis Function Neural Network
MRI	Magnetic Resonance Imaging
MLO	Mediolateral Oblique
MLP	Multilayer Perceptron's

MNN	Modular Neural Networks
NED	Neural Ensemble Based Detection
NN	Neural Network
PRNN	Pattern Recogonized Neural Network
PET	Positron Emission Tomography
PCA	Principal Component Analysis
PSOWNN	particle swarm optimized neural network
RBF	Radial Basis Functions
RBFN	Radial Basis Function Network
ROC	Receive Operating Characteristics
ROI	Region of Interest
RBST	Rubber Band Straightening Transform
SPF	Phase Fraction
SRG	Seeded Region Growing
SVM	Support Vector Machine
TP	True Positive
UWB	Ultra-Wideband
WBCD	Wisconsin Breast Cancer Diagnosis
WHO	World Health Organization

ABSTRACT

According to the World Health Organization, breast cancer diagnosis is the main cause of cancer death among women in the world. Breast cancer occurs generally in world especially undeveloped and developing countries mortality rates are still high, due to low availability of early detection technologies. From the clinical point of view, mammography is still the most effective diagnostic technology, given the wide distribution of the use and analysis of these images. The main propose of a method is to detect and classify mammographic injuries using the regions of attention of breast images. This research work proposes decomposing of each image using fuzzy level set rule algorithms and classification by using local linear radial basis functional neural network (LLRBFNN). Further to enhance the performance of accuracy by controlling parameters of level set evaluation are considered from the results of fuzzy clustering. This approach will combine image and shape of surface features, which can be applied for detection and classification of breast cancer diseases. The result of this research works the best methods needed to detect different classes of breast cancer such as benign or malignant (cancer).

Keywords: K-Mean Cluster, Local Linear Radial Basis Functional, Neural Network, Training Set,MIAS db and Tumor

CHAPTER 1

INTRODUCTION

Cancer is a word that is used to describe about 200 different diseases affecting organs or systems of the body [14]. Each type of cancer has its own possible causes, and develops and behaves in its own way. It is a diseases in which cells in the body grow, change and multiply out of control of cells forming a lump called a tumor. There are two kinds of tumor, benign and malignant (cancer). Most tumors in the breast are benign. This means they remain contained within a localized area, cannot spread and often do not require any treatment as they do not do any harm. Malignant breast tumors can also grow in the breast. These are different to benign tumors because they have developed, or can develop, the ability to spread either to surrounding tissue or elsewhere in the body.

Breast cancer cells can spread to dynamic organs (such as the liver or lungs) and affect their normal function. Often, cancer is named after the body part in which it originates as result, breast cancer refers to an inconsistent growth of cells that found in the breast tissue. According to the World Health Organization [14], breast cancer diagnosis is the main reason of cancer death among women in the world extremely increasing. Cancer is a leading cause of the most famous in the worldwide including Ethiopia which accounting for an estimated 2.09 million deaths people per year in 2018 G.C [14]. In 2016 G.C, about 188,800 of the estimated 595,690 cancer deaths in the US will be caused according to a recent study by American cancer society epidemiologists. About 595,690 Americans are expected to die of cancer in 2016 G.C, which translates to about 1,630 people per day [35].

Breast cancer is the most common cancer in women in India and accounts for 27% of all cancers in women. It is the most common malignant neoplasm among women in Ethiopia. The Addis Ababa cancer registry reports that breast cancer accounts for 34% of all female cancer cases, followed by cervical cancer at 16% [26]. In urban areas, 1 in 22 women develops breast cancer during her lifetime as compared to rural areas where 1 in 60 women develops breast cancer in her lifetime [35]. Hence breast cancer mostly occurs in an underdevelopment and developing countries mortality rates are still high, due to low availability of early detection technologies. Breast cancer occurs almost entirely in women, but men can get breast cancer, too [35] had applied deferent technologies such as general regression neural network, multilayer perceptron's (MLP), and probabilistic neural network [45] on Wisconsin breast cancer MIAS db. They show that the general regression

neural network the most accurate model for breast cancer classification [35, 32]. They called it neural ensemble based detection (NED) and used it to classify the images of the cancer cells. Radial basis functions (RBF) represents alternative approach to MLP's in universal function approximation [34]. Based on above technologies proposed medical images early detection for visual breast images. Early technologies use for detection breast cancer images are: X-ray, Ultrasound, and Computer Aided Tomography (CT), magnetic resonance imaging (MRI) and mammogram that are seen one by one under background.

1.1. Background

A. X-ray: The definition of imaging is the visual representation of an object. Medical imaging began after the discovery of x-rays by Konrad Roentgen 1896. The first fifty years of radiological imaging, pictures have been created by focusing x-rays on the examined body part and direct depiction onto a single piece of film inside a special cassette. The next development involved the use of fluorescent screens and special glasses to see x-ray images in real time. A major development was the application of contrast agents for a better image contrast and organ visualization. Its sometimes increase the hydrogen peroxide level of the blood, which may cause cell damage. Sometimes X-rays may change the base of DNA.

B. Ultrasound: Ultrasonic waves generated by a quartz crystal are reflected at the interfaces between different tissues, received by the ultrasound machine, and turned into pictures with the use of computers and reconstruction software. Ultrasound imaging is an important diagnostic tool, and there are great opportunities for its further development. Looking into the future, the grand challenges include targeted contrast agents, real-time 3D ultrasound imaging, and molecular imaging. Is helpful in the diagnostic follow-up of an abnormal screening mammogram. Provide guidance for biopsies and other interventions. Useful in evaluating the local extent of breast cancer. Can further evaluate masses or asymmetries and can differentiate a solid mass from a cyst. Color Doppler U/S can be used to see for signs of malignancy, but not sensitive.

C. Computer Aided Tomography (CT): Digital imaging techniques were implemented in the 1970s into conventional fluoroscopic image intensifier and by Godfrey Hounsfield with the first computed tomography. Digital images are electronic snapshots sampled and mapped as a grid of dots or pixels. These developments were made possible by analog to digital converters and computers. It is advanced engineering of X-ray imaging techniques,

where the X-ray images are taken at different angles. Contrast enhanced CT-scan may show the level of local structures involvement including lymph nodes.

D. Magnetic resonance imaging (MRI): The first MRI devices were tested on clinical patients in 1980 which is advanced of tomographic imaging techniques into diagnostic nuclear medicine. MRI is a real-time interactive imaging modality that provides both detailed structural and functional information of the body. Technique has been used widely in medical examinations, especially for cancer investigation for few decades [38]. For the diagnosis to be done properly, breast region should be extracted from other surrounding regions and tissues using image segmentation methods [39].Yearly MRI screening is not recommended for women whose lifetime risk of breast cancer is less than 15%. Women at high risk include those who have one or more of the following characteristics: a known BRCA gene mutation, a first- degree relative (parent, brother, sister, or child) with a BRCA gene mutation, but they have not had genetic testing themselves. A lifetime risk of breast cancer of 20% to 25% or greater, according to risk assessment tools that are based mainly on family history [40]. Women at high risk (greater than 20% lifetime risk) should undergo MRI and a screening mammogram every prevention and detection cancer year.

E. Mammography is one of the greatest current methods used in hospitals and clinics for early detection of breast cancer. It has been recognized effective to lessen mortality as much as by 30% [26]. The screening or diagnostic purpose of mammogram are: Is the only breast imaging found to consistently decrease breast ca related mortality rate, it is low dose(1-2mGy) x-ray evaluation of breast, two views need to be taken such as cranio-caudally and medio-lateral oblique. Up to 11%-25% ca could be missed if only single view is obtained. Mammography has false negative rate of 10%-30%, false positive of 10%. Over 90% of breast ca could be detected by mammography. The screening mammography machines is to early spot the cancerous tumor and eliminate it before the formation of metastases [40]. It assist interpretation classifier directly to the region of interest (ROI) image data and understanding the situation from the features extracted from the preprocessed image signals Advanced technology such as digital mammography, may help doctors read mammograms more accurately. Multiple factors affect accuracy of mammography are breast density, radiologist experience and body habitus. However, the primary signs for breast cancer challenging separated abnormalities scene due to contrast breast tissue [40]. The size of a breast cancer and how far it has spread are important factors in predicting the prognosis for a woman with breast cancer. Based on contrast

breast tissue mammogram have been limited, because they do not work as well in younger (below 40 aged) women and pregnant women which can hide a tumor. For this reason, the American Cancer Society now recommends MRI scans in addition to mammograms for screening in women at high risk.

Mammogram used to look for signs of breast cancer in women who are challenging problem due to presence of noise and dense tissue of body people especially young man. However, neural network methods is suitable to detect breast cancer diagnosis and abnormal categories in order to reduce false-positive results [1]. Accurate early detection can effectively reduce the mortality rate caused by breast cancer. Breast cancer that's found early, when it's small and has not spread, is easier to treat successfully. The two main types of breast changes originate with a mammogram are calcifications and masses.

Masses and micro calcification clusters are an important early signs of breast cancer [1].Currently the most effective method for early detection and screening of breast cancers is mammography. Masses are more difficult to detect than micro-calcifications because their features can be hidden or similar to normal breast functional part of tissue [16]. It must be classified as benign and malignant in order to improve the biopsy produce measurement. A mammogram is basically distinct with four stages of the intensities: background, fat tissue, breast parenchyma and calcifications with increasing intensity. Several studies have exposed a positive association of tissue type with breast cancer risks. Mostly speaking, masses with radiopaque and more irregular shapes are usually malignant, and those combined with radiolucent shapes are benign. Mammogram able to classification breast cancer in to multi-view. Numerous classification schemes have been designed in literature [24] for characterization of malignant and benign breast lesions but tragically could not achieve the encouraging results due to their in competence either in removing noise, lack of robust and differentiating features or selection of misfit classifier [1].High detection rate is mainly depends upon proper and state-of-the-art preprocessing techniques (noise restoration, exclusion of non-breast areas, and visual enhancement due to poor quality images), discriminating features and sophisticated classifier harmonized with the nature of data to detect cancer in order to avoid misclassification problems [31].

Several studies have been conducted in the literature [8] to rule out the malignancy from mammographic images and unfortunately couldn't acquire the desired results. The possible reason for not attaining higher detection accuracy rate is the possibility of

standard pre-processing techniques for enhancement, features selection and inclusion of unnecessary parts from breast cancer such as pectoral muscles. There are different types of breast cancer. Invasive and non-invasive are one of them. Non-invasive breast cancer has not yet developed the ability spread either within the breast or to another part of the body. Eg. Ductal carcinoma in situ. Invasive breast cancer has the potential to spread to other areas of the body and the region of abnormalities challenging to isolate each other's treatment aims to reduce the risk of this happening.eg invasive ductal carcinoma. Breasts are made up of lobules (milk-producing glands) and ducts (tubes that carry milk to the nipple). These are surrounded by glandular, fibrous and fatty tissue. Breast cancer started in the milk ducts and has spread into the surrounding breast tissue.

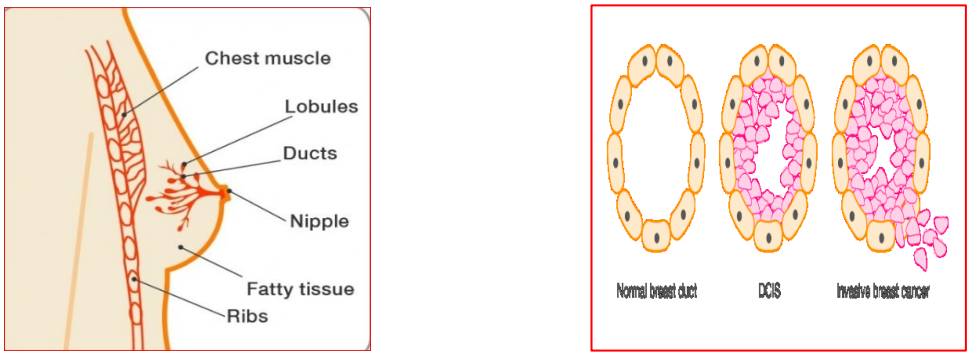

Figure 1. 1: Type of breast cancer

1.2. Statement of the Problem

A lot of researcher works have been investigated on breast cancer at different time to save people from deaths. It is often challenging to distinguish abnormalities class's breast tumor tissues benign and malignant because of their unclear appearance and confusing margins. The boundaries of a breast tumor are problematic to evaluation on screening mammograms and this expressions the spot of surface features in breast cancer detection. To overcome the above said difficulties for an identification and classification of the classes of breast cancer a new fuzzy level set algorithm and local linear radial basis function neural network has been proposed in this research work. The development of new algorithms for local linear radial basis functional neural network method is very important for clearly identification exact tumor. The aim of this research is to propose new method an efficient system for breast cancer classification.

1.3. Objectives

1.3.1. General objective

The general objective of this study is:-

To detect and classify the breast cancer tissues automatically using new fuzzy level rules and local linear radial basic function neural network.

1.3.2. Specific objectives

The specific objectives of this study are:-

- To enhance mammogram breast cancer image in detection using adaptive mean filter techniques.
- To apply new fuzzy level set algorithms for segmentation of exact tumor area for extraction features images.
- To perform classification of kind and unkind breast cancer using local linear radial basis function neural network.
- To evaluate the parameters performance for detection and classification of breast cancer.

1.4. Scope and limitation

There are different types of cancers which affect human bodies, the scope of the study focuses on breast cancer only in case the research time bounded. Breast cancer diagnosis detection use the way new fuzzy level and neural network to solve the problems. The study seeking to exist problem on simulation analysis, due to limitation of the cost to purchase required materials for working the hardware.

1.5. Significance

- The results of breast cancer detection and classification using new fuzzy level set rule algorithm and local linear radial basis function neural network may help to misclassification breast cancer.
- To provide documentary information about the breast cancer detection and classification use local linear radial basis function neural network for anyone who willing to do research work.
- To make the task of radiologist easier an automated system of detection and classification breast cancer.
- The method may reduce the confusion of breast cancer identification and classification.

CHAPTER 2

LITERATURE REVIEW

2.1. Fuzzy level set algorithms

The initial pre-processing is tasks by input mammogram to eliminate the noise, pectoral muscles and separate the breast region from the dark background and enhance contrast in the image. In these methods have been several approaches proposed to segment the breast profile in the mammogram [15, 29]. It is also, bring the image to that standard where that can be best suitable for further processing such as filtering, segmentation, features extraction, features selection and classification into benign and malignant cases. Some of them used one type of transform based or shape features to increase the contrast of images [32]. Fuzzy level set methods utilize dynamic variation boundaries for image segmentation.

2.1.1. Contrast enhancement:

Contrast enhancement [21] established a region-based adaptive neighborhood that adaptively develops the contrast of mammographic features of a varying size and shape. Advanced a mammographic image adaptive neighborhood contrast enhancement technique in which the contrast has been improved while compromising of the natural ness of the original image. Contrast stretching is a simplest method of increasing the contrast in an image [21]. It adjusts the image histogram so that there is a greater separation between foreground and background gray level distributions [13]. Thesis suitable when the gray level distribution is constricted due to poor illumination and lack of dynamic range in imaging sensors. However, this method is difficult to eliminate noise when the gray values of noise and the object are similar. A linear and non-linear rescaling transformation is introduced to rise and reduction the contrast in the image. [20] Proposed a modified contrast stretching algorithm in which the low frequency information is processed by conventional method and the high frequency is processed by log transformation.

Histogram equalization method is a contrast enhancement that enhances the image by considering the image histogram as a probability distribution. It is an effective and simple technique for contrast enhancement. The researcher used the histogram equalization [4] for mammogram contrast enhancement. However, the standard histogram equalization results in extreme contrast enhancement due to the lack of control on the level of enhancement. Contrast-limited adaptive histogram equalization (CLAHE). This technique has been

widely used by various researchers to perform contrast enhancement in mammogram images [2] proposed the histogram modified local contrast enhancement (HM-LCE) to adjust the level of contrast enhancement. This method provides important enhancement in the contrast and brings the local details present in the original image for more relevant reading. This multi-scale analysis constructed on the wavelet transform for mammogram contrast enhancement has been applied by numerous researchers [8] method for mammographic image enhancement by first derivative and local statistics.

The method enhancement mammographic be located fit for low-slung degree of gray level discontinuities in the mammogram images and as the mammograms are texture in nature, the method cannot handle these types of images. A comparative study of two multistate decomposition methods for measuring the contrast enhancement radiographies and mammogram images based on Laplacian pyramid and fast wavelet transform (FWT) has been accepted. Laplacian pyramid based improvement has applied to X-ray images whereas wavelet-based methods have been used in mammography. As proposed new image improvement technology based on multi-scale contrast measure the wavelet domain to modify the contrast of the image directly which is removing noise from input images.

2.1.2. Removing noise equalization

Investigators [9, 26] proposed a CAD system using initially all the noise has been removed using morphological operations. ROI is identified automatically by fuzzy c means clustering. Histogram features, gray level concurrence features and wavelet energy features are used for designing feature MIAS db. From the training set those samples that are not advantageous are deleted, but lack of optimal feature subset is a demerit. Technique is the modification of adaptive histogram equalization (AHE) where the histogram is calculated for the contextual region of a pixel. The enhancement is carried out by announcing a user-specified maximum is clip level to the height of the local histogram. Used this technique to re-scale mammographic images in order to equalize the noise [12]. Several techniques for improving the mammogram have been reported in literature, such as contrast extending, histogram equalizing, fixed and adaptive neighborhood, morphological operators, un-sharp masking, wavelet analysis and filtering techniques.

2.2. Filtering method

The approaches as adaptive background correction [4], density weighted contrast enhancement (DWCE), structured filtering fuzzy enhancement existing in the field of

mammogram enhancement for the detection of cancer in mammograms. This approach used a two stage algorithm for advertisement detection and shape extraction. In the first stage a weighted difference of Gaussian filter was applied for the noise invariant and dimensions specific detection of spots. A morphological filter duplicates the shape of the spots. The results of both filters were combined with a restricted thickening operation. The topology and the number of the bad skin were determined with the first filter and the shape by means of the second filter.

A filtering method that enhances speculations in mammograms as a portion of a speculated mass detection technique of image to obtain the enhanced image. To improve both masses and micro-calcifications scene of features based enhancement by contrast of various hybrid enhancement algorithms based on mathematical morphology, difference stretching, wavelet transform, anisotropic diffusion filter and CLAHEs are achieved on the mammogram images. The combination of mathematical morphology, anisotropic diffusion filter and CLAHE methods, produces superior image quality and offers more visibility for the suspicious regions.

Median filtering is a nonlinear smoothing filter, which is used to reduce random noise present in the mammograms. This filter agrees edge protection when compared with other smoothing filters. Using histogram equalization for image improvement and median filtering [17] for noise removal. Applied adaptive histogram equalization to improve the contrast of masked mammogram image. The diffusion algorithm is used to take away noise via a partial differential equation (PDE).The two scheme important for filtering are Gaussian filter and filters bank.

2.2.1. Gaussian filtering method

Filter method [19] developed an algorithm using calculated morphology to enhance local contrast of mammography. A new mammogram enhancement method which operates Gaussian smoothing filter based on standard deviation and morphological upper has filtering was proposed as part of their work for early detection of breast cancer. A laplacian edge enhancement filtering is used for mammogram enhancement as the part of the mass contour separation. A method for detection of cancer in mammograms planned approach used a two stage algorithm for spot detection and shape extraction. In the first stage a weighted alteration of Gaussian filter was applied for the noise invariant and size specific detection of features. A morphological filter duplicates the shape of the spots results of

both filters were combined with a conditional thickening task. The topology and the number of the features were determined with the first filter and the shape by means of the second filter. Currently X-ray mammography is the most widely used scheme for early detection of breast cancer. Many computer aided techniques are available to contribution the radiologist in taking crucial decisions. Several computers that use level set for separation of masses in digital mammograms was introduced. This technique uses the Gaussian filter for smoothing the image and noise reduction.

2.2.2. Filter bank method

Pectoral muscles are a condensed region close to the chest which may affect the mammogram mass diagnosis method. Due to its higher density than the surrounding tissues, the existence of the same may predicted false positive or false negative results. Therefore, it is mandatory to remove the pectoral muscle before mammogram mass discovery or segmentation process. A review of numerous pectoral segmentation methods have been given to know about the current state of research in this area [18] labelled a method for detection microcalcifications in mammograms. The method, the mammogram image was first processed by sub band decomposition filter bank.

The band pass sub image was divided into overlapping square regions in which skewness and kurtosis as measure of the asymmetry and impulsiveness of the spread were estimated. The detection method utilized those parameters. A region with great positive skewness and kurtosis was marked as region of interest. Simulation results have shown that the method was positive in detecting regions with microcalcifications detection method utilized in those two parameters. Digital mammography is believed to help breast image experts to detect breast cancer early. Accurate diagnosis also depends on the quality of the image presented to the experts. The study addresses the quality improvement of the image. A statistically based sub band filtering method was applied to enhance the mass and calcification shown in the digital mammograms by inhibiting noise.

The method was based on sub band transformation due to its decay characteristic and includes two steps: noise inhibition and boundary enhancement. Contrast ratios and frequency responses are measured to estimate the enhancement performance and distortion affect, respectively, to validate the effectiveness of the proposed and conventional patterns, mammogram image that contains of associated mammographic microcalcifications, breast gland and well-circumscribed mass was designed for model experiment. Moreover, the real

mammograms with microcalcifications were also applied in place the ordered enhancement ability by the proposed method.

The results in the study demonstrated that the proposed method improved the quality of the image more than other enhancement methods, according to these to standards. The comparison results have shown that not only the image quality is enhanced but also within less image distortion. Clusters of microcalcifications are the sign of breast cancer and their early detection is the key to increase breast cancer prognosis. Microcalcifications appear in mammogram as tiny granular points, which are difficult to observe by radiologists due to their small size. An efficient method for automatic and accurate detection of clustered microcalcifications in digitized mammograms is the use of computer Aided Diagnosis (CAD) systems. Novel approach based on multi-scale produces of eigenvalues of Hessian matrix.

Eigenvalue is finding microcalcifications achieved through decomposing the mammograms by filter bank based on Hessian matrix in to different frequency sub-bands, suppressing the low appearance sub band and finally reconstructing the sub bands containing only important high frequency features. The significant features are obtained by multi-scale products. Preliminary results have indicated that the proposed scheme was better in suppressing the background and detecting the microcalcifications clusters than any other detection methods.

The approach consisted of two steps are the first step, a filter algorithm was used to enhance the features and the second step, a filter was used to detect the spatial location with the enhanced features. Gabor filters and phase method portrait analysis to distinguish initial spots of tumor. The fractal dimension of each ROI was estimated using the circular average power spectrum technique. Analysis with established of four features, with fractal dimension and three texture features known as entropy, sum entropy and inverse difference moment had been carried out. Region based detection takings in to explanation the spatial information in contrast to pixel based methods. The features are straight correlated to important diagnostic information similar the shape and margin of extracted and segmentation regions.

2.3. Mass detection and segmentation

Mammographic use single and multiple view to detect masses. Segmentation of breast area is suggestively very important in automated examination of mammogram images [8].

Numerous researchers attempted to review the mammographic mass detection and segmentation techniques. The literatures created on mammogram detection and parting is clustered together according to the computer vision based procedures.

Discovery represents identification of potential lesions in the mammogram. It produces a marker at the potential lesion. Segmentation represents detecting exact boundary of the potential lesions. The terms potential and suspicious are identical. Based on the literature there are three possible products for mass detection/segmentation algorithms: detection and/or segmentation of potential lesions, classification of detected lesions as false positive or true positive and diagnosis of a lesion as benign or malignant.

The mass detection mechanisms in full mammograms, the mass segmentation works in small patch or a given seed point from a mammogram. The detection and segmentation of the mass can also labor in full mammograms. Depending on the images ROIs, single mammograms, pairs of mammograms or full four-mammogram images. The main aim of segmentation in mammograms is to isolated the breast tissue and unwanted regions from breast part in order to limit the area of interest. The most commonly used segmentation algorithm for pectoral removal is the seeded region growing (SRG) algorithm which is simple and effective. Several authors worked with SRG algorithms with modifications to suppress the pectoral muscle in the mammogram. The advantage of mammogram use single and multi-view detection images.

2.3.1. Single view based mass detection

Thresholding based segmentation is measured as partitioned clustering methods that can be applied to obtain an initial rough representation of suspicious regions. In subsequent step, the result is refined using region or contour based segmentation methods. In model based approaches, at first, the system is trained to detect the specific objects. Subsequently the system has to be able to detect and classify new images based on the presence or absence of similar objects. The training step covers instances with and without mass present in the image. The mammograms containing mass have been learned through possible location and the discrepancy in shape and size of the mass. The mammograms without mass have been learned through the features that represent normality. The training phase made the system to learn about the features that can be used to investigate when a new image is presented. Pattern matching has been used by many investigators in the field of mass detection in mammograms [12].

They used regularized cross-correlation distance as the similarity measure. But this approach had a difficulty to account for the large variation in the mass shapes. A probabilistic template matching scheme has been offered to detect masses. A novel application specific instrumentation technique was designed by [20] and it was used for the simulation of breast cancer diagnosis system using the ultra-wideband (UWB) sensors. The problems with generic instrumentation systems are that the human interpreter is expected and is very costly; the ASIN removed both these problems. The RBF based ANN was used to detect the presence of the tumor and the finite difference time domain method was used for the simulation. In the histogram based thresholding technique along with morphological operations has been used to segment the pectoral muscles. Otsu's thresholding method connected component labeling (CCL) to remove the pectoral muscle. Along with intensities, gradients have also been extensively used to find the line of separation of the pectoral muscle.

2.3.2. Multiple views based mass detection

Multiple views based mass detection has also been done using matching scheme the different mammographic images of same person. The comparison is between either left and right mammograms or cranial-caudal (CC) and Medio-lateral oblique (MLO) views of the same breast or same view mammograms taken at different times. The literature contains the algorithms used for the detection of suspicious masses using many views of the mammograms. The significant observations have been made when comparing different mammograms of same women. Smooth though one breast may larger than other, the internal structures have been quite symmetric over broad parts. The overlapping tissues form summation shadows and variations in normal tissues highlight un-significant asymmetries. In instruction to differentiate masses and asymmetric breast tissues, the characteristic such as size, density, edge and shape have been considered into account. A general method for mass detection using multiple views of mammograms is bilateral subtraction. In this methodology, both the left and right breast images have been aligned first and subtracted.

The alignment of the breast is the critical issue in this process. One approach for the alignment of the breast has been carried out by considering the anatomical features like position of nipple, internal regions or assumptions on the compression of the breasts [17]. Second approach has been done via the segmentation of profile of both breasts. Later method has a drawback that failed to register the breast interior correctly. The distortion of

the internal organizations has not been considered in this approach. The comparison between CC and MLO views are known as ipsilateral comparison. In this approach, the mass detection has been performed independently in both mammograms then a mapping of suspicious region has been done by a correspondence algorithm.

A comparison has been achieved to ensure that the detected regions are real masses or not. The communication process has been used to validate that the suspicious region identified in both views was same. It helps an algorithm to detect a mass in the second view once a probable mass was detected in first view. It extracted joint features of both views for a posterior classification step. FCM algorithm separation suspicious region multi-view mammogram with an ipsilateral system. The ipsilateral multi-view scheme for mass detection to improve the detection accuracy. The correspondence algorithms rely on the fact that radiologists use the distance from the nipple to the center of a lesion to correlate the lesion in both views [4].

To validate the mass in both views, the distance from the mass to the nipple has been calculated and compared. The breast boundary calculate Cartesian coordinate system used the skin-line for fit an ellipse based model where one of the axes intersects. A Bayesian network framework that considers both the lesion region and the links between the regions to locate the mass in mammograms. Another method of mass detection by multiple views mammograms temporal contrast of mammograms. Here the mammograms of the same breast have been temporally segmented. Radiologists used this methodology to assess how a suspicious region has evolved. A method to classify the important control points and establish association between them.

Those method presented an approach to identify ROI on most recent mammograms. Then, the nipple scene was used to align mammograms and locate the detected regions in the previous mammograms. [20] Extracted significant control points from the internal linear structures to establish the correspondence between the mammograms. These control points were extracted using features such as orientation and width of the structures. The removed the spot at the junctions of curvilinear structures to establish the correspondence. It performed a comparison on the performance of CADx scheme based on breast imaging reporting and data system BI-RADS descriptors from one/two views. A multi-thresholding mass detection via combined wavelet analysis and genetic algorithm with multiple views

of mammograms. In multi-view mammogram useful feature extraction from reference image to target images.

2.4. Feature extraction and classification

In feature extraction, the features that describe the specific regions are calculated and the significant features are selected for the classification of the ROI as normal or abnormal and mass as benign or malignant. The feature space is great and complex due to the wide diversity of normal and abnormal tissues. Some of the features are unimportant when observed alone, but combination with other features can be significant. The features are generally categorized into intensity regular and texture. The regular features are also called as morphological shape features. Features provided a detail description of features in this category [11]. Recently, multi-resolution features also place an important role in CAD of breast cancer. Various effective methodologies for classifier have been proposed such as Bayesian classifier, MLP classifier, and adaptive neuro-fuzzy inference scheme o adaptive network-based fuzzy inference system (ANFIS) classifier, RBF, KNN [12], decision tree classifier and SVM. Some system performs a FP reduction via feature extraction and classification [11]. In adaptive ribbons of pixels across the margins of masses to classify the regions detected as true mass regions or FPs segment.

Segmenting mass regions are extra classified with step-wise discriminant analysis as benign or malignant disease by computing texture features based on gray level co-occurrence matrix (GLCM) and using the features in a logistic regression method. This method describe the identified suspected regions with features based on the iris filter output and, gray level, texture, contour-related, and morphological sorts extracted from the image. BPNN classifier has been trained to decrease the number of false positives executed the elimination of FP segments using shape analysis. Used LBP for on behalf of the textural properties of the masses.

The basic LBP histogram descriptor extended into a spatially enhanced histogram encodes both the local region appearance and the spatial structure of the masses. SVM was then used for identify the true masses from the normal parenchyma. FP reduction system, by wavelet features are extracted from the detected ROI to decide between TP and FP regions using SVM. Achieving an evaluation of texture extraction using ridge let, wavelet and co-occurrence feature based methods. Feature reduction by Genetic algorithm with random for classification has been applied to FP reduction in computer-aided detection of masses.

Spherical wavelet transform for feature extraction with SVM classifier to classify the detected ROI and decrease the FP. Extracting texture features and geometry features from the ROI containing the segmented suspicious regions and the boundaries of the segmentation. The texture features were figured from GLCM and LBP. Finally the FP reduction was performed by means of SVM, with supervision provided by the radiologist. Some scheme performs the mass classification using feature extraction and classification. A method for differentiating malignant from benign masses [17] in which a computer automatically extracts lesion features related to the margin and density of each mass and merges them into an estimated likelihood of malignancy [10].

A sequential forward floating selection features algorithm has been used to select a best subset from temporal feature set and support vector machine has been used as a classifier. The feed-forward and back-propagation neural network has been used with gradient descent learning rule with momentum. Classification method innate programming to classify masses into benign and malignant class [17], which possesses feature selection implicitly. The features extracted contain edge, sharpness measures, shape factors and statistical texture features. Using a fuzzy binary decision tree classifier with a sequences of radiographic and density-related features. Identification breast tissue using simple image statistics such as its intensity level of histogram (by using different parameters mean, standard deviation, smoothness, third moment, uniformity ,kurtosis, correlation and entropy).

Principal component analysis (PCA) scheme, feature extraction module using independent component analysis and a feature subset selection module using rough set model to decrease the effect of data inconsistency. Finally, a fuzzy classifier was combined into the classification to label sub images into normal or abnormal regions. Proposed the technique for detection of mass on digital mammograms. They used k-means clustering algorithm for image segmentation and gray level [20] co-occurrence matrix to describe and analyze the texture of segmented structures in the image. Classification of these structures was achieved through Support Vector Machines, which separate them into shape and texture descriptors.

K-means algorithm was employed by [20] to segment a mammogram images and co-occurrence matrix to label the texture of segmented structures. The directional features were extracted at dissimilar orientation and frequencies. PCA with proximal SVM was

employed to diminish the dimension of filtered data and to classify them. Proposed a new, genetically optimized neural network (GONN) algorithm [13] to identify breast cancer tumors as benign or malignant based on the features given in the test MIAS db. KNN classifier method to classify the masses as benign or malignant in mammograms. [22] Performed breast cancer diagnosis using multi-scale curvelet transform to extract the features from the ROI. GLCM and wavelet features were extracted from the ROI of a mammogram.

The applicable features extracted through true-test and false-test were used in a BPNN classifier for classification.

2.4.1. Feature extraction techniques

Extracted features from the mammogram images can produce better results for the diagnostic of abnormality and deliver higher classification accuracy rate. Redundant, insignificant and non-representative features assumed to classifier as an input carry no weight in terms of accuracy rate and may yield misleading results [12]. The malignant cancer cell can be effectively diagnosed. The performance of the unsupervised and supervised neural network for the detection of breast cancer has been presented [20]. According to paper [21] the values of the features like cluster thickness, uniformity of cell size, uniformity of cell shapes are first normalized. The lower classified features were removed using the information gain method and the higher ranked attributes were breast-fed to the ANFIS (as shown in figure 2.1) which were processed and the accuracy of this method when applied to the Wisconsin breast cancer diagnosis (WBCD) MIAS db was originate to be 98.24% but no attention was paid to the computational time.

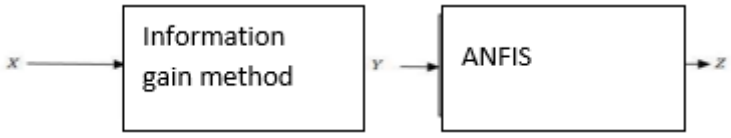

Figure 2. 1: General Structure of the Proposed Method [21].

The features extracted from the images were fed to the neural network [5]. The fuzzy co-occurrence matrix and fuzzy entropy method were used for features' extraction and the data was fed to feed-forward multilayer neural network to classify the biopsy images into three classes. The FCM though has small dimensions yet is more accurate than the ordinary co-occurrence matrix. The performance of the method was found to be better than the other conventional methods as the fuzziness of the data was also considered.

2.4.2. Classification techniques

The classification process is mainly depends on correct feature extraction methods. The extracted features should be accomplished to differentiate between benign and malignant masses [20]. To finding solutions doubtful regions detect the in poor contrast image is done by filtering, DWT (enhancement) thresholding (feature extraction) and classification is done by SVM Classifier. MIAS db (75 images) is used providing 88.75% accuracy [43].Proposed a paper that uses histogram equalization to increase the image quality. The intensity features are extracted and computed to calculate volumetric values. Detecting using Gabor filter (feature extraction) histogram equalization (enhancement) by k-means clustering algorithm. MIAS db is used providing 99% accuracy [44].

Using GLDM and Gabor features as extraction methods with SVM and KNN classifiers obtain MIAS db from MIAS and Gabor feature along with wavelets are used. Basic idea of SVM was to find a hyper-plane to separate. D-dimensional data in to two classes finely. KNN classify objects based on nearest training samples in the feature space. Using sequential floating forward (SFFS) as feature selection and PNN method as classification is done [31].

The mammogram images analysis the help of contourlet coefficient co-occurrence matrix method by histogram equalization in ROI. To classify and detect breast cancer by WNN possess both wavelet and neural network properties, here the ROI detection is done through Global thresholding technique. WNN along with PSO proves to be best for classification as it decreased false negatives and false positives. From the mammographic images the laws texture energy measures are extracted with an abnormality detection algorithm. The textural features are extracted through a windowing operation and by convolution kernels applied to ROI. Detecting mammographic images by wavelet neural network and classification using particle swarm optimized neural network (PSOWNN).MIAS db (216) is used providing 93.67%accuracy [46].

The accuracy of GLDM + SVM, Gabor Filter + KNN and PNN methods results 95.83%,71.83%[25] and 92.5% respectively. Proposed multi-scale curvelet transform to sense breast cancer [22]. The largest coefficients are extracted from large scale levels by transforming ROI's. In these way designed mean for classification using feature SVM; MIAS MIAS db is used. Accuracy at different scale levels are computed and found that the smallest scale having additional accuracy than largest scale of twice. The scale rises the

redundant data also increases. The Computer-aided-diagnosis has been proposed for the medical diagnosis [18].

The fuzzy logic and artificial neural network form the basis of the intelligent systems. The methods have included many artificial neural networks architectures such as convolution neural network[4], radial basis function neural network (RBFNN) [33], general regression neural network (GRNN) [33], probabilistic neural network (PNN) [33], resilient back propagation neural network [26] and hybrid with fuzzy logic [21]. Most of the papers used MATLAB, a high performance and easy to use setting; for the diagnosis and classification of the breast cancer. According to a supervised artificial neural network [4, 7] was used to help classify the breast lesions into cancer and non-cancer classes by processing the computer cytology images [17]. Accuracy of trained neural network was originate to be 82.21%.

The ANN has been established as a healthy scheme for the diagnosis of breast cancer [11]. There is a complex connection between different biomarkers which were identified for the diagnosis of this cancer [33], the MLP neural network was simulated for the diagnosis using four biomarkers (DNA ploidy, phase fraction (SPF), cell cycle delivery and the state of steroid receptors) and it was originate that this method is better an analysis of the methods employed for breast cancer diagnosis. An analysis of the means employed for breast cancer diagnosis previously used techniques like logistic regression [11]. Altered combinations of the biomarkers were applied to the MLP and it was concluded that DNA had no effect on the outcome thus it can be excluded from the prognosis. Only an unsupervised NN will support in assessing the medical expert in case of a patient with no previous diagnosis. The results from wavelets were fed to the ANN method.

The methods are create to be 96%-97% accurate and the system successfully combined the intelligent methods with the image processing thereby increasing the sensitivity of the diagnosis. Occasionally, even after the primary treatment breast cancer can return. The prediction of the recurrent cancer is a very challenging task; [7] developed a method for the aforesaid. The conventional imaging (CI) with an accuracy of up to 20% or the complex and expensive methods like magnetic resonance imaging (MRI) or Positron emission tomography (PET) with an accuracy of 80% are used for such diagnosis thus that paper used the RBF, MLP and PNN for the same.

The NN algorithm designed was originate to be accurate but the PNN performed poorly. The MLP and RBF gave good performance but the performance of MRI and PET is very high; established a CAD system for differentiating the non-cancer breast nodules from the cancer nodules. The perception capability of the features extracted from the sonograms was tested by the SVM, ANN and KNN classifier. It was found that the SVM gave the greatest accuracy while the ANN had the highest sensitivity. In the back propagation algorithm is compared with the Genetic algorithm for the CAD diagnosis of breast cancer by means of the receiver operating characteristics (ROC) [2]. The GA slightly outperformed the BP for training of the CAD schemes but not significantly. The GA is better used for the feature selection. Most of the methods designed/used/tested in various papers use soft computing to identify, classify, detect, or distinguish benign and malignant tumors. Majorly all the methods used ANNs at some stage of the process or the other and different combinations of NNs were shown to give better results than the use of a single type of NN.

There are several techniques available in the literature for the detection and classification breast cancer. Many researchers have contributed their ideas in this tumor. Several domains and concepts have been used identify breast cancer in different methods. Such as neural network, image processing, Convolution Neural Network [4], Radial Basis Network [33], General Regression Neural Network [33],Probabilistic Neural Network Fuzzy level set and etc. However, clearly detection and classification of the breast cancer there are great challenge.

CHAPTER 3

MATERIALS AND METHODS

3.1. Materials requirement

Required software MATLAB R2014a.

3.2. Methodology

Different methods were used to investigate detected and classified breast cancers. This paper proposed new method, local linear radial basis function neural network Addition to existing method new fuzzy segmentation and the results of accuracy was compared with that of previous values. This thesis has written program code for each function and model proposed in block diagram of the system figure 3.1 based on breast MIAS db.

3.2.1. Data collection

This breast cancer MIAS dbs and database for screening mammography (DDSM) was collected [41]. MIAS db contained number of instances 400 ten plus the class attribute. Each instance has one of 2 possible classes: benign (229) and malignant (171). The arranging data were ID, nine variables measured and class attribute respectively coded. In addition to the code for the identification and diagnosis, each record of Wisconsin breast cancer diagnose (WDBC) presents 9 variables descriptors related to the cell nucleus and modelled. The highest values predicted are malignant by depending on process such as: clump thickness, uniformity of cell size, uniformity of cell shape, marginal adhesion, single epithelial cell size, bare nuclei, bland chromatin, normal nucleoli and mitoses. The medical diagnosis problem is clearly classification of tumor. The accuracy of collected half MIAS db of 369 instances was 93.5% [1]. Different algorithms was applied to the same MIAS db and obtained better accuracy of 93.7% [2].Samples collected were 60 benign and 100 malignant masses from desire of Digital Database for Screening Mammography (DDSM) data provided by [43] masses and calcifications [14]. The collection of MIAS db was not normalized for computer reading as binary image, color image and grayscale image. For this reason, prepared suitable for design in required normalization MIAS db for recognized as essential images.

3.2.2. Normalized MIAS db

Normalized MIAS db attributes between zero and one (0, 1) range by multiplying zero point one (0.1) by all instances of attribute except ID of patient.

The last attribute class converted logical 0 or 1 to one if it's true or zero if it's false with the help of supervised learning with neural network. The classes is either benign or malignant when the output zero (0) and one (1) respectively. Then neural network is powerful for classification MIAS db using training sets, and now a training set was created to help us with the breast cancer classification problem. Many researcher used neural network for detection and classification cancer, similarly in this method started from that point.

3.3. General block diagram proposed method

The attained system was designed based on general block-diagram of this method was followed. Breast cancer was detected and the exact point of scheme was showed by new fuzzy mean segmentation and classified as benign and malignant by local linear radial basis function neural network depending on the following steps of diagram.

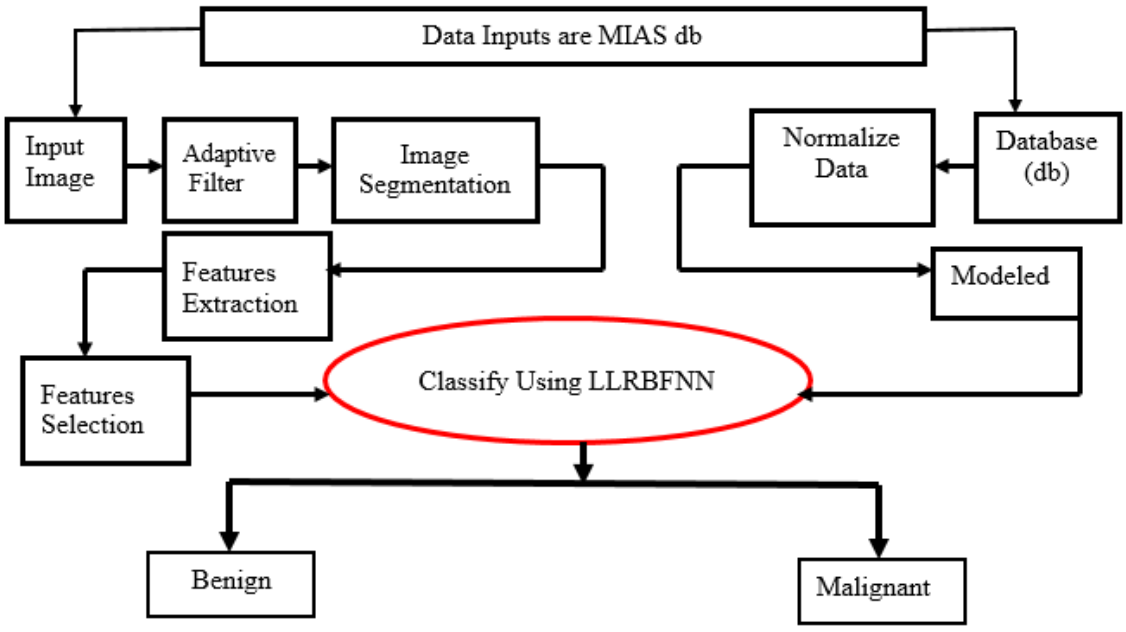

Figure 3. 1: General block-diagram of proposed new method.

3.4. Detection method

An importance point detection, extracting feature descriptors, and point feature matching using local features enables these algorithms to better handle scale changes, rotation, and

removed blob. The detectors and the descriptors can be mixed and matched depending on the requirements of proposed figure 3.1 computational well-ordered. The new fuzzy level set rule method automated the initialization and parameter shape where discovered the interest object of tumor, using the schemes such as enhanced medical input image, filtering, segmentation and extraction features and images taken from mammogram. All related codes are available under appendix.

3.4.1. Medical input image

An image defined as a function I (i,j) in 2D space or I (i,j,k) in 3D space, where i = 0,1,3 …M-1,j = 1,2,3 …N-1 and k = 0,1,3 …D-1 denote spatial coordinates. The values amplitudes of the functions and are intensity values and are typically represented by a gray value in mammogram of the breast; as seen in figure 4.1. Every image consists of a finite set of image elements called pixels in 2D space or voxels in 3D space. Each image element separately specified by its intensity value and its coordinates for pixels and voxels which was described by size. Mammogram input images identified potential abnormalities and segmented color image and regions of a contrast margin [35, 37]. The systems use image processing correlation and de-correlation algorithms analyzed mammograms help of the histogram and scattering selected variables to plot. Image represented three way in pixels. Such as binary number zero (black) and one (white) intensity, color RGB integer values and grayscale (0-255) values in 8bit classes. Those are arranged in two or three dimensional plane.

i. Color images: Color images are represented by three intensity components as follow a similar storage strategy to specify pixels' intensities. The representation of color is based on the relationships between colored light and perception such as eliminated by normalizing color images. It has two function a high-level function and a low-level function. A high-level function that calls new plot to determine where to draw the graphics objects and sets the axes properties XLim and YLim to enclose the image view the result in [0 90] axes. A low-level function that adds the image to the current axes without calling new plot. Such application features can be used to reduce color images to gray level. The advantages for using color representation is to reduce memory requirements and disadvantage is that the quality of the image is reduced since only a reduced collection of colors is actually used [5].

ii. Grayscale images: Grayscale level calculated given below equation formula of the gray conversion for reduced dissimilarity color. In image compression, there were ways to measure the quality of the reconstructed image [18].

$$\text{Gray(G)} = 0.299 * \text{R} + 0.587 * \text{G} + 0.114 * \text{B} \quad \ldots 3.1$$

Where RGB represented red, green and blue respectively. Parameters are evaluated the uniformity of an image and focuses on the partial characteristics of the image. Some of parameter which measures the quality images are mean (m) and standard deviation (sdt) that are normalized distributor shape of data that centers the distribution and that determines the spread of the distribution respectively.

GLCM (Grey Level co-occurrence matrix) scheme:

Other parameters variance (var) and correlation (f) are measured each observation data and measured variables are related similarly.

$$\text{Mean}(\mu) = \frac{1}{\text{MN}} \sum_{\text{i}=1}^{\text{M}} \sum_{\text{j}=1}^{\text{N}} \text{P(i,j)} \quad \ldots 3.2$$

$$\text{Standard deviation } (\delta) = \sqrt{(\frac{1}{\text{MN}} \sum_{\text{i}=1}^{\text{M}} \sum_{\text{j}=1}^{\text{N}} (\text{P(i,j)} - \mu)^2} \quad \ldots 3.3$$

This feature puts relatively high weights on the elements that differ from the average value of P (i, j).

$$\text{variance(var)} = (\text{sdt})^2 \quad \ldots 3.4$$

Correlation reflects a definite gray value along a certain direction of extended length. The correlation value will be larger if extended or if made longer.

$$\text{Correlation(f)} = \sum_{\text{i}=0}^{\text{Ng}-1} \sum_{\text{j}=0}^{\text{Ng}-1} \text{Pd}, \theta\text{(i,j)} \quad \ldots 3.5$$

It is measured of gray level linear dependence between the pixels at the specified positions relative to each other. Where μx, μy and σx, σy are the means and standard deviations of px and py. Where Ng is gray tone, i,j coordinate of function P(i,j).

Contrast indicates the range of dissimilarity between pairs of pixels over the whole image. So it reveals the clarity of the image by extracting the edge information of the objects. [40]

$$\text{Contrast(f)} = \sum_{n=0}^{Ng-1} n^2 \left\{ \sum_{i=0}^{Ng-1} \sum_{j=0}^{Ng-1} Pd, \theta(i,j) \right\}^2 \ldots\ldots\ldots\ldots\ldots\ldots\ldots\ldots\ldots\ldots\ldots\ldots\ldots\ldots\ldots\ldots\ldots\ldots 3.6$$

It is measured local intensity variation favored contributions from P (i, j) away from the diagonal, i.e. i not equal j. Kurtosis is a parameter that describes the shape of image a random variable's probability distribution.

$$\text{kurtosis(k)} = \{\frac{1}{MN} \sum_{i=1}^{M} \sum_{j=1}^{N} \frac{[p(i,j) - \mu]^4}{\delta}\} - 3 \ldots\ldots\ldots\ldots\ldots\ldots\ldots\ldots\ldots\ldots\ldots\ldots\ldots\ldots\ldots\ldots\ldots\ldots 3.7$$

Above parameters measured the distribution information of images by histogram and scatter plotting graphs then passed to filtering method.

3.4.2. Filtering method

Image filtering used to converts an input image to its smoothed variety, where small intensity difference between neighboring pixels was minimizing by edge detection and removing noise. The goal edge detection and removing noise in filter techniques were smoothing image. The two filtering method linear filters and nonlinear filters are based on its scheme, in linear operations addition and constant multiplication, whereas nonlinear operations, minimum value selection used.

Edge detection: Edge detection is a set of pixels with a large change in pixel value. For an image with a white-filled circle on a black background. The basic idea of edge detection filtering is to calculate the first-order or the second-order derivatives of pixel value. From a view point of signal processing, this combination use of two filters results in a band-pass filter, where the smoothing filter works as a low-pass filter and the edge detection filter as a high-pass filter. It finds the correct places of edges and testing wider area around the pixel.

Smoothness: Relative smoothness, R is a measure of grey level contrast that can be used to establish descriptors of relative smoothness. The smoothness is determined using the formula:

$$R = 1 - \frac{1}{1 + \delta^2} \ldots\ldots\ldots\ldots\ldots\ldots\ldots\ldots\ldots\ldots\ldots\ldots\ldots\ldots\ldots\ldots\ldots\ldots\ldots\ldots\ldots\ldots\ldots\ldots\ldots\ldots\ldots\ldots\ldots\ldots\ldots\ldots 3.8$$

Where, σ is the standard deviation of the image

Removing noise: Smoothing filter to minimize gray-level difference among neighboring pixels. The gray-level difference is often caused by noise and thus smoothing is useful for noise removal. Median filter are useful replaces the original pixel value by an average pixel value around the pixel and by the median pixel value among the current pixel and its neighboring pixels respectively. Since the averaging operation cancels noise, the resulting image becomes smooth and a median filter can remove salt-and-pepper noise.

Gaussian filter used to reduce the amount of noise present in a signal at small value of the variance, wiener2 performs more smoothing the sum of the true pixel value and a random, Gaussian distributed noise value, which is using Gaussian noise with a fixed variance.

3.4.3. Segmentation

Binary images were using for difference between dark regions and bright regions becomes more apparent. Usually, it is better to remove such a difference in advance to further processes; without the removal, a parameter value suitable for images. Segmented colors in an automated fashion using the L*a*b* color space. Global thresholding method and Otsu's method used for separation of bright target objects from dark background and determined maximum threshold value that evaluated the separation of region by given threshold value respectively. Homogeneity designed of segmented lesion, with p (i, j) being probability of pixels with number of grey-levels.

$$\text{Homogeneity(H)} = \sum_{\text{i ,j}}^{\text{M}} \frac{\text{P(i, j)}}{1 + |\text{i} = \text{j}|} \dots\dots\dots\dots\dots\dots\dots\dots\dots\dots\dots\dots\dots\dots\dots\dots\dots\dots\dots\dots\dots\dots 3.9$$

Entropy is a measure of disorderliness of intensity distribution in the image. If there were no textures in the image, the entropy value would be near to zero, and on the other hand, a bigger entropy value indicates a more complex texture.

$$\text{Entropy(f)} = \sum_{\text{i=0}}^{\text{Ng}-1} \sum_{\text{j=0}}^{\text{Ng}-1} \text{Pd}, \theta(\text{i, j}) \log\big(\text{Pd}, \theta(\text{i, j})\big) \dots\dots\dots\dots\dots\dots\dots\dots\dots\dots\dots\dots\dots\dots 3.10$$

It is measured the variation of scenes when low first order entropy that was inhomogeneous, while a homogeneous scene high entropy. Inverse difference movement (IDM) is influenced by the homogeneity of the image. Because of the weighting factor (1+ (i−j) 2) $^{-1}$. The low IDM value relatively higher value for homogeneous images.

$$\mathrm{IDM} = \sum_{i=0}^{G-1} \sum_{j=0}^{G-1} \frac{1}{1+(i-j)^2} p(i,j) \ldots\ldots\ldots\ldots\ldots\ldots\ldots\ldots\ldots\ldots\ldots\ldots\ldots\ldots\ldots\ldots\ldots\ldots\ldots\ldots\ldots\ldots\ldots\ldots 3.11$$

Skewness calculates of the segmented lesion, with i,j being the number of pixels inside the region delimited by the contour. Gray level intensity of the i^{th} pixel inside the contour the mean.

$$\mathrm{Skewness(s)} = \frac{1}{MN} \sum_{i=1}^{M} \sum_{j=1}^{N} \frac{(P(i,j)-\mu)^2}{\delta} \ldots\ldots\ldots\ldots\ldots\ldots\ldots\ldots\ldots\ldots\ldots\ldots\ldots\ldots\ldots\ldots\ldots\ldots\ldots\ldots\ldots\ldots 3.12$$

Root mean square level (RMS) computed N-by-M matrix along the first non-singleton dimension.

$$(\mathrm{RMS}) = \frac{1}{N} \sum_{i,j}^{N} |P(i,j)|^2 \ldots\ldots\ldots\ldots\ldots\ldots\ldots\ldots\ldots\ldots\ldots\ldots\ldots\ldots\ldots\ldots\ldots\ldots\ldots\ldots\ldots\ldots\ldots\ldots\ldots\ldots 3.13$$

iii. Binary image: Is useful segment tumor of bright target objects from dark background and determined maximum threshold value that evaluated the separation of region by given threshold value.

3.4.4. Extraction features

Extracting outlier's features the segmented tumor in section 3.4.3 and dimension reduced that efficiently represents interesting parts of an image as a dense feature vector. Speeded-up robust features (SURF) algorithm is used for extracting a specific object based on finding point correspondences between the reference and the target image. It has been four steps interest point detection, local neighborhood description, matching and detected the object points. Extraction features can detect objects despite a scale change or in-plane rotation. This method of object detection works best for objects that exhibit non-repeating texture patterns, which give rise to unique feature matches. This technique is not likely to work well for uniformly-colored objects, or for objects containing repeating patterns.

3.4.5. Feature selection

In this, paper reduced dimension MIAS db by using principal component analysis (PCA) method. Dimensionality reduction was an important factor in predictive modeling. Various proposed above methods have presented different approaches done by graphically comparable filtering [36]. See in section 4.1.1. It worked a higher dimensional space is mapped to data in a lower dimension space, the variance of the data in the lower

dimensional space should be maximum. Selecting feature reduced the space and time complexity as well as increase the accuracy of classification and clustering for supervised learning [47].The features evaluated by the segmentation methods were a set of equations that described in different properties of the mammograms image. The above calculations parameters used new fuzzy set algorithm to detect mammograms image and transmitted all detected mammograms images to section 3.5 by performance parameter. See appendix 6.

3.5. Classification method

Designing the network input and output in this paper was used the following neural network. GRNN design code newgrnn, PNN design code newpnn and RBFNN design code newbre. RBFNN is base of this research was focused with the help of training method based on validation method. Validation method used hold validation and cross validation to classify and evaluated the output accuracy with the help of feed-forward neural network (FFWNN), fit function neural network (FFNN) and pattern regression neural network (PRNN).In this chapter those were designed each method by MATLAB code and their outputs in chapter four could was obtained with code sim. The three neural networks have similar block diagram except the second layers only RBF both layers have biases and each function contain the following layers.

The input layer vector: The input vector is the P_R-dimensional vector that are trying to classify. The entire input vector is shown to each of the RBF neurons.

The RBF layer: Each RBFNN neuron compares the input vector to its weight, and outputs a value between 0 and 1 which is a measure of similarity. The distance between the input and weight increase, the response falls off exponentially towards zero. The shape of the RBF neuron's come to curve, as showed section 4.2.2 figure 4.24.

Linear layer: Computed classification by taking a weighted sum of the activation values from every RBF neuron. Because each output node is computing the score for a different category, every output node has its own set of weights. The output node will typically give a positive weight to the RBF neurons that belong to its category, and a negative weight to the others. All classification methods model mathematically based on the following formula according to each method required. Mathimatically calculation based on its parameters such as weights and bias is given simple operation of training network with its operation below.

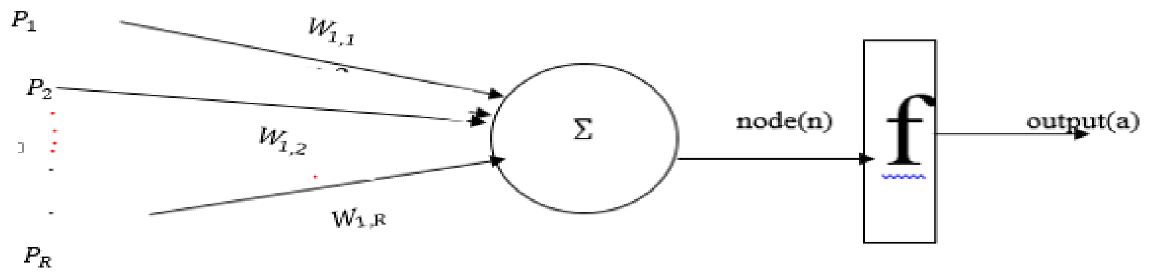

Figure 3. 2: Simple operation training network

The output the node is processed using activation function (φ) with the transfer function such as linear function and log-sigmoid function are used. Activation function determines the behaver of a node. Several connection summesion are connected at each nodes such as input layer,hidden layer and output layer. Those are calculated based on delta rule algorithm. The layer between input and output nodes where there are two or more than two founded name as deep neural network not accessible (hidden layer). Deep neural network given as

$P = P_1, P_{2,\ldots} P_R$ Where $P_1,P_2,\ldots,P_n$ inputs are (features)

$$P = \left(P_{1,P_2}, \ldots P_R\right)^{transpose} \ldots\ldots\ldots 3.14$$

$$W = [W_{1,1}W_{1,2}W_{1,R}$$

$$W_{2,1}W_{2,2}W_{2,R}$$

.

.

.

$$W_{S,1}W_{S,2}W_{S,R}] \ldots\ldots\ldots 3.15$$

Weighted sum equation is given by:

$$V = W_1P_1 + W_2P_2 + \cdots + W_RP_R + b = WP + b \ldots\ldots\ldots 3.16$$

Where p is input data,W is weighted ,S is number of neuron in layer,R is number of elements in input vector,v is weighted sum. An output (a) calculated with helped of transfer function equation generalized delta rule. Reduced error adjusted the weights of the network calculated as below equation.

$$e_i \triangleq t - a \ldots\ldots\ldots 3.17$$

Where e is error of the output node i,t is corrected output and a $\left(a = \varphi(v)\right)$ is output

$$a = \varphi(v) = \varphi(WP + b)$$

The weighted sum transmitted to output by using linear function that updates the weights according to generalized delta rule from equation (3.15 and 3.16) given by:

$$W_{ij} \leftarrow W_{ij} + \alpha\delta_i P_i,$$

$$\delta_i = \varphi'(V_i)e_i \ldots\ldots\ldots\ldots\ldots\ldots\ldots\ldots\ldots\ldots\ldots\ldots\ldots\ldots\ldots\ldots\ldots\ldots\ldots\ldots 3.18$$

Where w_{ij} are updates and previous values,α is alpha learning rate it's value range (0,1) and $\varphi'$is the fist derivative of activation function of node in linear functon is one that means $(\varphi'(V_i) = 1)$ be comes $\delta i = ei$ it is valid only linear function. Sigmoid function computed updates weighted value using activation function $(\varphi(p) = \frac{1}{1+e^{-P}})$ and $\varphi'$is the fist derivative of activation function of node sigmoid function substitute in equation 3.17 is.

$$\delta i = \varphi(V_i)(1 - \varphi(V_i))e_i \ldots\ldots\ldots\ldots\ldots\ldots\ldots\ldots\ldots\ldots\ldots\ldots\ldots\ldots\ldots\ldots\ldots\ldots . .3.19$$

3.5.1. Generalized regression neural networks

GRNN is proposed for function approximation purposes [45]; however in some tasks, it is applied to classification [46, 45, 28].It has two layers radial basis layers and special linear layer as shown in figure. 3.3[45, 34, 32]. The net might recall from the notation section of the preface that conversion of the layer weight matrix from math to code for a particular network. In special linear function required additional treatment to normalized data by the sum of first weight element by other MATLAB code function that was consumed time. Newgrnn creates a two-layer network. The first layer has radbas neurons, calculates weighted inputs with dist and net input with netprod. The second layer has purelin neurons, calculates weighted input with normprod and net inputs with netsum.

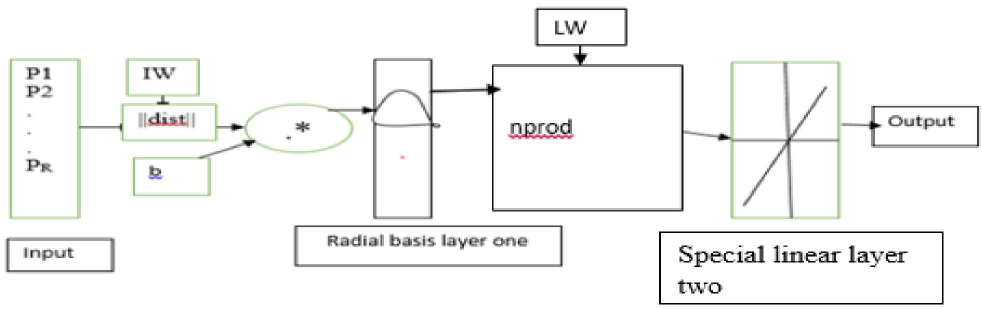

Figure 3. 3: Architecture for the GRNN.

Each cluster from a center computed using squared Euclidean distance and applied to activation function with help of exponential function according to the MATLAB code. The simulation of the GRNN method based on their code graphically as shown that observed an

error based on confusion matrix and histogram in chapter four. MATLAB code design given as inputs X, targets confusion matrix scheme one of performance evaluation focus the predictive capability of model rather than classified breast cancer in to two classes as showed table below.

Table 3. 1: Confusion matrix.

	Predicted class (observation)		
Actual class(patient)		Class = M	Class = B
	Class = M	MM	MB
	Class = B	BM	BB

Where MM = TP (true positive), MB = FP (false negative), BM = FP (false positive) and BB = TN (true negative). The smoothing line diagonal stands increasing true predicted value where the broken line diagonal stands increasing false predicted. The most widely used confusion matrix evaluation accuracy computed as this formula. Accuracy calculated as the sum of correct classifications divided by the total number of classifications.

$$\text{Accuracy} = \frac{\text{sum of true positive} + \text{true negative}}{\text{sum of all predicted value}} = \frac{\text{MM} + \text{BB}}{\text{MM} + \text{MB} + \text{BM} + \text{BB}} \dots 3.20$$

The limitation of accuracy high when the prediction predicted only one class BB or MM the accuracy misleading because model does not detected any other classes. The range of correct outputs were 0 to 1 indicating benign or malignant patients respectively. According to table 3.1 the probability outcome was 0.5 then taken the threshold value greater than probability of them to get 1's and 0's accuracy top.

Model GRNN for detected true positive and true negative rate used as inputs and targets MIAS db of breast cancer showed below. T taken as target, X as inputs and radial basis functions (spread = 100), X = 9x400 size, 28800 class double and T = 2x400 size, 6400 class double, net = newgrnn (X,T,spread) and displayed results sim(net,x).

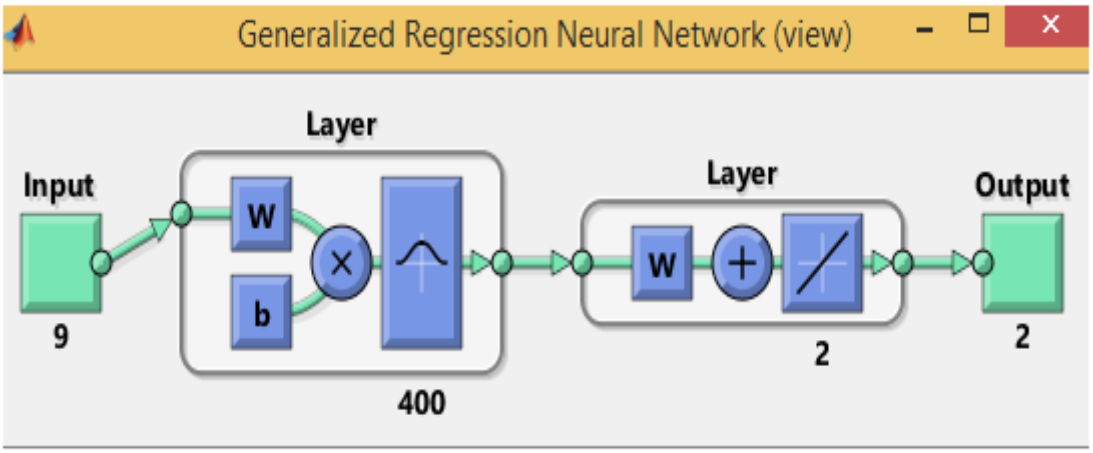

Figure 3. 4: Design GRNN network.

As seen figure 3.4, 9 input MIAS db, 400 amount of neuron in vectors and 2 output. Only first layer has bias in the second layer has not bias. Detected error used confusion matrix and histogram was plotted across all samples measured error for the GRNN method designed. See table 4.1 and figure 4.11.

3.5.2. Probabilistic neural networks

PNN also proposed for function approximation purposes [45]; however in some tasks, it is applied to classification problem [1]. PNN has two radial basis layer and competitive layer shown in figure. 3.5[45, 34]. In competitive function, target vectors has a 1 only in the row associated with that particular class of input, and 0's elsewhere that used MATLAB code function ind2vecis to create the proper vector hence the network has classified large input data into a specific one output. In this case dropped original information data thus, have seen from simulation. Newpnn creates a two-layer network. The first layer has radbas neurons, and calculates its weighted inputs with dist, and its net input with netprod. The second layer has compet neurons, and calculates its weighted input with dotprod and its net inputs with netsum.

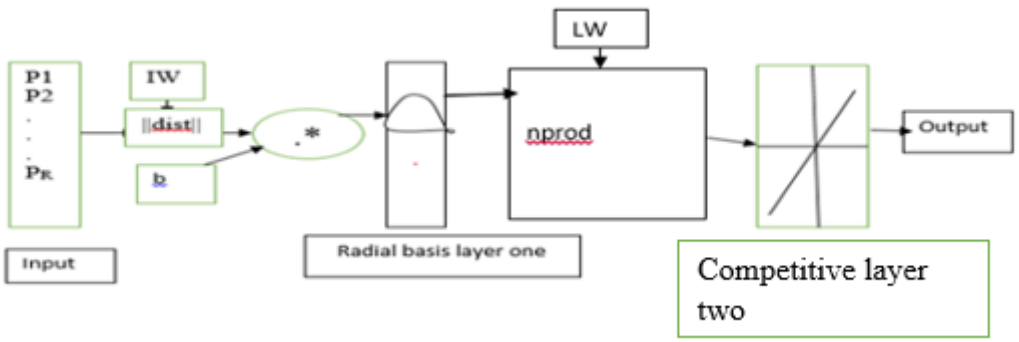

Figure 3. 5: Architecture for the PNN.

Each cluster from a center to inputs and weighted sun computed using squared Euclidean distance and applied to activation function with help of Gaussian function according to the MATLAB code. Design a PNN network given inputs X, targets T and radial basis functions (spread = 100), X = 9x400 size, 28800 class double and T = 2x400 size, 6400 class double, net = newpnn (X,T,spread) and displayed results sim(net,x).

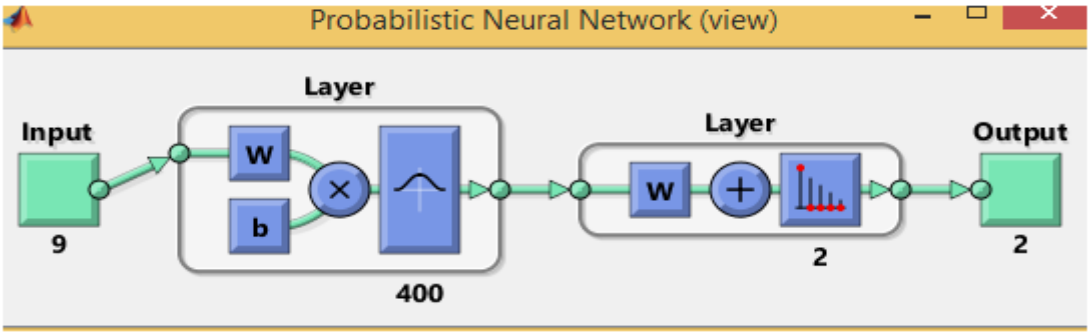

Figure 3. 6: Design PNN network.

As seen figure 3.6, 9 input MIAS db, 400 amount of neuron in vectors and 2 output. Only first layer has bias in the second layer has not bias. Detected error used confusion matrix and histogram was plotted across all samples measured error for the PNN method designed. See table 4.2 and figure 4.12.

3.5.3. Radial basis function neural network

RBFNN is a famous feed forward network that is used for approximation. The output of the layer two close to first layer input data in case of linear function because the first derivative activation function is one this used to reduced error to zero. RBF networks can be used to approximate functions designs with zero error as soon as saved time during simulation processed. It contains one input and two layers are radial basis layer and linear layer as showed diagram below.

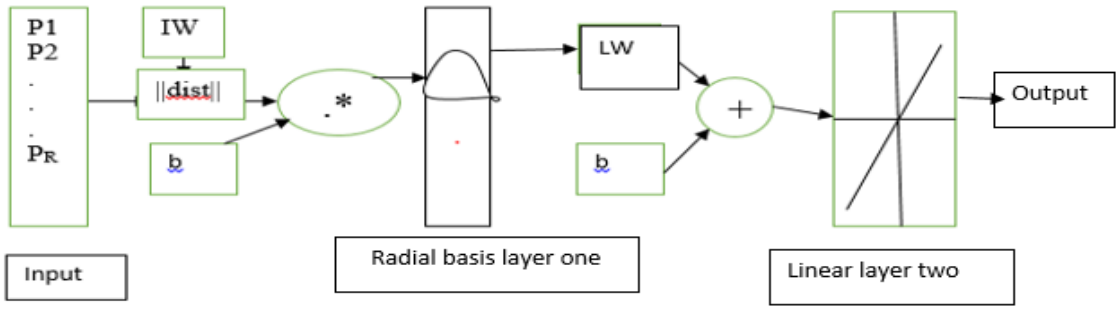

Figure 3. 7: Radial basis function network.

The above illustration shows the typical architecture of an RBF network. It consists of an input vector, a layer of RBF neurons, and an output layer with one node per class of data. Design a RBF network given inputs X, targets T and radial basis functions (spread = 100) , X = 9x400 size, 28800 class double and T = 2x400 size, 6400 class double, net = newrbe (X,T,spread) and displayed results sim(net,x).

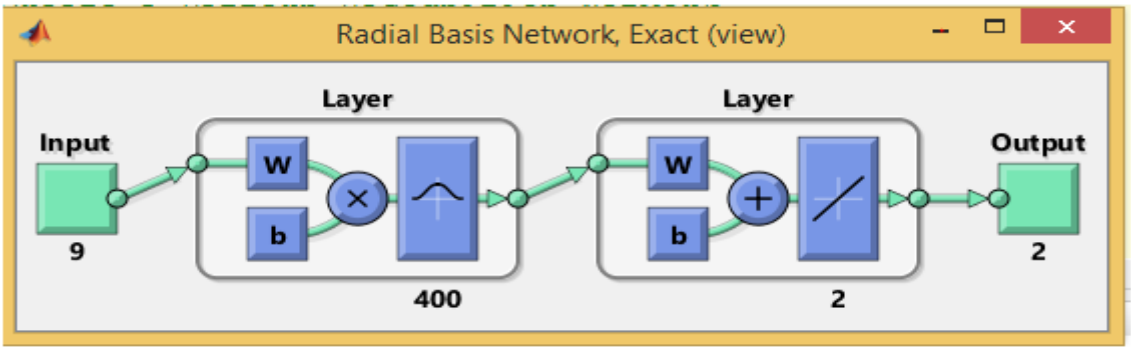

Figure 3. 8: Design RBN network.

As seen figure 3.8, 9 input MIAS db, 400 amount of neuron in vectors and 2 output. Both layers have bias in the first and second layer. Detected error used confusion matrix and histogram was plotted across all samples measured error for the RBNN method designed. See table 4.3 and figure 4.13.

3.6. Design training neural network method

In this method training used as RBF that the two layers computed both weighted sum and bias as observed from RBF diagram. Reduced error by calculated linear activation function with sigmoid function and update weighted sum generalized delta rule. Each train data error computed separately by stochastic gradient descent (SGD) scheme. This system immediately updated weighted sum that advantage saved time during training processing. MATLAB code called according to theirs train function in the specified loop sequence of inputs, output, and error and updated weights. In this paper the supervised training method was used in section 3.2.2 for normalized MIAS db and an unsupervised training techniques used, for adjustted weights by rand instance, to identified groups of data. Training network kinds of linear networks are designed directly as showed figure 3.7. Designed training based on learning rule medhod that produced desgin block diagram individual function established on theirs code. Train error decreased any network as long as its weight, net input, and transfer functions have derivative functions.The validation vectors are used to stop training early if further training on the primary vectors will hurt generalization to the

validation vectors. It measured network performance vectors fails to improve or remains the same for max_fail epochs in a row.

Hold-out validation this algorithms, the mostly large MIAS db is randomly divided to three subsets. Training set is a subset of the MIAS db used to build predictive models. Validation set is a subset of MIAS db used to assess the preformance of model build in training phase. It provides a test platform for fine tuning model's parameters and selecting the best performing model. Test set is a subset of MIAS db to assess the likely future performace of a model.It provides avoid overfitting in validation occoured. Overfitting which have very complecated model does not reduced error MIAS db.Test vectors are used as a further check that the network is generalizing well, but do not have any effect on training. It estimated generalization error due to weight training; performance of fielded network where validation set represent novel designs not yet classified.

Cross-validation is other validation set which is limited amount of MIAS db available, achieved unbiased estimate of model performance well used k-fold cross-validation. K-foldcross validation split data into k-sub groups in identical size. Receive operating characteristics (ROC) olso measured the performance of training neural network that showed the accuracy under ROC and the value ROC between the probabilty table 3.1 and one (0.5<ROC<1). Showed the relationship between true positive rate and false positive rate.

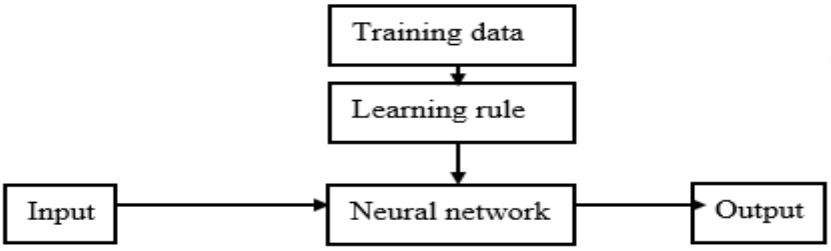

Figure 3. 9: Blok diagram of designing training data.

The behavior of training data neural network designated under performance graphed,fit graphed and received operating characteristic graphed.This is crooked while understanding the process of training data. Some function used for training such as feed-forward neural network(FFWNN),fitting function neural network (FFNN) and pattern recogonized neural network(PRNN) help full function measuring the performance parameters of the training network.

3.6.1. Feedforward neural network

Hidden layer- a layer of a network that is not connected to the network output. (For instance, the first layer of a two-layer feed forward network). Input layer- a layer of neurons receiving inputs directly from outside the network. The neurons in a feed-forward neural network are grouped into a sequence that neurons in any layer are connected only to neurons in the next layer [28]. Also communication proceeds layer by layer from the input layer through the hidden layers up to the output layer, can fit any finite input-output mapping problem.Computed according to this formula.

$$y_k = \sum_{j=0}^{N} W_{ki} a_i \ldots\ldots\ldots\ldots\ldots\ldots\ldots\ldots 3.21$$

Where W_{ki} is weighted link hidden layer to output,y_k is output layer in k classes

Designed FFWNN it's weighted inputs with dist, and its net input with hidden layer. MATLAB code is calculated as given inputs X and targets T , X = 9x400 size, 28800 class double and T = 2x400 size, 6400 class double, net = feedforwardnet(hidden layer sizes = 40) , [net,tr] = train(net,X,T); and displayed output sim(net,X) was.

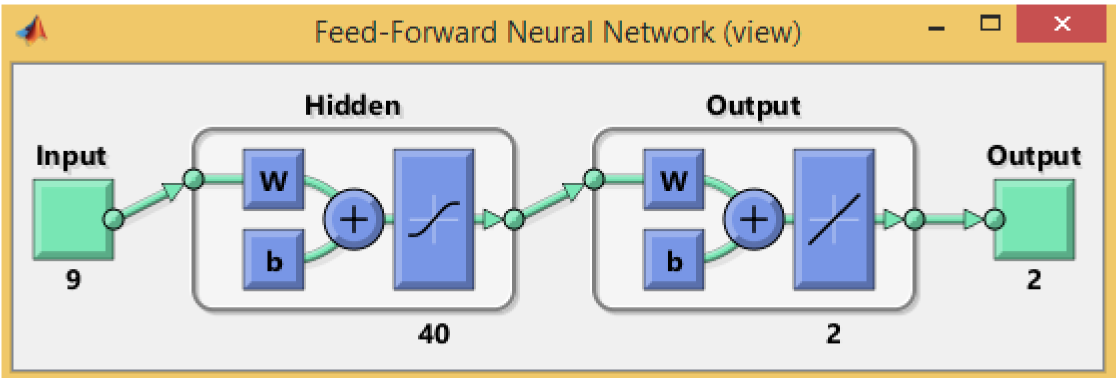

Figure 3. 10: Design FFWN network.

As seen figure 3.10, 9 input MIAS db, 40 number of neuron vectors in hidden layer and 2 output. Both layers have bias in the first and second layer. Detected error used performance for hold-validation and performance for cross-validation was plotted for 40 neuron samples measured error for the FFWNN method designed. See figure 4.14 and figure 4.15.

For estimating test error of FFWNN, FFNN and PRNN designed network measured ROC using validation set. The validation set approach was used on the error data set in order to estimate the test error that results from predicted mpg using polynomial function of breast MIAS db horsepower. Illustrating in the estimated test error given as:

$$mpg = f(x^n, x) \ldots\ldots\ldots\ldots\ldots\ldots\ldots\ldots 3.22$$

Where mpg is f (polynomial function) describe at which the MSE minimum as given degree of polynomial along epoch's line (x^n, x) in this case indicated least error (1, 2 …n)is degree polynomial and x is breast cancer MIAS db.

In section 3.6 described cross-validation (fitting curve) classification technique that measure the performance by comparison different breast cancer MIAS db. Fitting curve was the best estimate of the unknown functional relationship from a set predicted value at given actual data with polynomial function. In fit function error observed three set given as:

$$e = t - y \ldots\ldots\ldots\ldots\ldots\ldots\ldots\ldots\ldots\ldots\ldots\ldots 3.23$$

Where e is error, t is target and y is output. When t > y, e is positive, t = y, e = 0, and t < y, e is negative value those were indicated the relationship between benign and malignant.

In section 3.6 described ROC also classification technique that measure the performance by comparison deferent breast cancer MIAS db. The ROC is a metric used to check the quality of classifiers. For each class of a classifier, roc applies threshold values across the interval [0, 1] to outputs. For each threshold, two values are calculated, the true positive ratio, and the false positive. ROC was the best measured accuracy under area curve (45 degree) diagonal that showed the trade-off between true positive rate and false positive rate using logistic regression method. Simple figure below define the best accuracy area as increased up on the left hand the accuracy of data also increased.

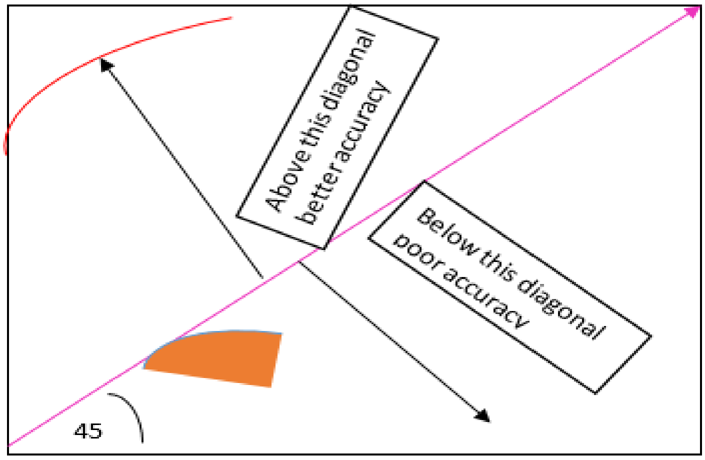

Figure 3. 11: Classification model.

This figure show the relationship between above diagonal and below diagonal as actual MIAS db given, accuracy define based on predictor observation.

3.6.2. Function fitting neural network

Designed FFNN it's weighted inputs with ||dist|| and its net input with hidden layer. MATLAB code is calculated as given inputs X and targets T, X = 9x400 size, 28800 class double and T = 2x400 size, 6400 class double,net = feedforwardnet(hidden layer = 40) , [net,tr] = train(net,X,T); and displayed output sim(net,X) was.

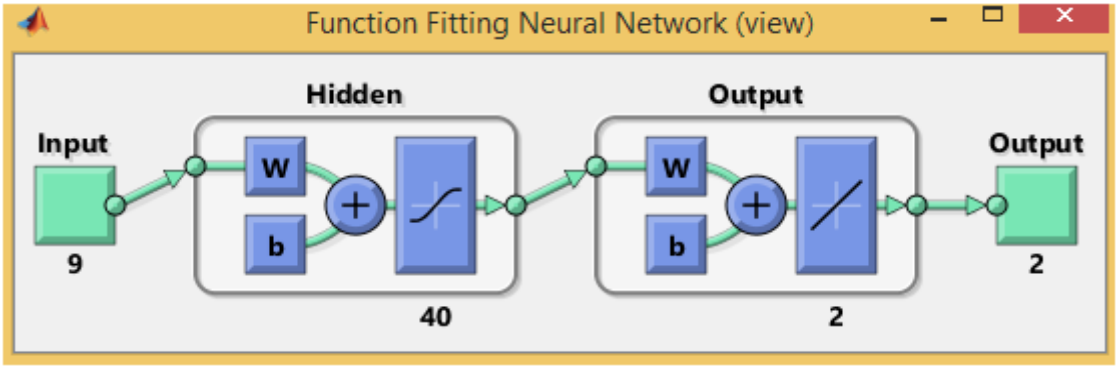

Figure 3. 12: Design FFN network.

As seen figure 3.12, 9 input MIAS db, 40 number of neuron vectors in hidden layer and 2 output. Both layers have bias in the first and second layer. Detected error used performance for hold-validation and performance for cross-validation was plotted for 40 neuron samples measured error for the FFNN method designed. See figure 4.17 and figure 4.18.

3.6.3. Pattern recognition neural network

Designed PRNN it's weighted inputs with ||dist|| and its net input with hidden layer. MATLAB code is calculated as given inputs X, and targets T, X = 9x400 size, 28800 class double and T = 2x400 size, 6400 class double,net = feedforwardnet(hidden layer = 40) , [net,tr] = train(net,X,T); and displayed output sim(net,X) was.

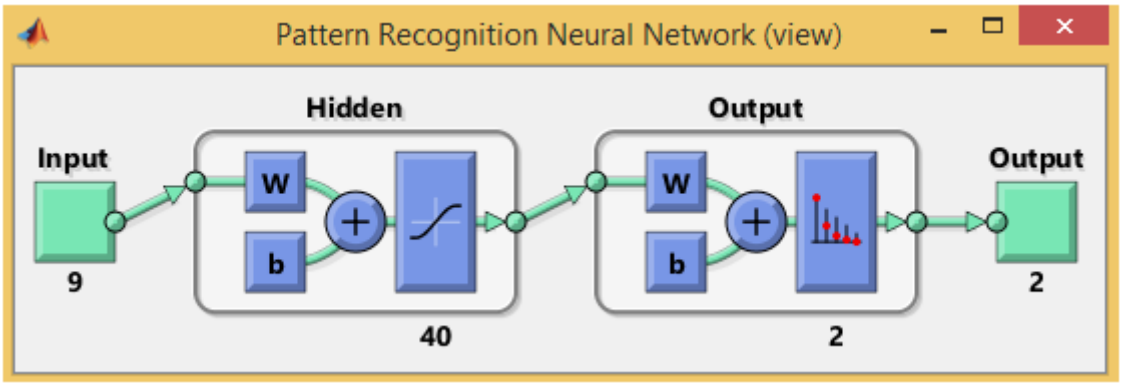

Figure 3. 13: Design PRNN.

As seen figure 3.13, 9 input MIAS db, 40 number of neuron vectors in hidden layer and 2 output. Both layers have bias in the first and second layer. Detected error used performance for hold-validation and performance for cross-validation was plotted for 40 neuron samples measured error for the PRNN method designed. See figure 4.20 and figure 4.21.

3.7. Model local linear radial basis function neural network

RBFNN is proposed as local linear radial basis function neural network (LLRBFNN). The architecture of the proposed LLRBFNN is given in figure 3.14. Local linear models provide a frugal interpolation in high dimension spaces when modeling samples are sparse. A local linear model replaces the connection of weights between the hidden layer and output layer of conventional RBFNN to have faster convergence speed. In comparison of LLRBFNN and RBFNN, the LLRBFNN requires less number of neurons than the RBFNN to approximate the same nonlinear system thus the LLRBFNN is more efficient because the ability of approximation has been increased by placing a local linear model instead of the hidden layer units [27]. The input and number of hidden layer nodes are equal which reduces overall node requirement.

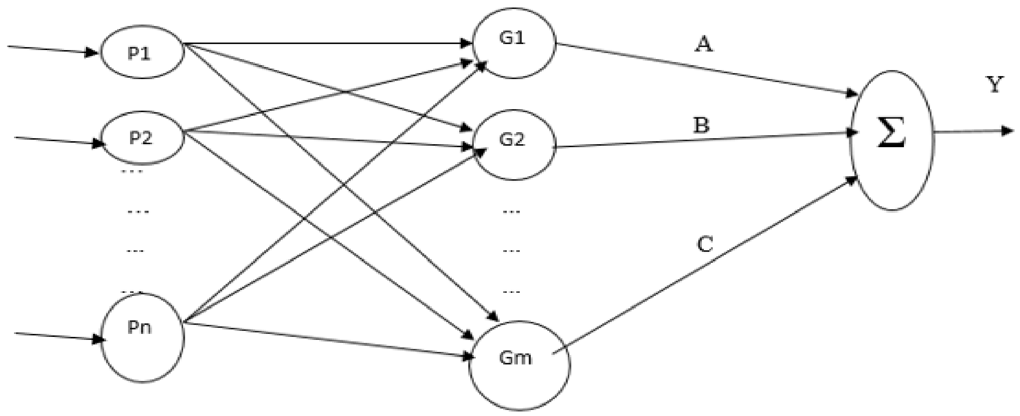

Figure 3. 14: Architecture LLRBFNN.

The linear equation each output node local linear given by:

$$A = W_{10} + W_{11P_1} + \cdots + W_{1nP_n} \ldots \ldots \ldots \ldots 3.24$$

$$B = W_{20} + W_{21P_1} + \cdots + W_{2nP_n} \ldots \ldots \ldots \ldots 3.25$$

$$\vdots$$

$$C = W_{m0} + W_{m1P_1} + \cdots + W_{mnP_n} \ldots \ldots \ldots \ldots 2.26$$

Where P_1, P_2…P_n are inputs (features), and G_1, G_2… G_m are the Gaussian activation function in the hidden units, A, B and C are linear equation.

RBFN have a hidden layer whose activation functions are calculated based on distance of the inputs and center of the activation functions. The hidden layer takes the local linear weight as the input and computes the output. The activation function of the M^{th} hidden layer sizes is defined by a Gaussian Kernel as:

$$\mathrm{Gm(p)} = \mathrm{e}\left(\frac{-||\mathrm{p}-\mathrm{cm}||^2}{2\delta m^2}\right) \ldots\ldots\ldots\ldots\ldots\ldots\ldots\ldots\ldots\ldots\ldots\ldots\ldots\ldots 2.27$$

Where $\delta m^2$the parameter for controlling the smoothness of the activation is function, cm is the center of the hidden node and $||p-cm||^2$indicates the Euclidean distance between the inputs and the function center. LLRBFNN is characterized by localized activation of the hidden layer units. The connecting weights associated with the hidden nodes can be viewed as locally accurate linear models. The mapping function of the network with Gaussian activation function and weighted linear summation in output neuron is given as:

$$\mathrm{Y} = \sum_{\mathrm{m}=1}^{\mathrm{M}} \mathrm{LmGm(Lm)} \ldots\ldots\ldots\ldots\ldots\ldots\ldots\ldots\ldots\ldots\ldots\ldots\ldots\ldots 3.28$$

Where $\mathrm{G_m(L_m)} = \mathrm{e}\left(\frac{-||\mathrm{Lm}-\mathrm{cm}||^2}{2\delta \mathrm{m}^2}\right)$

Form equation 3.23 the local linear model is given by

$$[L]_{m=1}^{M} = [A] \ldots\ldots\ldots\ldots\ldots\ldots\ldots\ldots\ldots\ldots\ldots\ldots\ldots\ldots 3.29$$

From equation 3.23, 3.24, 3.25the complete local linear weight matrix is given by

$$\mathrm{L} = [\mathrm{A}; \mathrm{B}; \mathrm{C}]^{\mathrm{T}} \ldots\ldots\ldots\ldots\ldots\ldots\ldots\ldots\ldots\ldots\ldots\ldots\ldots\ldots 3.30$$

The output at the output layer is given by

$$\mathrm{Y} = \sum_{\mathrm{m}=1}^{\mathrm{M}} \mathrm{A\,G_m L_m} \ldots\ldots\ldots\ldots\ldots\ldots\ldots\ldots\ldots\ldots\ldots\ldots\ldots\ldots 3.31$$

Thus in matrix notation the weight matrix L is given as

$$[\mathrm{L}]_{1\mathrm{xM}} = [\mathrm{P}]_{1\mathrm{xn}} \,\mathrm{x}\, [\mathrm{W}]_{\mathrm{Mxn}} \ldots\ldots\ldots\ldots\ldots\ldots\ldots\ldots\ldots\ldots\ldots\ldots\ldots\ldots 3.32$$

Here each column of the weight matrix L denotes the connecting weights associated with a single hidden node. The objective function is to minimize the error and the mean square error is given by

$$\mathrm{MSE(e)} = \frac{1}{\mathrm{M}} \sum_{\mathrm{m}=1}^{\mathrm{M}} (\mathrm{D_m} - \mathrm{Y_m})^2 \ldots\ldots\ldots\ldots\ldots\ldots\ldots\ldots\ldots\ldots\ldots\ldots\ldots\ldots 3.33$$

Where "D" is the desired vector

3.7.1. Weight updating for local linear

In this network the weights are initialized to zero and optimized by using Widrow Hoff's Least Mean Square (LMS) algorithm [34, 38]. Initializing the weight to zero is very convenient as only the weights associated with the disturbance classes present in the input set need to be modified. In each epoch i.e., the learning cycle, the input pattern vectors are presented in a sequential manner, and the output vector is obtained. The error is calculated by subtracting the actual output from the desired output vector:

$$e_{m=Dm-Ym} \quad \ldots\ldots 3.34$$

The network weight is now updated by using Widrow Hoff's Least Mean Square algorithm:

$$W_{mn}(X+1) = W_{mn}(X) + \eta[p]{P_{kn}}^{T} e_{km} \quad \ldots\ldots 3.35$$

k = 1, 2, 3… K, n = 1, 2, 3… m = 1, 2, 3… M

Here 'X' is the number of learning cycle and the learning rate parameter 'η' is a function of 'X'. The weights are updated during training data model description is given in figure 3.15.The LLRBFNN model uses a simple approximation pattern classification model, which needs a reduced number of hidden nodes than the normal RBFNN model. Normally the number of hidden nodes taken is equal to the clusters present in the data. Thus each node acts as an approximation for a particular data cluster.

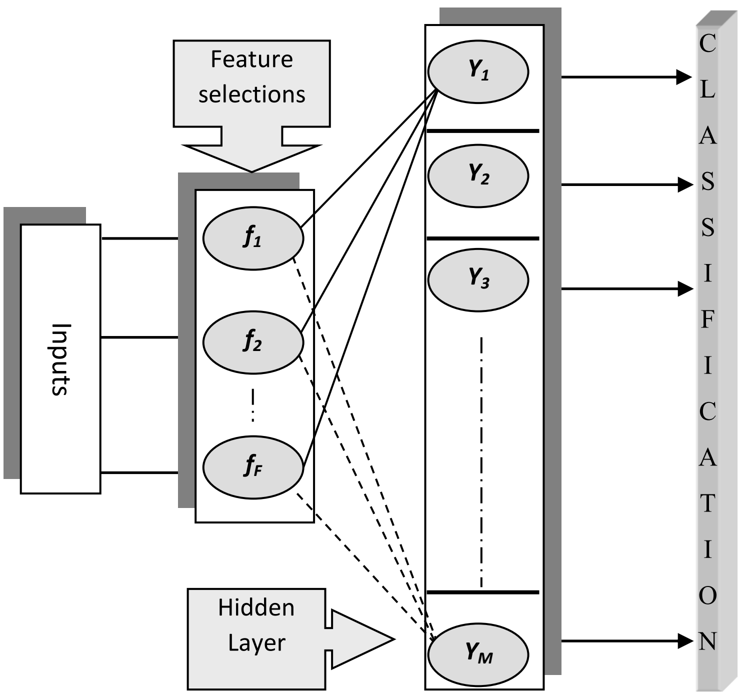

Figure 3. 15: LLRBFNN model description.

The proposed model consists of three layers. The model description of the network layers are given below.

Input layer: The input layer provides the features needed by the network to perform the classification task. The number of nodes is equal to the dimensionality of the input vector that is the number of features in each training vector. The features provided are normalized in between zero and one, which plays a key role in maintaining network stability during training.

Input weights: In this network a randomized set of connecting weights is used in between the feature input layer and approximation hidden layer. The weights are initialized to zero and optimized by using Widrow Hoff Least Mean Square (LMS) algorithm. Initializing the weight to zero is very convenient as only the weights associated with the disturbance classes present in the input set need to be modified. Other connecting weights remain unchanged, as they contribute no output.

Hidden layer: The hidden layer takes the local linear weight as the input and computes the output associated with a particular class. The activation function used is a simple Gaussian Kernel given as

$$G(p) = \exp\frac{-(p-c)^2}{2\sigma^2} \quad \text{.....3.36}$$

Here the spread parameter sigma (σ) is taken to be one .The center is also fixed at one. This reduces the kernel to

$$G(p) = \exp\frac{-(p-1)^2}{2} \quad \text{.....3.37}$$

3.7.2. Local linear weight

LLRBFNN are characterized by localized activation of the hidden layer units. The connecting weights associated with the hidden nodes can be viewed as locally accurate linear models. The output of the m^{th} unit in the hidden layer is given as

$$Y_m = L_m G_m(L_m) \quad \text{.....3.38}$$

Where m = 1, 2, 3……M ,'M' is the number of classes and L_m represents a local linear model .The local linear model L_m is given by

$$[L_m]_{m=1}^{M} = \sum_{f=1}^{F} p_f w_{fm} = [p_1 w_{1m} + p_2 w_{2m} + \ldots\ldots\ldots + p_F w_{Fm}]_{m=1}^{M} \quad \ldots\ldots\ldots\ldots\ldots\ldots\ldots\ldots 3.39$$

Where, L_m is the local linear weight associated with m[th] hidden node, f = 1, 2, 3…F is number of features selections. Thus the output of the m[th] hidden node is given by

$$Y_m = \sum_{f=1}^{F} P_f w_{fm} \exp - \left(\frac{(P_f w_{fm} - 1)^2}{2} \right) \quad \ldots\ldots\ldots\ldots\ldots\ldots\ldots\ldots\ldots\ldots\ldots\ldots\ldots\ldots\ldots\ldots\ldots\ldots\ldots\ldots 3.40$$

Thus for an input vector

$$[P_k]_{k=1}^{K} = [P_1, P_2, \ldots\ldots\ldots\ldots P_F] \quad \ldots\ldots\ldots\ldots\ldots\ldots\ldots\ldots\ldots\ldots\ldots\ldots\ldots\ldots\ldots\ldots\ldots\ldots\ldots\ldots\ldots\ldots\ldots\ldots 3.41$$

k =1, 2, 3 ……K (numeral of input pattern)

The complete local linear weight matrix is given by

$$L = \begin{bmatrix} A \\ B \\ . \\ . \\ C \end{bmatrix}^{T} \quad \ldots\ldots\ldots\ldots\ldots\ldots\ldots\ldots\ldots\ldots\ldots\ldots\ldots\ldots\ldots\ldots\ldots\ldots\ldots\ldots\ldots\ldots\ldots\ldots\ldots\ldots 3.42$$

Thus in matrix notation the weight matrix L is given as

$$[L]_{1\times M} = [P]_{1\times f} \times [W]_{f\times M} \quad \ldots\ldots\ldots\ldots\ldots\ldots\ldots\ldots\ldots\ldots\ldots\ldots\ldots\ldots\ldots\ldots\ldots\ldots\ldots\ldots\ldots\ldots\ldots\ldots 3.43$$

Here each column of the weight matrix L denotes the connecting weights associated with a single hidden node. Therefore out of M number of classes only one output of the output layer will deliver the output. The output is given as

$$Y = [L]_{1\times M} \cdot \times [G]^{T}{}_{1\times M} \quad \ldots\ldots\ldots\ldots\ldots\ldots\ldots\ldots\ldots\ldots\ldots\ldots\ldots\ldots\ldots\ldots\ldots\ldots\ldots\ldots\ldots\ldots\ldots\ldots\ldots 3.44$$

Where ‘G’ is the hidden node output given as

$$\exp \frac{-(L-1)^2}{2}$$

Weight update

In each epoch (learning cycle), the input pattern vectors are presented in a sequential manner, and the output vector is obtained. The error is calculated by subtracting the actual output from the desired output vector [28]:

$$e_m = D_m - Y_m \quad \ldots\ldots\ldots\ldots\ldots\ldots\ldots\ldots\ldots\ldots\ldots\ldots\ldots\ldots\ldots\ldots\ldots\ldots\ldots\ldots\ldots\ldots\ldots\ldots\ldots 3.45$$

m=1, 2, 3…M

The network weight is now updated by using Widrow Hoff’s Least Mean Square algorithm [38].

$$W_{fm}(X+1) = W_{wf}(X) + \eta(X) P_{kn}{}^{T} e_{km} \quad \ldots\ldots\ldots\ldots\ldots\ldots\ldots\ldots\ldots\ldots\ldots\ldots\ldots\ldots\ldots\ldots\ldots\ldots 3.46$$

For k = 1, 2, 3… K, f = 1, 2, 3… F, m = 1, 2, 3… M and 'X' is the number of epochs and the learning rate parameter 'η' is a function of 'X'. From the above equation that can the weights connecting the feature nodes to the m^{th} hidden node are changed only when there is an error obtained at m^{th} node. Thus the weight is purely a local phenomenon, which presents a need based weight model. The number of weight column thus needed completely depends on the number of classes present in the MIAS db that used an adaptive learning rate parameter to train designed network in order to find the optimum weight matrix. The learning rate, which is a function of the epoch number, is given as:

$$\eta(X) = \frac{\eta_0}{1 + \frac{X}{T}} \quad \ldots\ldots\ldots\ldots\ldots\ldots\ldots\ldots\ldots\ldots\ldots\ldots\ldots\ldots\ldots\ldots\ldots\ldots\ldots\ldots\ldots\ldots 3.47$$

Where, T is number of training pattern, X is epoch number

This is called LLRBFNN, by gradually decreasing value of η_0 as observed parameters ensure that the weights converge to the optimum value within a few epochs. The design of LLRBFNN was comparing with FFWNN, FFNN, PRNN and RBFNN for breast cancer MIAS db classification by 9-fold cross validation test. Performance of LLRBFNN was comparing with MATLAB 14astandard neural network toolbox RBFNN and train function such as FFNN and PRNN implementations.

3.8.K-mean clustering classification scheme

K-means is a method of clustering observations into classify number of MIAS db of disjoint clusters. The"K" refers to the number of clusters species. Various distance measures exist to determine which observation is to be appended to which cluster. The algorithm aims at minimizing the measure between the centroids of the cluster and the given observation by iteratively appending an observation to any cluster and terminate when the lowest distance measure is achieved. Common distance measures used the Euclidean squared distance. The Euclidean measure corresponds to the shortest geometric distance between two points.

$$c = \sum_{i=1}^{N} (x_i - y_i)^2 \quad \ldots\ldots\ldots\ldots\ldots\ldots\ldots\ldots\ldots\ldots\ldots\ldots\ldots\ldots\ldots\ldots\ldots\ldots\ldots\ldots\ldots\ldots\ldots\ldots\ldots\ldots\ldots\ldots\ldots\ldots\ldots\ldots 3.45$$

Where input data, specified as an N-by-P matrix. N is the number of observations, and P is the number of variables. i = 1, 2, 3…N, x_i and y_i is two points coordinates and c is centroid distance between center points to coordinate points.

As observed in literature review many researcher described a big challenge problem was detected and classified breast cancer. In this paper breast cancer detected and classified into classes according to the following scheme. Neural network which was showed the output launches a window that specified in net as a graphical diagram. RBF (radial basis function) which stood centers of RBF model and width data from RBF model. Centers is returns an array of size number of centers by number of variables. Width is usually a single value, but can also be of size 1 by number of variables in the case of the width per dimension algorithm, or number of centers by number of variables in the case of linear classification. Linear local is an object that stores the linear estimate nonlinear as linear arranged data was taken from the LRBFNN that detected and classified breast cancer by cosine and sine function as x input data and t target data the MATLAB code. The simulation results of all above methods described in chapter four

CHAPTER 4

RESULT AND DISCUSSION

4.1. Simulation results

Different simulation results were described for different detection and classification as given below.

4.1.1. Simulation results for detection

The simulation results for medical input image, filtering images, segmentation images and extraction features were described separately in this chapter was used code fuzzy level set rule. .

Output result for medical input image compared original image, true color image and grayscale image by histogram and scatter plot system.

Figure 4.1 showed the original image was displayed with the RGB color values left as a subplot figure 4.1a and subplot of the same image was displayed the transformed intensity image as a heat map right figure 4.1b.

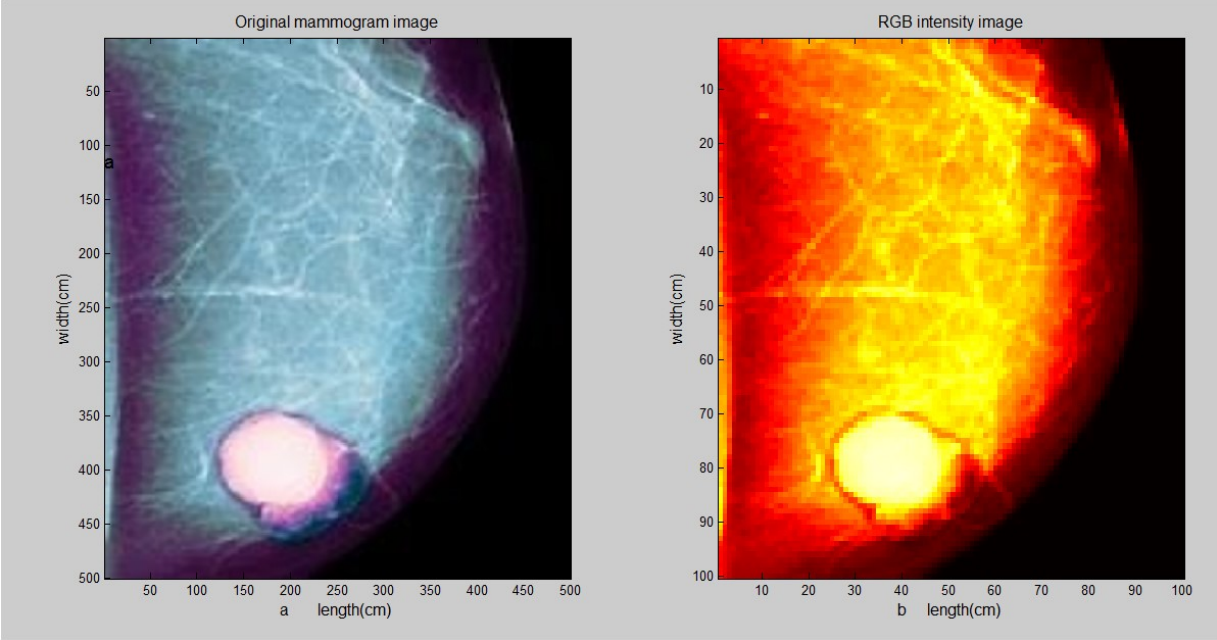

Figure 4. 1: Comparison variation dimension true color with original images.

Figure 4.1a (original image) was stored as a size (500-by-500) cm values in the same range as indexed (RGB) image. Figure 4.1b image was stored as a size (100-by-100) cm values in the range. It was decreased by 400cm when compared with original mammogram image

but colors were unbalanced. From the graph, it can be seen that the size of image was diminished.

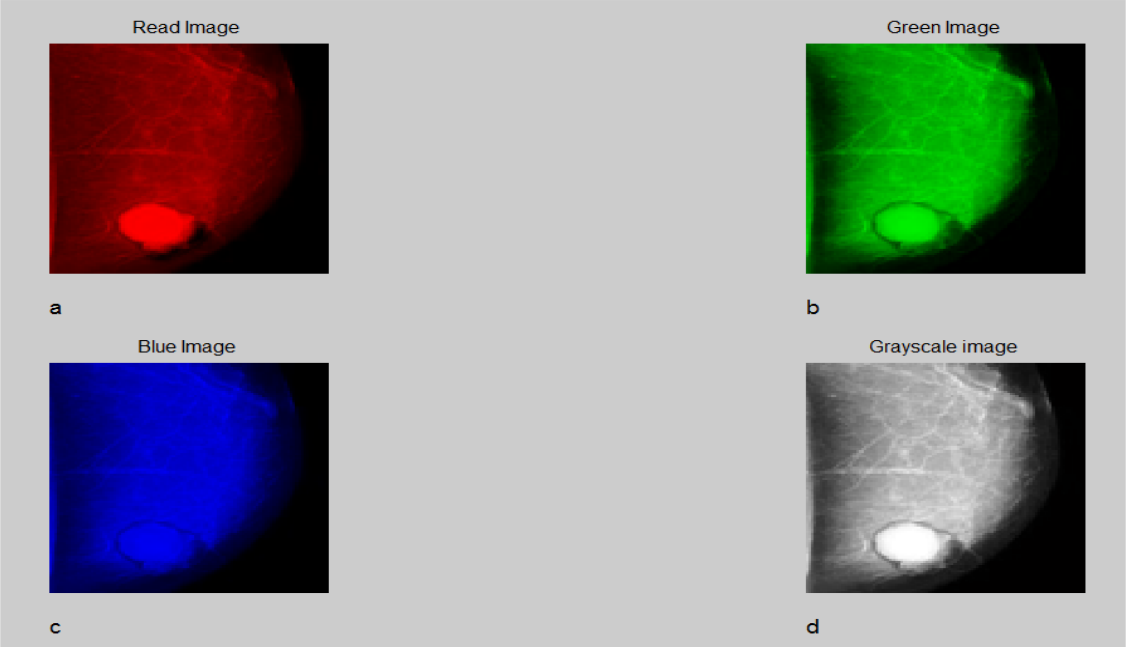

Figure 4. 2: Comparison difference three color with grayscale images.

Grayscale (figure 4.2d) has the highest quality value than RGB (figure 4.2a, b and c) component. Gray-level transformation for contrast enhancement was better than RGB color image. Figure 4.2d showed an extreme case of gray-level transformation for measured image enhancement parameters. From figure 4.2, it can be illustrated that the three color images was lower contrast image as compared with grayscale image. For the cause that grayscale image conversion for reduced dissimilarity color.

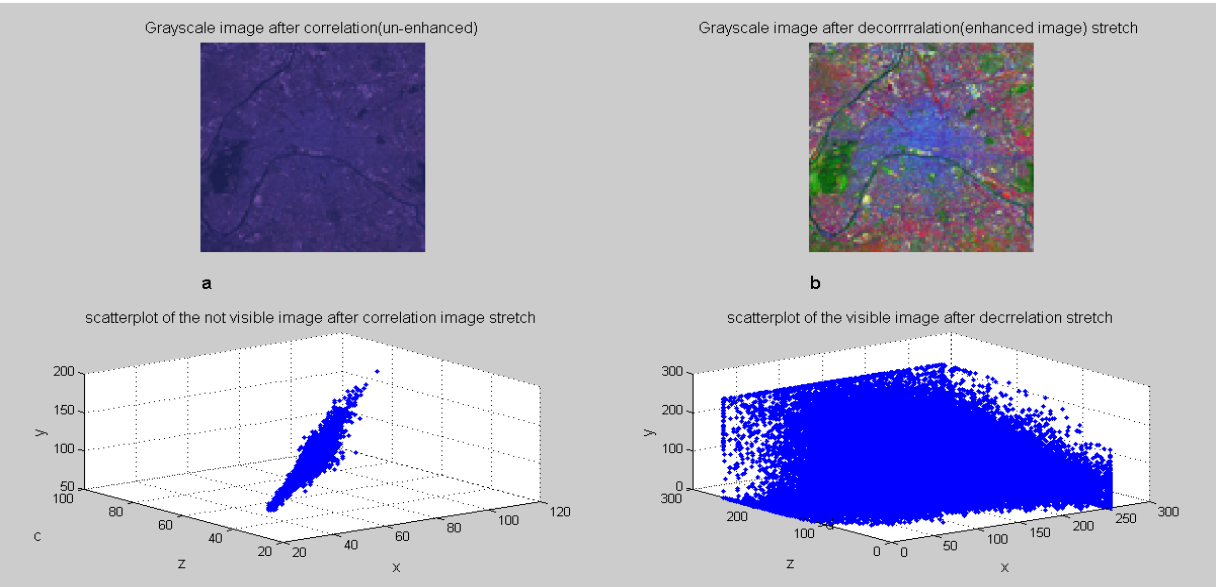

Figure 4. 3: Comparison grayscale image correlation with de-correlation.

Used to correlation required for grayscale figure 4.3d composited. A grayscale image the figure 4.3a composited in case correlation stretch, figure 4.3c shadowed across highly correlated. The visible image figure 4.3d were highly de-correlated. The two and three scatter plots figure 4.3b, d were an excellent way to gauge the degree of the de-correlation among contrast images. This was performed by applying de-correlation stretch, adjusting parameters value ('Tol was 0.01') of a linear contrast stretch.

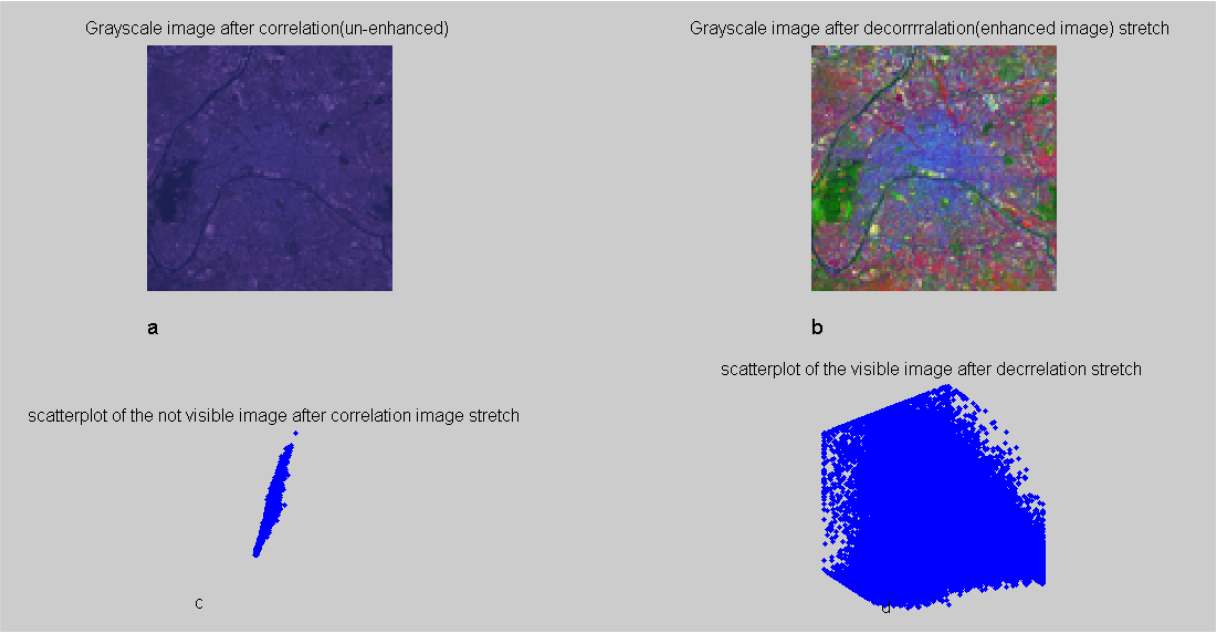

Figure 4. 4: Comparison grayscale image after remove axis tick correlation with de-correlation.

Remove the axis tick marks and tick labels for figure 4.4c, d. Figure 4.4c, d compared with figure 4.3c, d. Image adjust maps the intensity values in grayscale image to new values in figure 4.4c, d such that 1% of data is saturated at low and high intensities of grayscale image. That increases the contrast of the output image of figure 4.4d. Set the feature ratio to obtain separation interested shapes. The de-correlation stretch extremely decreased in the correlation image. Hence the surface features have become more clearly visible.

Grayscale and true color images analysis after de-correlation by histogram was observed as different shapes on the right hand histogram greater contrast than the left histogram sides figure below.

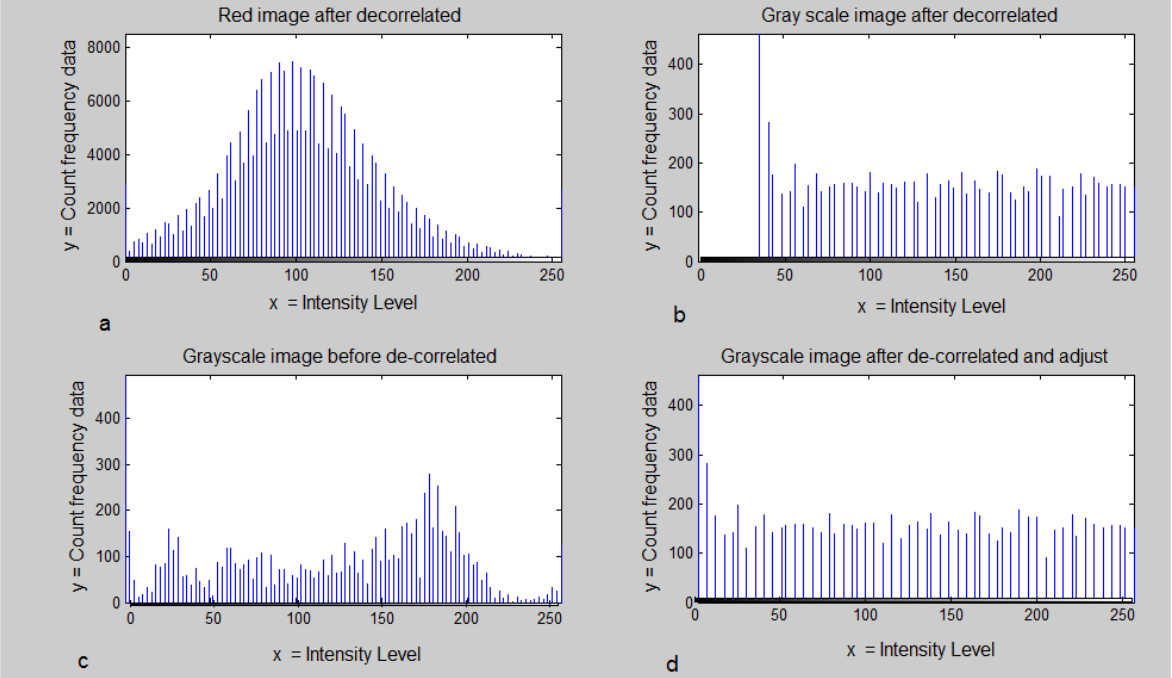

Figure 4. 5: Comparison red color image with grayscale image analysis on histogram.

Generated quality image histogram with helped C++ code from MATLAB after de-correlated figure 4.4b and figure 4.2d obtained figure 4.5. Figure 4.5b more contrast than figure 4.5a as shown in histogram. The maximum value on the y-axis count data 8000 was automatically reduced to 450, since outlier points do not dominate, so its edge was easily detected. Separation suited that evaluated histogram clearly seen into two regions.

Output simulation result for filtering evaluated mean filter, median filter and adaptive mean filter used grayscale image.

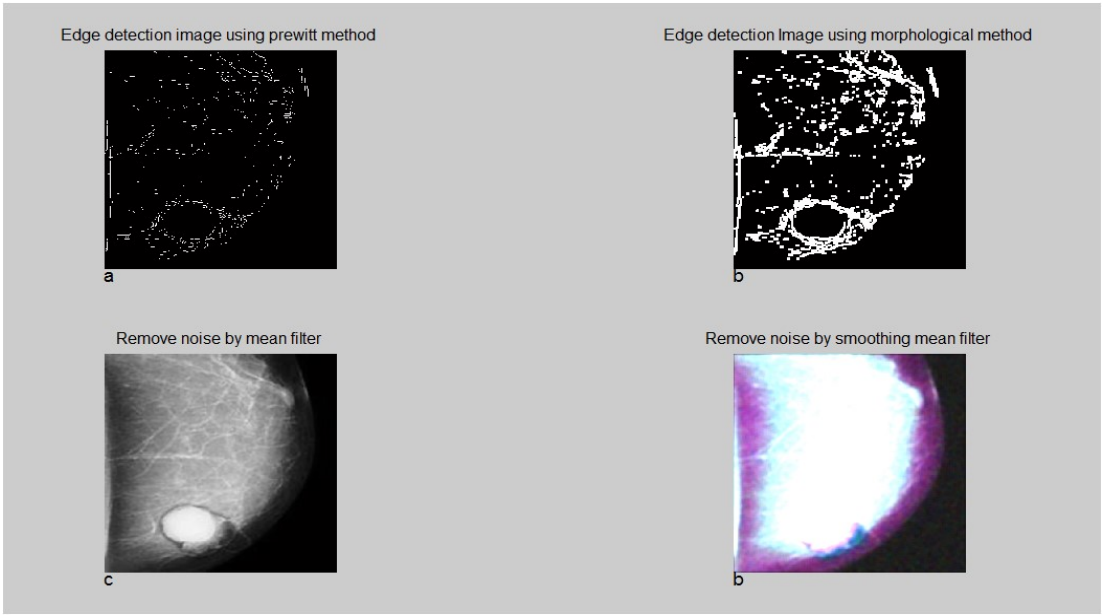

Figure 4. 6: Remove noise and edge detection of images by mean filter.

Figure 4.6a, b showed edge detection and the rest two showed remove noise on the region of images. From figure 4.6b, it can be seen that it has more edge detection than figure 4.6a. It was morphological operation on the binary image. Figure 4.6c, d, remove inner pixels to leave an outline of the shapes and filter the noisy image with an averaging filter and display the results.

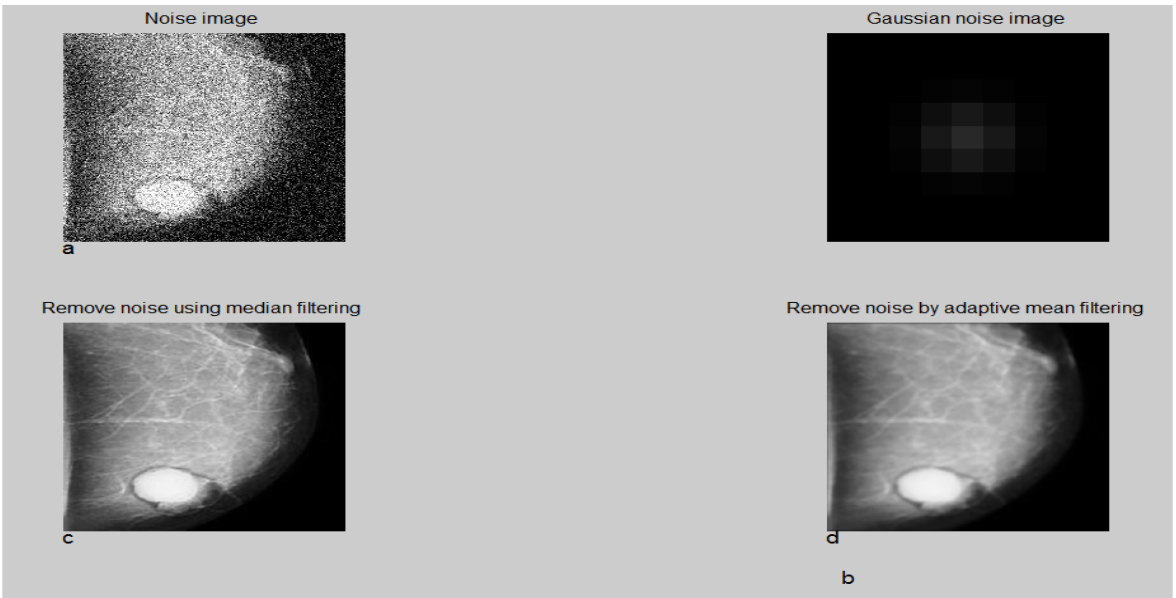

Figure 4. 7: Remove noise and edge detection of images different filter methods.

Figure 4.7a, adds noise of intensity image constant mean (0) and variance (1) because, de-noise an image using Gaussian filters. Figure 4.7b, add Gaussian noise to the image and then displays the image in case of quite large black that showed only a portion of the image. Negative values have been set to zero for the rows with Gaussian noise, matching the effect that a typical detector does not produce negative values. Figure 4.7c, median filter to filter the noisy image and display the results using medfilt2 scheme removing noise, with less confusing of edges. Figure 4.7d remove the noise, used the wiener2 function scheme was the best smoothed binary image. The adaptive mean filter used as preserved edges and other high-frequency parts of an image using a Weiner filter this noise can be reduced to very much extent.

Output simulation result for segmentation. The tumor Segmented used original image.

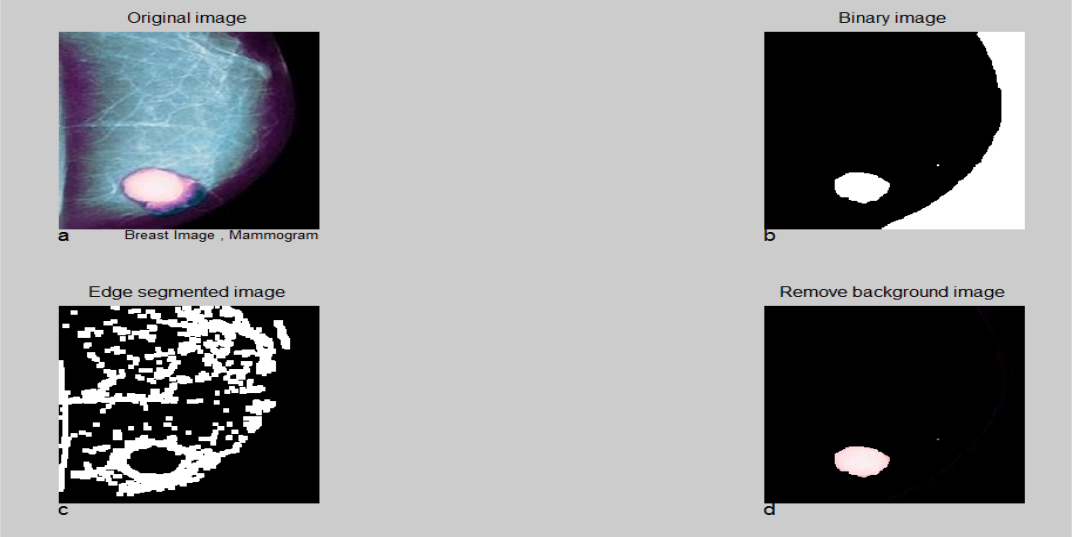

Figure 4. 8: Segmentation of the binary images.

Figure 4.8a, original image and figure 4.8b, separation of bright target objects from dark background. The resulting image contains connected component black-pixel regions and also white-pixel regions, the size and the shape of each target object was analyzed as its corresponding connected component was observed. Figure 4.8c, determined maximum threshold value that evaluated the separation of region as given threshold value. Figure 4.8d, the grayscale distributions of bright (1) binary target objects and dark (0) background binary over the image in this case segmented tumor scene.

Output simulation result for extraction features.

Matched tumor scene from reference image to target image and extracted the outlier's spot at the end.

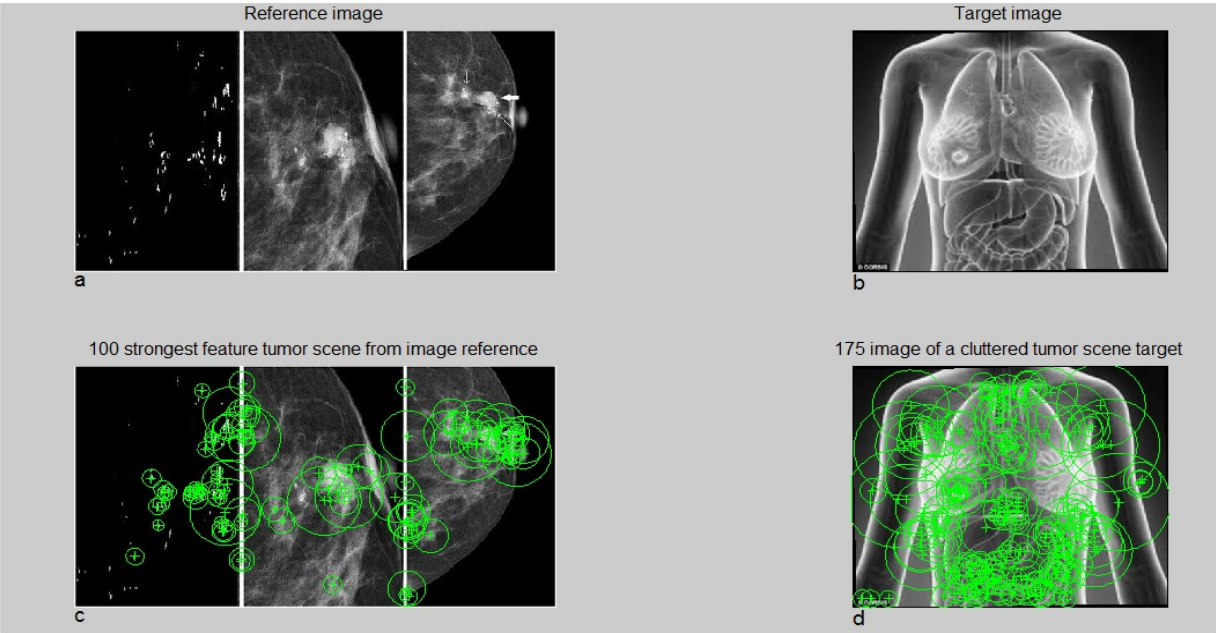

Figure 4. 9: Extraction features different thresholding values.

Figure 4.9 (a, b), represented by reference image and target image respectively. Figure 4.9 (c, d) showed as detected feature scene in both images which was visualized the strongest feature scene found in both images. `The index of reference image (120,163) computed the location tumor detected.`

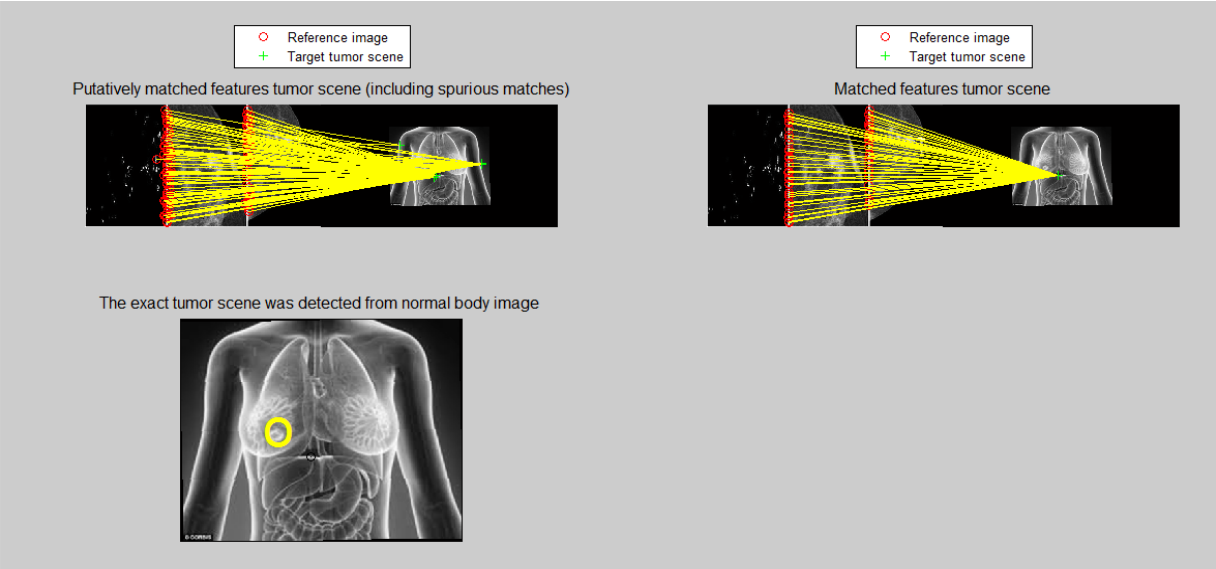

Figure 4. 10: Detected exact tumor scene.

Figure 4.10: Extract feature at the interest points in both images. Matching inliers and outliers features using estimate geometric transform calculated the transformation relating the matched points. Eliminated outliers and localized the tumor in the scene.

4.1.2. Simulation results for classification

The output simulation results of the same data used for the GRNN, PNN and RBF given below respectively. Those outputs result analyzed the error by confusion matrix and histogram plot.

The output simulation result for GRNN presented table 4.1 the percentages of correct classification green squares on the matrices diagonal and incorrect the red squares classifications. As seen the table below the overall percentages of correct classification was 57.3% and incorrect classification was 42.8% obtained.

Table 4. 1: Confusion matrix for GRNN.

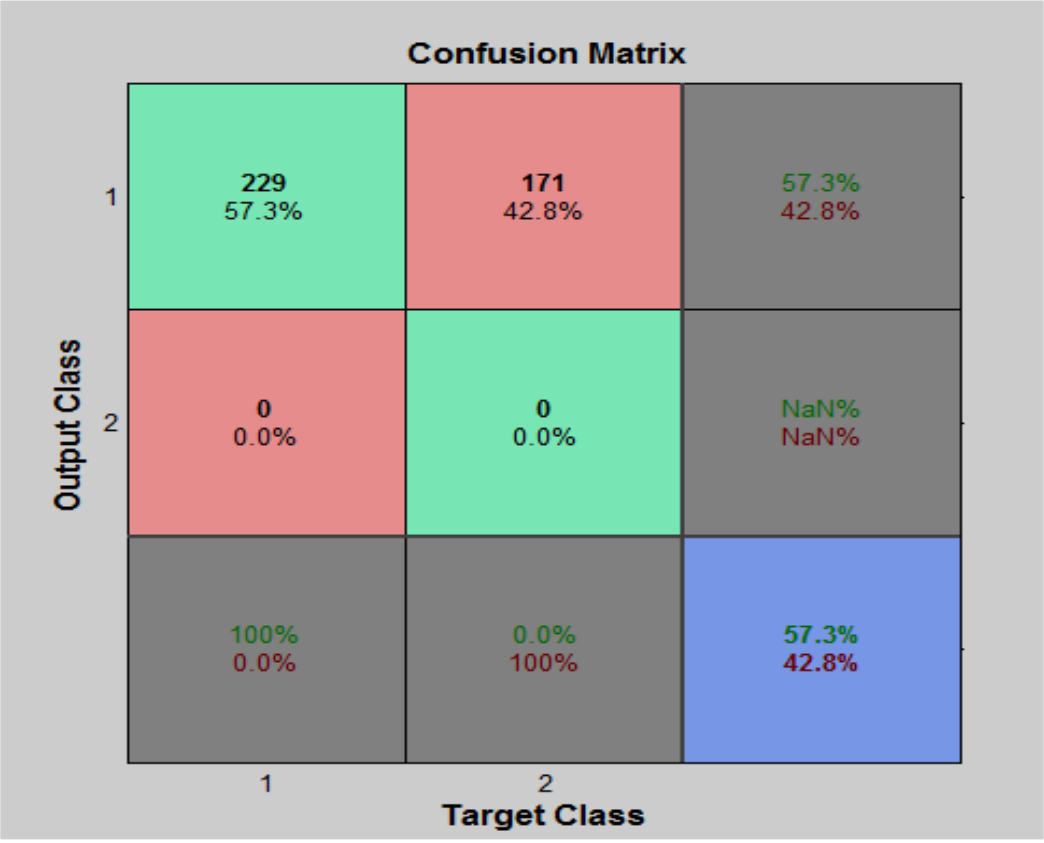

Table 4.1, the X axis represents the simulation result actual (target) class and the Y axis determines the predictive (output) class that was showed percentage error by histogram in figure 4.11. Histogram simply visualized those 400 breast cancer MIAS db, it was sorted plot of MIAS db into 20 equally spaced bins made a histogram.

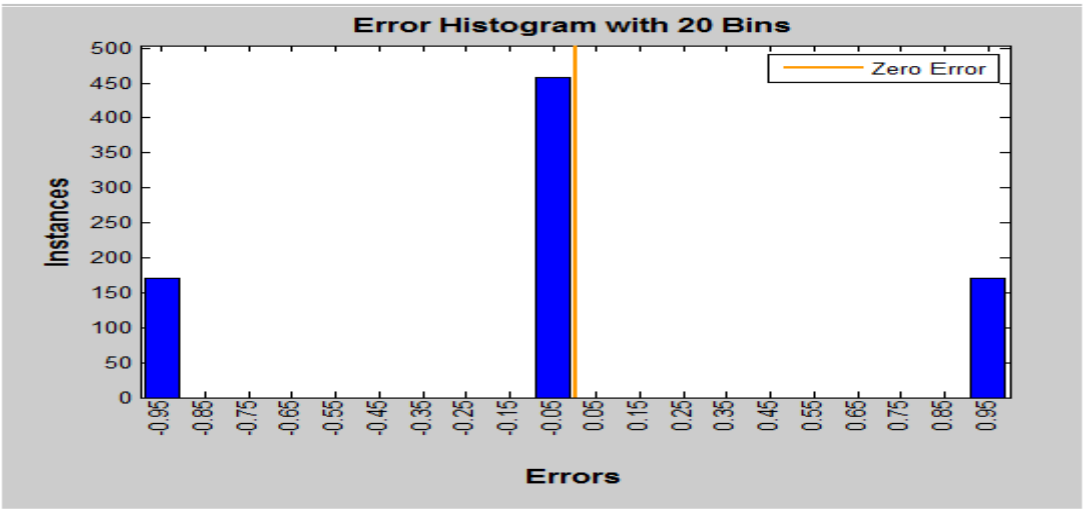

Figure 4. 11: Histogram error MIAS db for GRNN.

The X axis of the above graph represents the simulation result error in percentage and the Y axis showed the instances attributes MIAS db in GRNN. This graph showed the mean error GRNN for higher at the number of bins -0.96 and 0.96 error occurred around 175 instances. In this histogram sorts the values in MIAS db among 20 equally spaced bins between -0.96 and 0.96, the error values occurred at the number of bins -0.05.

The output simulation result for PNN presented table 4.2 the percentages of correct classification green squares on the matrices diagonal and incorrect the red squares classifications. As seen the table below the overall percentages of correct classification was 57.3% and incorrect classification 42.8% obtained.

Table 4. 2: confusion matrix for PNN.

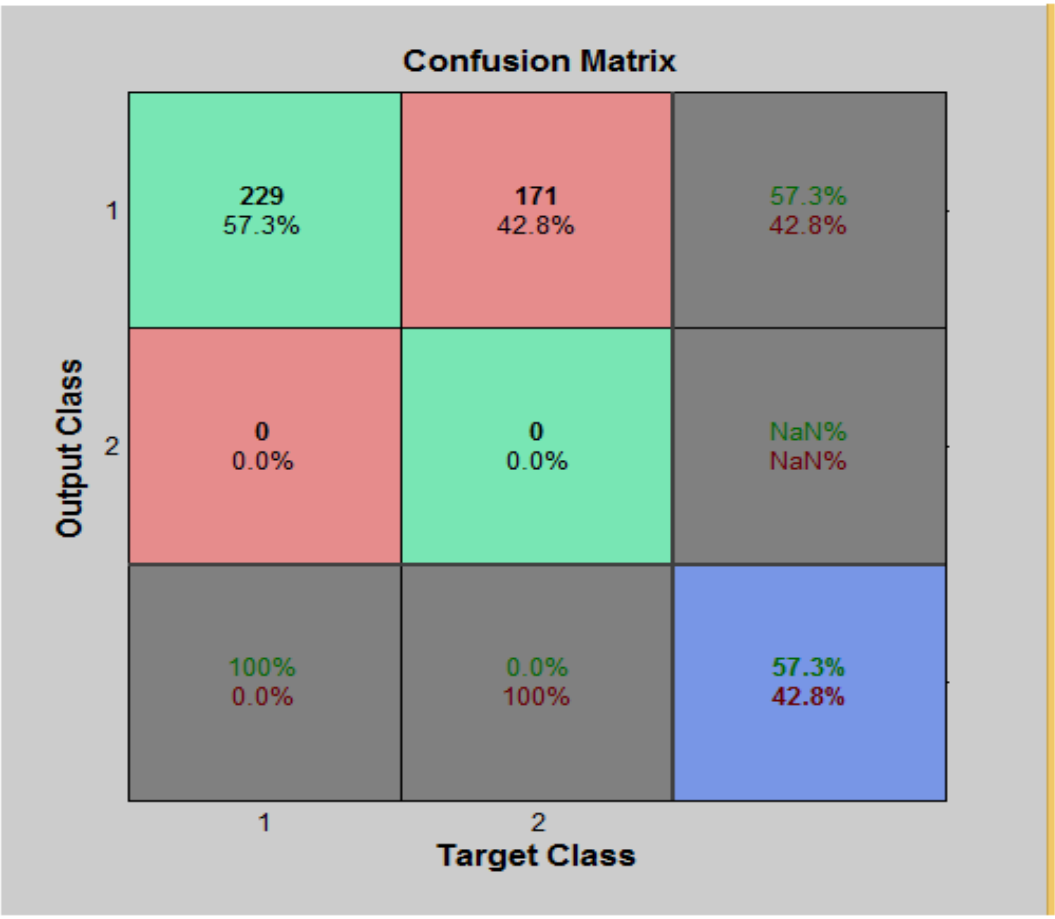

The X axis of the above table represents the simulation result actual (target) class and the Y axis determines the predictive (output) class that was showed percentage error by histogram below. Histogram simply visualized those 400 breast cancer MIAS db, it was sorted plot of MIAS db into 20 equally spaced bins made a histogram in PNN.

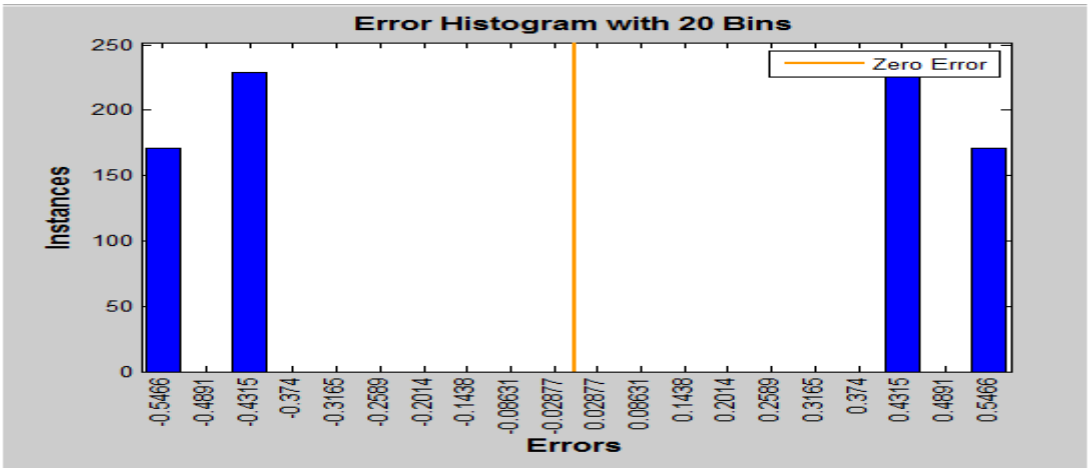

Figure 4. 12: Histogram error for PNN.

The X axis of the above graph represents the simulation error in percentage and the Y axis showed the instances attributes MIAS db in PNN. This graph showed the mean error PNN for higher at the number of bins 0-.4515 and 0.4515 error occurred around 175 instances. In this histogram sorts the values in MIAS db among 20 equally spaced bins between -0.5466 and 0.5466 the error values occurred.

The output simulation result for RBNN showed table 4.3 the percentages of correct classification green squares on the matrices diagonal and incorrect the red squares classifications. As seen table below the overall percentages of correct classification was 100% and incorrect classification 0% obtained.

Table 4. 3: Confusion matrix for RBF.

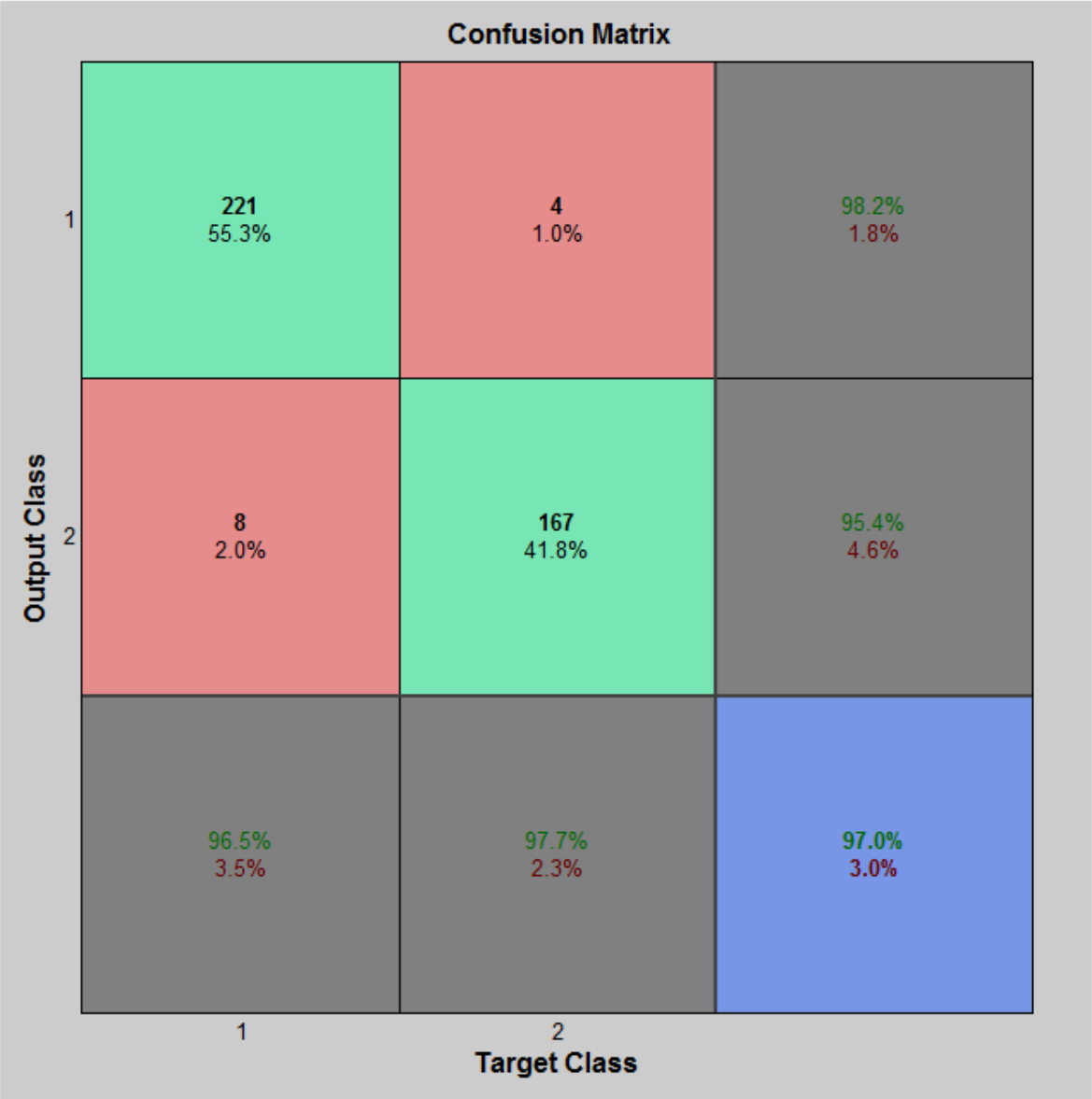

The X axis of the above table represents the simulation actual (target) class and the Y axis determines the predictive (output) class that was showed percentage error by histogram below. Histogram simply visualized these 400 breast cancer MIAS db it was sorted plot of data into 20 equally spaced bins made a histogram in RBF.

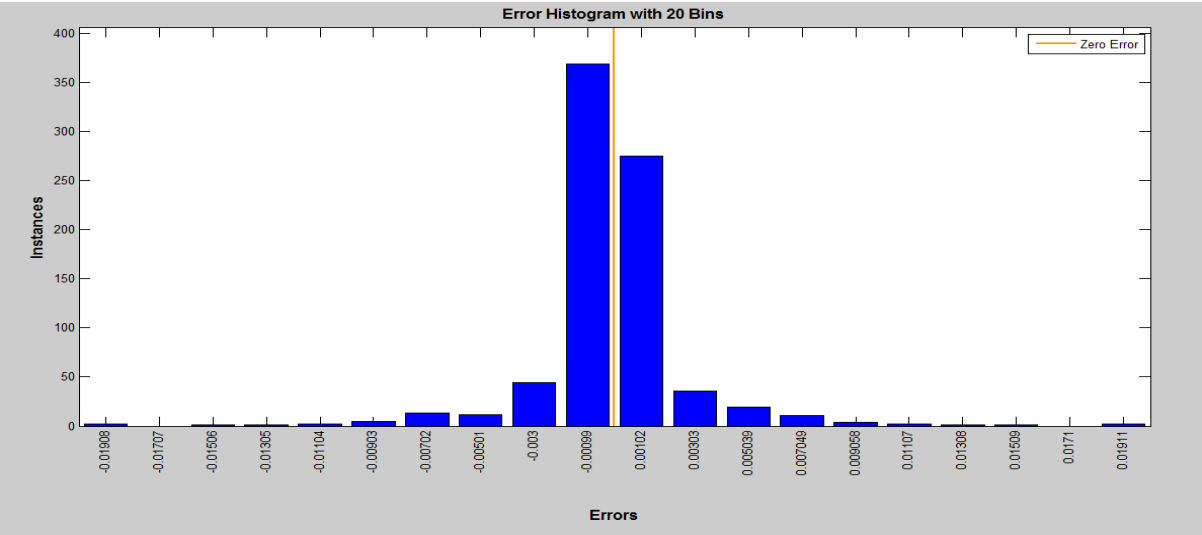

Figure 4. 13: Histogram error RBF.

The X axis of the above graph represents the simulation error in percentage and the Y axis showed the instances attributes data RBF. This graph shows the removed far from mean error RBF highest instances error occurred around zero.

The output of training set simulation results of comparison performance of test error for FFWNN, FFNN and PRNN by hold-validation and cross-validation given below respectively. The accuracy of classification was observed using ROC. Those outputs result analyzed the error and accuracy from the following figures.

The output simulation results of comparison performance by hold-validation for FFWNN was at 8 epochs given below.

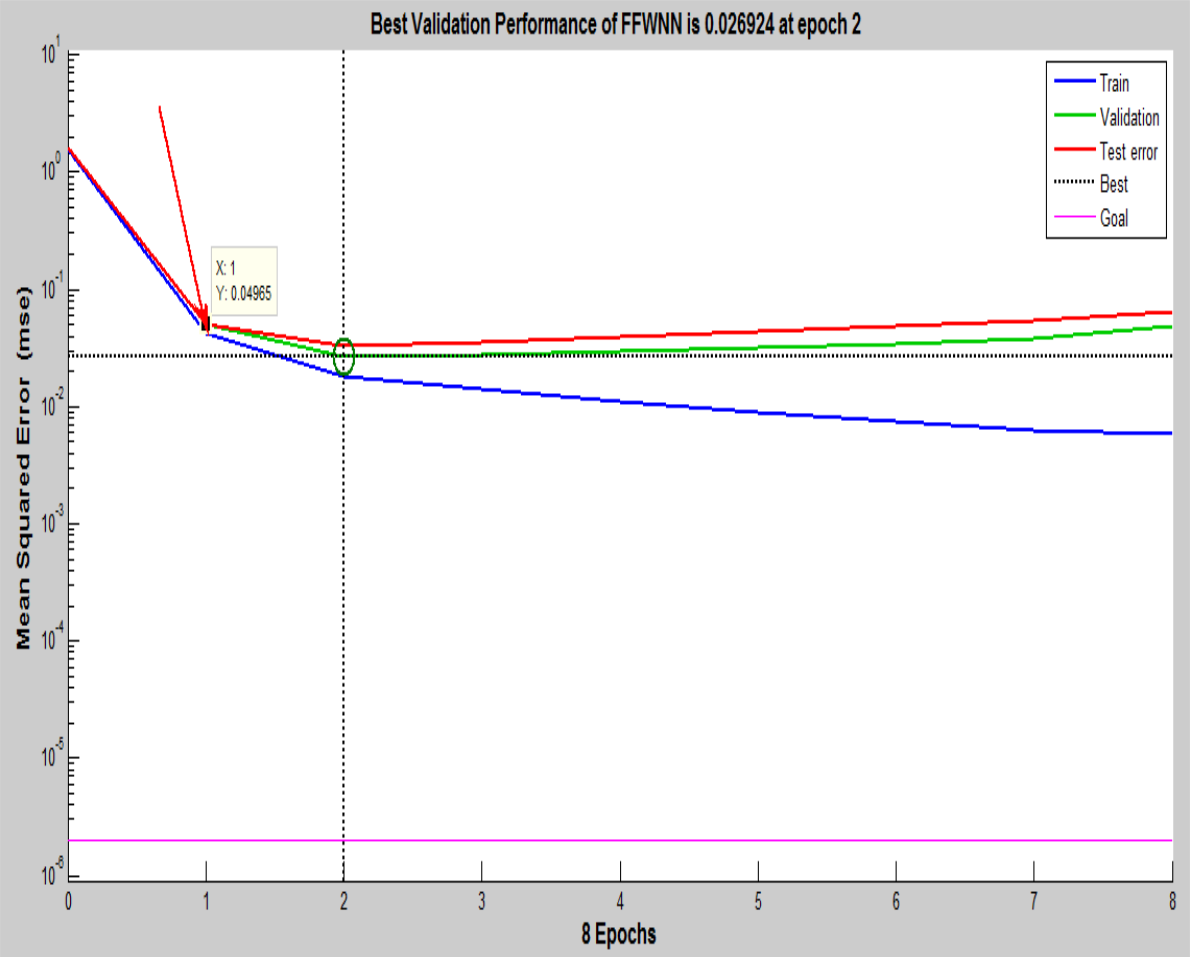

Figure 4. 14: Comparison of performance for hold-validation of FFWNN.

The X axis of the above graph represents the simulation result iteration (epochs) and Y axis determines mean squared error (MSE). A set of MIAS db observations were randomly split into training (as showed in red), validation set (showed in blue) and test set (showed in cyan). This graph showed test error at began quite biggest when epoch increase error linearly decreased extent epoch one (1) and after that test error did not gotten much degrade error. The best validation error performance of FFWNN was 0.02692 at epochs 2. Those were crossing best at 2 epochs and the statistic of this test error was giving in the table 4.5.

The output simulation results of comparison fit by cross-validation for FFWNN given below.

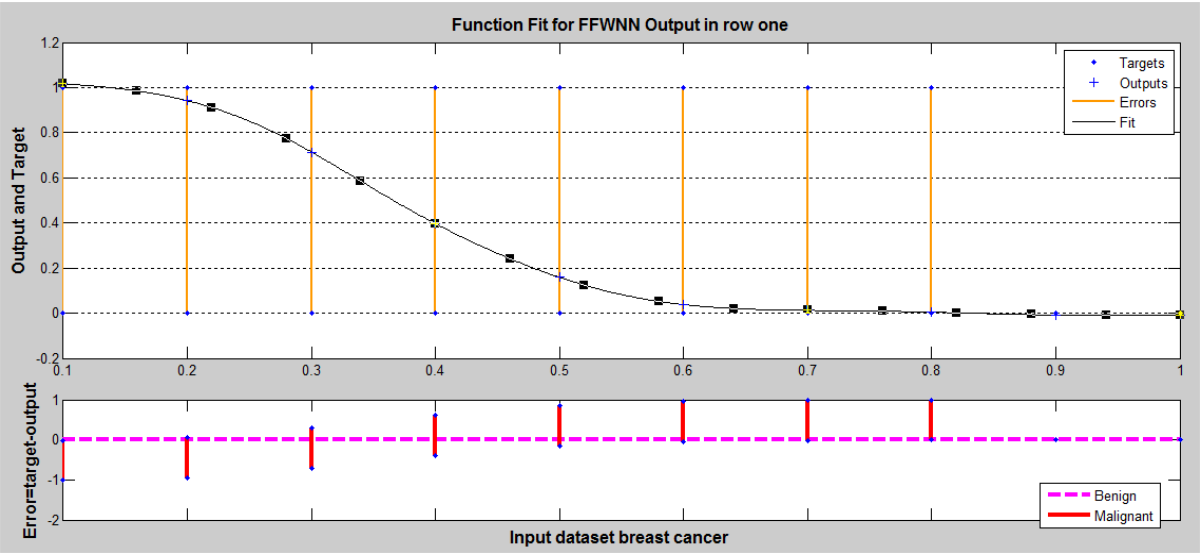

Figure 4. 15: Comparison of performance for cross-validation of FFWNN.

The X axis of the above graph represents the simulation input breast cancer MIAS db and Y axis output and target. A set of MIAS db observations were error (as showed in [1 0.84 0 (yellow)]), output (showed +), target (showed *) and fit (as showed in black). From above graph it can be observed that at the beginning, the fit decreased extremely extent 0.8. After that fit was approach to zero error due to low variation between target and output.

The output simulation results of comparison ROC by cross-validation for FFWNN given below.

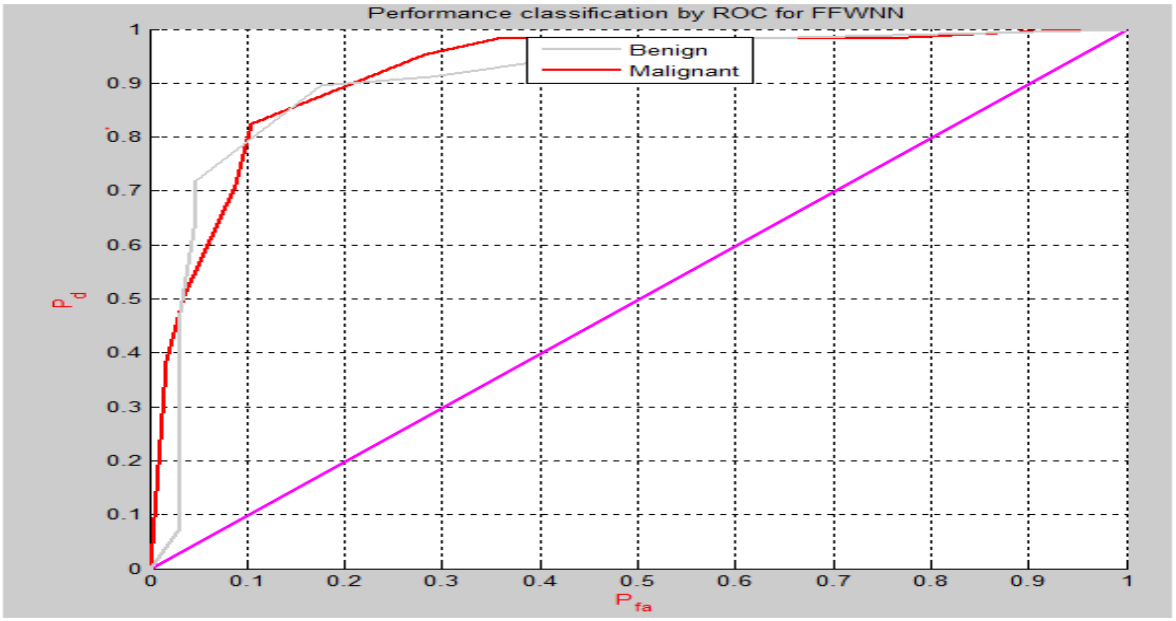

Figure 4. 16: Comparison of performance accuracy for ROC of FFWNN.

The X axis of the above graph represents the simulation detection probabilities corresponding to the false-alarm probabilities (P_d) rate and Y false-alarm probabilities in a row (P_{fa}). As seen from graph the ROC curves a detector's performance above threshold (diagonal at 0.5) the quality of classify was high. A set of MIAS db observations were benign (as showed in [0. 8 0.8 0.8]), malignant (showed red) as seen benign more accuracy than malignant because the benign graph more approach to true positive rate curve.

The output simulation result of comparison performance by hold-validation for FFNN was at 10 epochs given below.

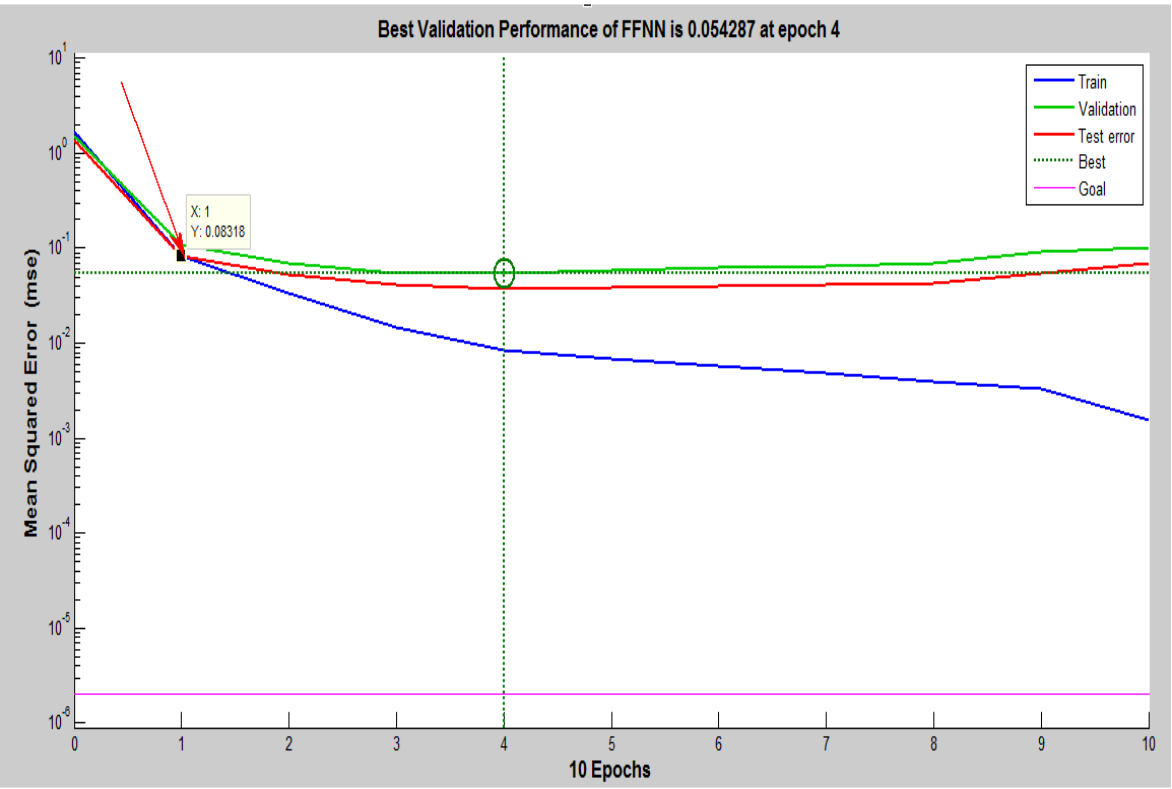

Figure 4. 17: Comparison of performance for hold-validation of FFNN

The X axis of the above graph represents the simulation result iteration (epochs) and Y axis determines mean squared (MSE). A set of MIAS db observations were randomly split into training (as showed in red), validation set (showed in blue) and test set (showed in cyan). This graph showed test error at began quite biggest when epoch increase error linearly decreased extent epoch one (1) and after that test error did not gotten much degrade error. The best validation error performance of FFNN was 0.054287 at epochs 4. Those were crossing best at 4 epochs and the statistic of this test error was giving in the table 4.5.

The output simulation results of comparison fit by cross-validation for FFNN given below.

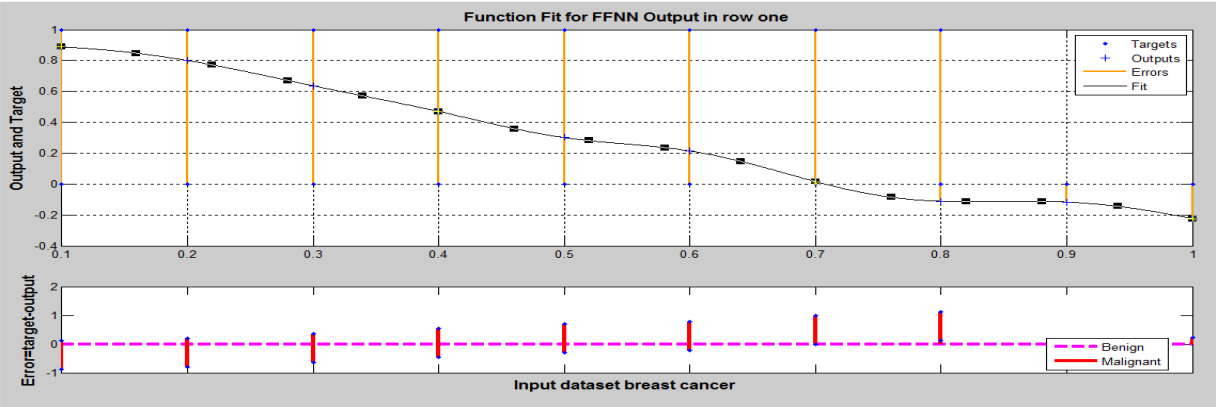

Figure 4. 18: Comparison of performance for cross-validation of FFNN

The X axis of the above graph represents the simulation input breast cancer MIAS db and Y axis output and target. A set of MIAS db observations were error (as showed in [1 0.84 0 (yellow)]), output (showed +), target (showed *) and fit (as showed in black). From above graph it can be observed that at the beginning, the fit decreased extremely extent 0.7. After that the fit was below zero due to the predicted value (output) greater than target value.

The output simulation results of comparison ROC by cross-validation for FFWNN given below.

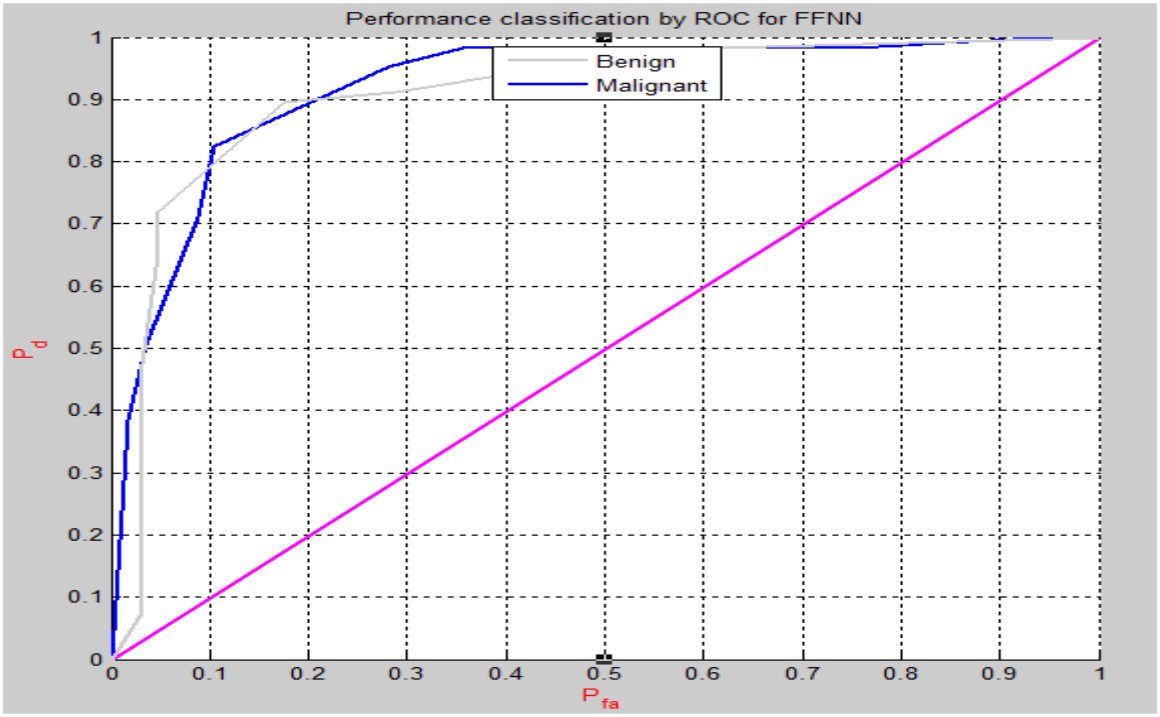

Figure 4. 19: Comparison of performance accuracy for ROC of FFNN.

The X axis of the above graph represents the simulation detection probabilities corresponding to the false-alarm probabilities (Pd) rate and Y false-alarm probabilities in a row (Pfa). As seen from graph the ROC curves a detector's performance above threshold (diagonal at 0.5) the quality of classify was high. A set of MIAS db observations were benign (as showed in [0.8 0.8 0.8]), malignant (showed blue) as seen at the beginning malignant more accuracy than benign because the malignant graph more approach to true positive rate curve but at the end benign more accuracy than the malignant as figure 3.11 observed the relation accuracy curve.

The output simulation result of comparison performance by hold-validation for PRNN at 36 epochs given below.

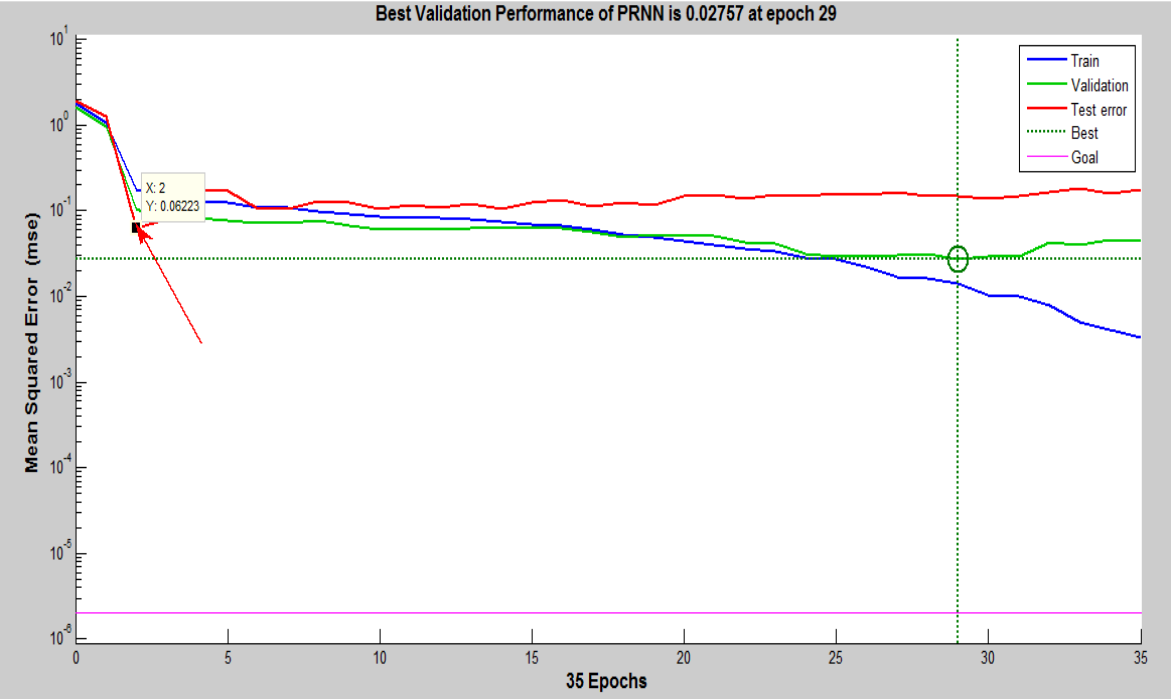

Figure 4. 20: Comparison of performance for hold-validation of PRNN.

The X axis of the above graph represents the simulation result iteration (epochs) and Y axis determines mean squared (MSE). A set of MIAS db observations were randomly split into test error (as showed in red), validation set (showed in blue) and training set (showed in cyan). This graph showed test error at began quite biggest when epoch increase error linearly decreased extent epoch two (2) and after that test error did not gotten much degrade it. The best validation error performance of PRNN was 0.02757 at epochs 29. Those were crossing best at 29 epochs and the statistic of this test error was giving in the table 4.5.

The output simulation results of comparison fit by cross-validation for PRNN given below.

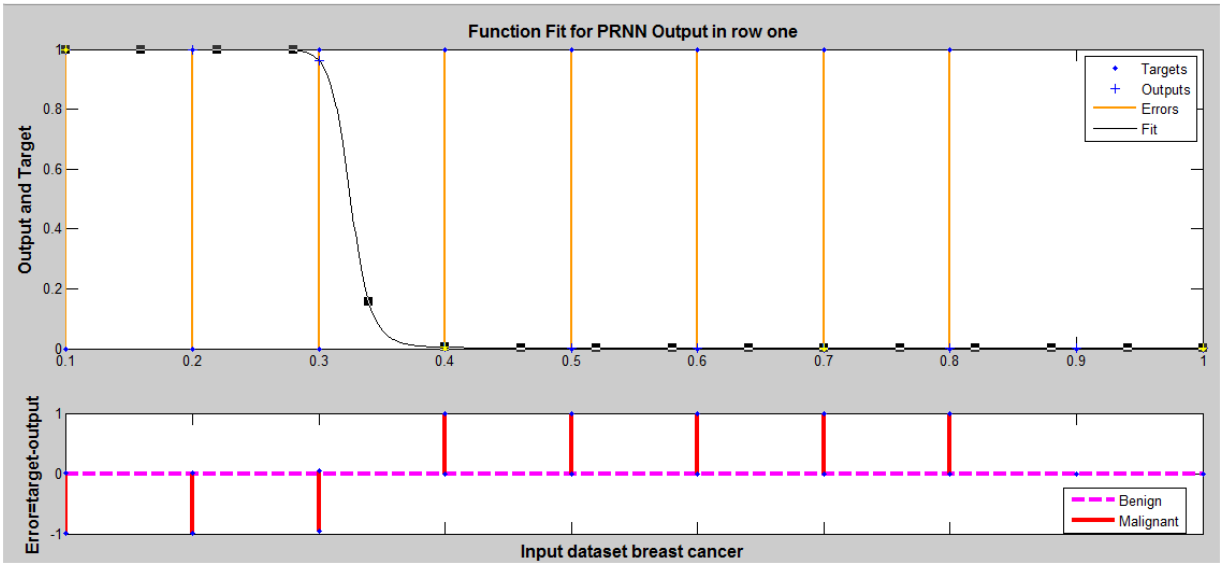

Figure 4. 21: Comparison of performance for cross-validation of PRNN.

The X axis of the above graph represents the simulation input breast cancer MIAS db and Y axis output and target. A set of MIAS db observations were error (as showed in [1 0.84 0 (yellow)]), output (showed +), target (showed *) and fit (as showed in black). From above graph it can be observed that at began to 0.3 input MIAS db fit was highest value this reason target value was one where output value was zero. From 0.3 to 0.4 fit extremely decreased in case of target value and output value altered. After that fit was approach to zero error due to low variation between target and output.

The output simulation results of ROC by cross-validation for FFWNN given below.

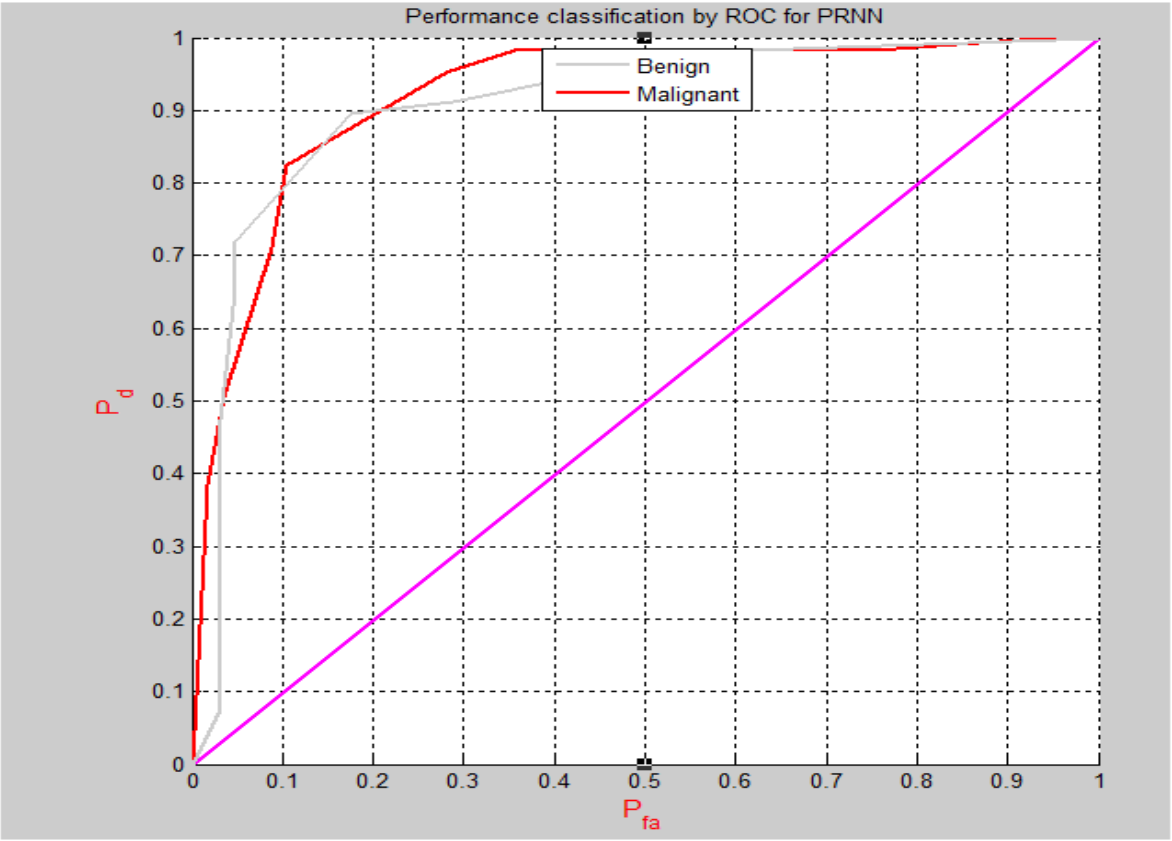

Figure 4. 22: Comparison of performance accuracy for ROC of PRNN.

The X axis of the above graph represents the simulation detection probabilities corresponding to the false-alarm probabilities (Pd) rate and Y false-alarm probabilities in a row (Pfa). As seen from graph the ROC curves a detector's performance above threshold (diagonal at 0.5) the quality of classify was high. A set of MIAS db observations were benign (as showed in [0.8 0.8 0.8]), malignant (showed red) as seen at the beginning malignant more accuracy than benign because the malignant graph more approach to true positive rate curve but at the end benign more accuracy than the malignant as figure 3.11 observed the relation accuracy curve. The ROC of PRNN over crossing benign and malignant less when compered ROC of FFNN, which means the predicted class in PRNN more accuracy than in FFNN and the statistic of this test error was giving in the table 4.5.

The output simulation result for LLRBFNN provides reduced error showed figure below. From figure 4.23 the Y axis of represents the simulation result error in number and the X

axis showed the number of iteration of LLRBNN. RMS performance of LLRBFNN is 0.0013 at iteration 67.

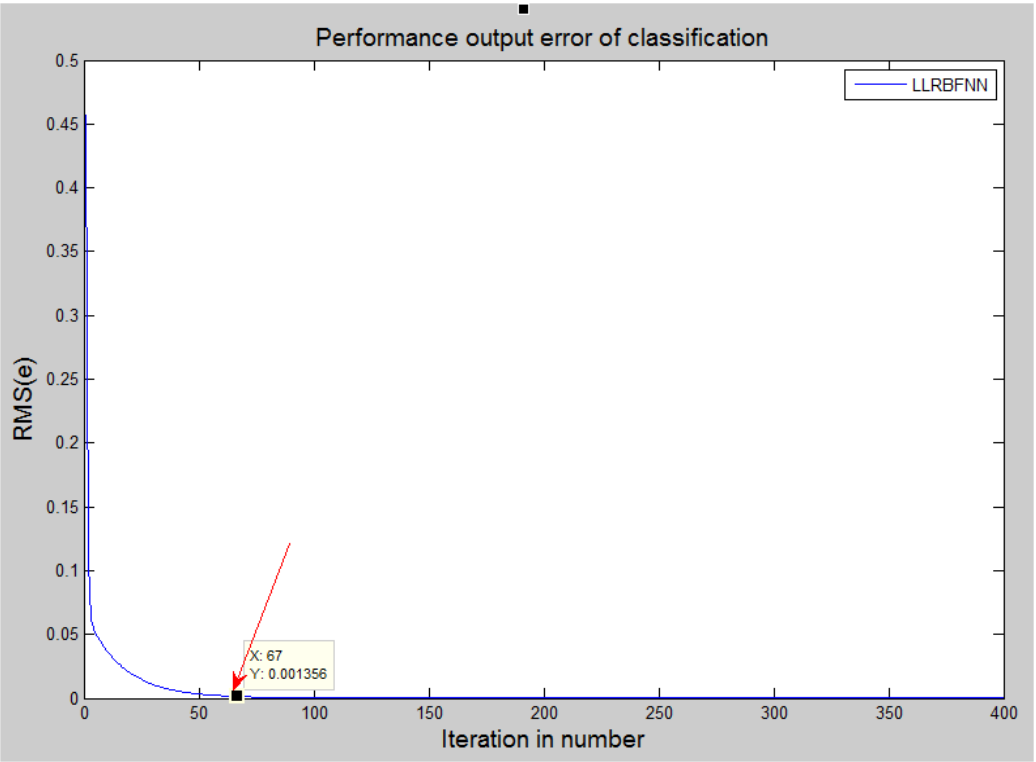

Figure 4. 23 : LLRBFNN methods measured MSE for classification.

The output simulation results of the overall designed for classification the combination of RBFNN, FFNN, and PRNN were obtained from MATLAB simulation showed figure 4.24 that observed LLRBFNN provides better classification performance among the others. From simulation results it is very difficult to separate the error of LLRBFNN and PRNN at minimum database. In order to distinguish that errors large dataset was used. At large dataset it was observed that the error of LLRBFNN is easily converged approach to zero than PRNN.

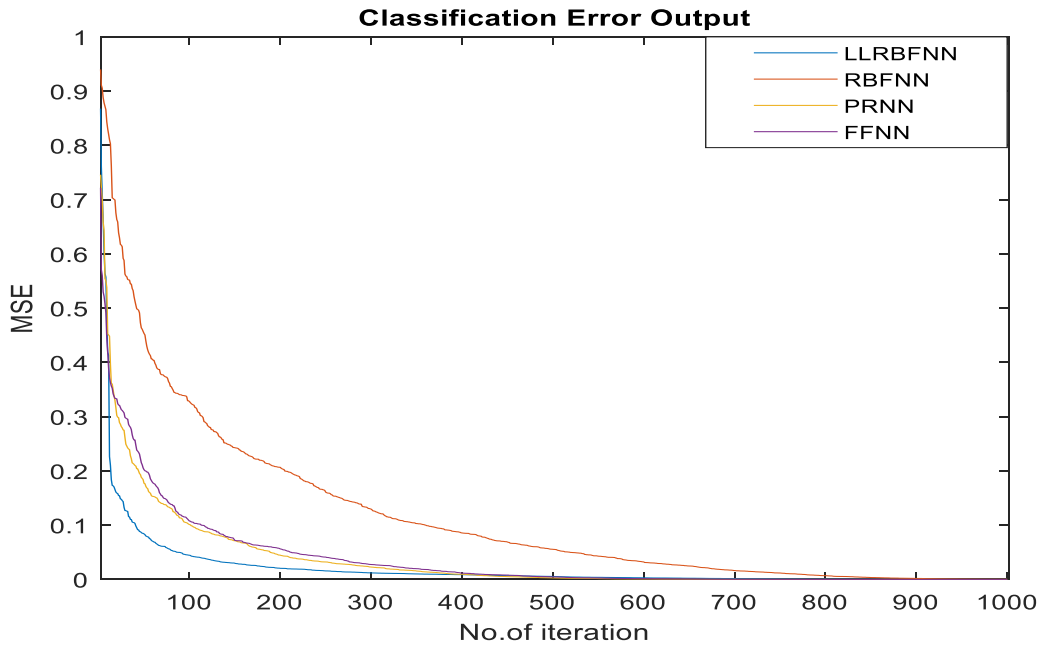

Figure 4. 24: Comparison of different methods measured MSE for classification.

The X axis of this graph represents the simulation number of iteration and the Y axis demonstrates the MSE in percent. The proposed LLRBFNN graph was the blue line, steadily approaching convergence at 500 iterations. Whereas graphs were the red, yellow and magenta lines, steadily approaching convergence at 550,560 and 950 iterations respectively. The statistic of this parameters is given in the table 4.5.

The output simulation result K-mean clustering for detection and classification showed below graph. Those graphs clearly detected and classified the two tumor.

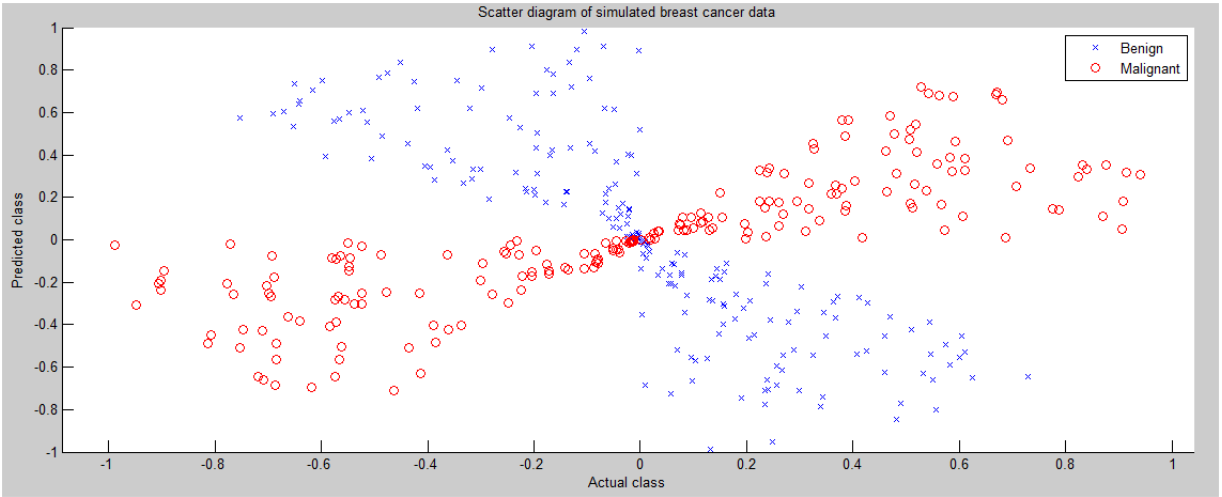

Figure 4. 25: classified actual without centroid.

The X axis of the above graph represents the simulation actual class and Y axis determines predicted class. This graph shows the groups of instances (data points) into the representation space which no centroid and nonlinear.

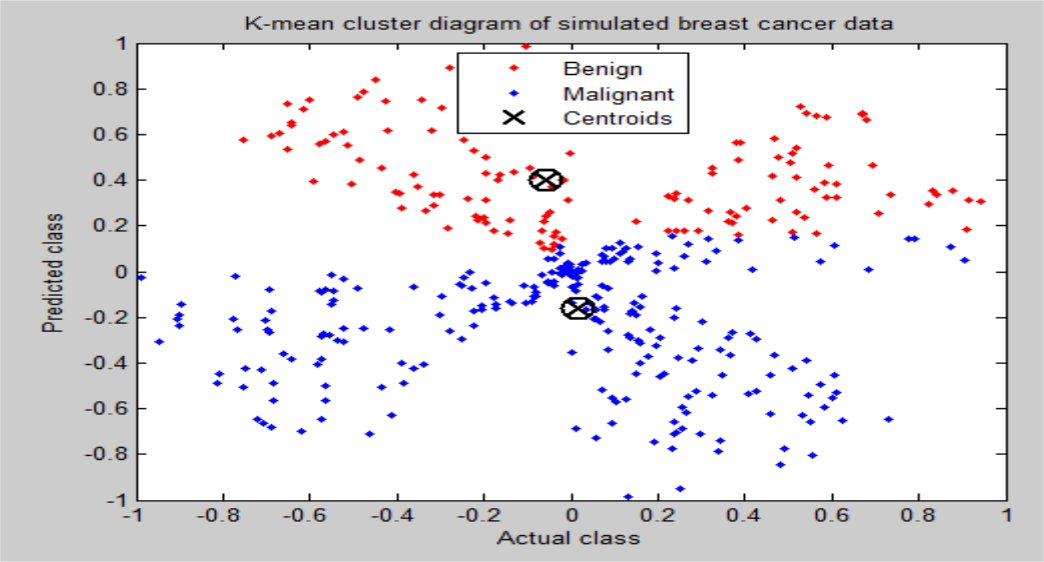

Figure 4. 26: classified actual with centroids.

The X axis of the above graph represents the simulation actual class and Y axis determines predicted class. This graph shows the groups of instances (data points) into the representation space which contained centroid and identified the groups (clusters) which were significantly different (distant) from each other.

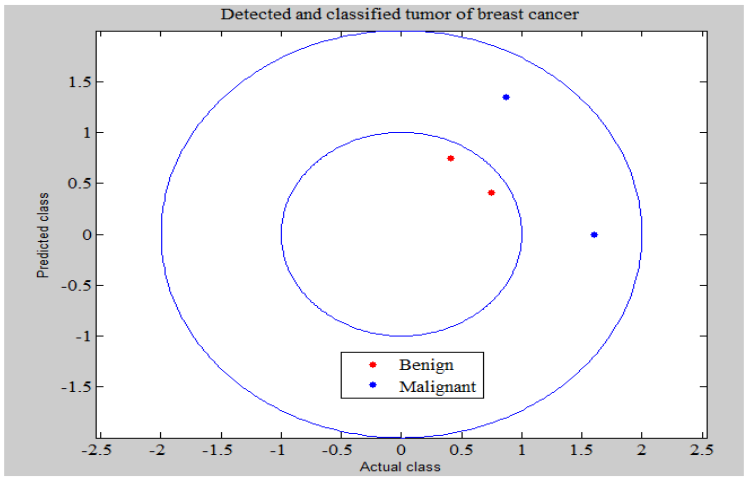

Figure 4. 27: Detected and classified type of breast cancer.

The X axis of the above graph represents the simulation actual class and Y axis determines predicted class. From the above circle, observed that malignant separated from benign and

segmented in specific place. In this simulation paper, breast cancer clearly detected and classified in two tumor that was answered the statement problem in section 1.2.

Table 4. 4: Statistics for detection.

For benign tumor						
Parameters	Contrast	Correlation	Entropy	Homogeneity	Mean	STD
Results	0.3017	0.1718	2.8777	0.9461	0.0045	0.0897
Parameters	Variance	Smoothness	Kurtosis	skewness	RMS	IDM
Results	0.0081	0.9432	14.6858	1.2732	0.0898	0.4217
For malignant tumor						
Parameters	Contrast	Correlation	Entropy	Homogeneity	Mean	STD
Results	0.3017	0.1718	3.0100	0.9358	0.0035	0.0897
Parameters	Variance	Smoothness	Kurtosis	skewness	RMS	IDM
Results	0.0080	0.9284	9.1671	0.7342	0.0898	1.2596

Table 4. 5: Statistics for classification.

Neural network scheme	Parameters (%)	Hidden layer (N)		
		N =20	N = 40	N = 60
GRNN	MSE	0.427	0.427	0.427
	net error	0.683	0.683	0.683
	Accuracy	96.667	98.333	96.667
PNN	MSE	0.428	0.428	0.428
	net error	15.409	15.409	15.409
	Accuracy	98.333	96.667	96.667
RBFNN	MSE	0.030	0.030	0.030
	net error	0.0876	0.876	0.876
	Accuracy	95	98.333	96.667
Training validation		Hold-validation	Cross-validation	

scheme			
N = 40			
FFWNN	MSE	3.70	1.86
	Test error	0.0381	0.032
	Accuracy	97.145	98.095
FFNN	MSE	1.83	1.9
	Test error	0.046	0.0455
	Accuracy	97.145	98.968
PRNN	MSE	0.99	0.99
	Test error	0.029	0.051
	Accuracy	98.095	99.045
Hidden neuron(N) =1			
LLRBFNN	MSE	0.130	0.130
	Accuracy	99.020	99.307

Table 4. 6: Comparison of accuracy in different methods for previous and this paper.

Previous Methods	Reference	Previous accuracy (%)	In this research work Methods	This research work of accuracy (%) consider only cross validation
K-Means clustering algorithm	[44]	99%	LLRBFNN	99.307
SVM	[25]	95.5	PRNN	99.045
KNN	[25]	71.83	FFNN	99.045
PNN	[31]	92.5	RBFNN	98.33

4.2. Discussion

As experienced from the result on graphs it can be seen that figure 4.7 and figure 4.8 detect screen mammogram image can be seen by adaptive mean filter and new fuzzy level set method to performs smoothest and segment exact tumor respectively. For classification design of LLRBFNN reduce error best among the others as observed figure 4.24. Among training set methods PRNN training performs best accuracy among the other as observed table 4.5. In this research works performance of different parameters have been considered.

All parameters in detection schemes are used to measure the enhancement of mammogram image by removing noise, edge detection, increase smoothing image, minimize the variation neighboring pixels and increase contrast image.

RMS and MSE are the key parameters to measure the performance of the error breast cancer for detection and classification correspondingly. Network error (net error) is also one of the parameter which measure the error at each net neural network that error is vary based on bias. Bias is an important factor which has a great impact on the radial basis function. Radial basis function becomes high if the bias is small. Another cause of radial basis function is disparity of output configuration distance between input and weights. It is possible to reduce error with adjust radial basis function by taking bias value above 0.9.

The main factor of parameter is accuracy which has great impact on the true positive rate and false positive rate predict to classify tumor based on the range of ROC. Its range always found in $0.5<ROC<1$ because the probability outcome is 0.5. The accuracy degrades when either benign or malignant or both graph come under the curve area of the ROC and accuracy is high when both benign and malignant graphs increase above area ROC.

Test error is best parameters among training scheme which has great impact on the breast cancer MIAS db classification. To illustrate the variability of estimated MSE of results. Test error becomes decrease if breast MIAS db is linear and other case of test error is nonlinear from second degree polynomial to the end of epochs. It is possible to reduce the MSE by converting nonlinear breast MIAS db to the linear with the help of local linear radial basis function. In other case it is potential to satisfy for reliable test error in terms of minimizing MSE by deploying the proper cross-validation scheme. However, in hold-out validation scheme difficult to reduce error because a huge MIAS db randomly classify while cross-validation scheme spilt small MIAS db that is useful for classification MIAS db.

In order to measure the statistics, few detection and classification have been considered for different types of breast cancer. In order to manifest the statistics of the simulation in terms of different parameters for both scheme are providing in table (4.4 and 4.5).

CHAPTER 5

CONCLUSION AND RECOMMENDATION

5.1. Conclusion

The classification of breast cancer is a complex and difficult task. This research work proposes a novel LLRBFNN classification model for breast cancer classification. The images are decomposed using fuzzy level set rule segmentation. For detection of breast cancer areas, adaptive mean filter is employed to have better smooth image than median filter, as it is preserving edges and other parts of an image, hence enhanced the mammogram image. In order to classify breast tumor clearly mammogram image required LLRBFNN.

LLRBFNN has been proposed to increase the accuracy of breast cancer classification, as it is potential to take proper initiative in different levels of hidden layer and spread of radial basis functions implementation. Appropriate parameters use in the neural network can be one of the ways to improve the accuracy of classification. For proper parameters of classification, accuracy management should be considered for each neural network. The K-mean clustering has also been considered for classification. It can support the cluster by minimizing distance of the centroids. In the case of nonlinear distance between benign and malignant it's difficult to separate one from the other with k- mean cluster only. So to overcome this barrier LLRBFNN can play an effective role by converting nonlinear to linear and split the pass overhead in the two tumor using k-mean cluster.

The PRNN has better accuracy among training neural network due to reduction of the false negative and false positive predicted class as well as improve true positive and true negative predicted class of breast cancer MIAS db. The features are extracted using the GLCM scheme and fed as input to the proposed model. The FFNN, FFWNN, PRNN also has been taken into consideration and the classification results are shown in the results section. The accuracy of LLRBFNN has better among other neural network which is presented in the result section along with the comparison results of the other mentioned methods. As observed from table 4.5 that when the number of hidden layer decreases, the error also decreases and the accuracy increases. The key existing parameters such as MSE, test error, accuracy and RMS in mammogram image classification has been presented.

With this experimental results, it can be concluded that the performance of detection and classification achieved by LLRBFNN for mammogram image is superior to the PRNN and FFNN method.

5.2. Recommendation

The mammogram is the common platform for all other technologies to interact properly. In order to make efficient services for the patient, it is important to design a common classification scheme for the common platform. This research works recommend to design a new model of common classification scheme that include young people to improve the overall service for the breast cancer.

MATLAB is corporate platform software for many methods recognizing its library methods for working simulation known. In order to make efficient task for the design of LLRBFNN classification method, it is significant to design a common classification scheme for the common platform. This research works recommend that, if MATLAB will recognize LLRBFNN method as model based calibration toolbox design a new model of common classification scheme; the accuracy of the breast cancer classification will be develop.

References

[1] A.F.S. Tahmasbi, "Classification of benign and malignant masses based on Zernike noments.," in Computers in biology and medicine , 2011, pp. 726-735.

[2] A.Jalalian, S. Mashohor, B. Mahmud, H. R., Saripan, M. I. B. Ramli, A. R. B. & Karasfi, "Computer-aided detection/diagnosis of breast cancer in mammography and ultrasound," A review Clinical imaging, vol. 3, pp. 420-426, 2013.

[3] A.M.Fadzilah.,"Web-Based Neurofuzzy Classification for Breast Cancer,"in Proceedings Second International Conference on Artificial Intelligence in Engineering &Technology, Sabah, 3rd-4th, 2004

[4] B. Sahiner, C. Heang-Ping, N. Patrick, D. M. A. Wei, D. Helie, D. Adler, And M.M., "Classification of Mass and Normal Breast Tissue: A Convolution Neural Network Classifier with Spatial Domain and Texture Images," IEEE Transactions on Medical Imaging, vol. 15, no. 5, pp. 598- 610, 1996.

[5] C. M. Chen, Y. H. Chou, K. C. Han, G. S. Hung, C. M. Tiu, H. J. Chiou, S. Y. Chiou., "Breast Lesions on Sonograms: Computer Aided Diagnosis with Nearly Setting-Independent features and Artificial Neural Networks," Radiology, vol. 226, pp. 504-514, 2003.

[6] D. B. Burke, "Comparing Artificial Neural Networks to other Statistical Methods for Medical outcome Prediction," IEEE World Congress, vol. 4, pp. 2213-2216, 1994.

[7] F. E. Ahmed, "Artificial Neural Networks for Diagnosis and Survival Prediction in Colon Cancer," Molecular Cancer, vol. 4, p. 29, 2005.

[8] G. Karthikeyan, "Automated diagnosis of mammogram images of breast cancer using discrete wavelet transform and spherical wavelet transform features: a comparative study," 3, 2014, pp. 605-615.

[9] G. Karthikeyan, "Computer-aided breast cancer detection using mammograms: a review," in IEEE Reviews in biomedical engineering, 6, 2013, pp. 77-98.

G. Schwarzer, W. Vach, M. Schumacher, "On the Misuses of Artificial Neural
[10] Networks for Prognostic and Diagnostic Classification in Oncology," Statistics in Medicine, vol. 19, pp. 541-561, 2005.

[11] H. B. Burke, P. H. Goodman, D. B. Rosen, . E. Henson, J. N. Weinstein, F. E. Harrell, J. J. R. Marks, D. P. Winchester, D. G. Bostwick, "Artificial Neural Networks Improve the Accuracy of Cancer Survival Prediction," cancer, vol. 79, pp. 857-862, 1997.

[12] H. Cheng and X. Shi, "Approaches for automated detection and classification of masses in mammograms," Pattern Recognition, vol. 4, 2006.

[13] H. Vazirani, R. Kala, A. Shukla and R. Tiwari, "Diagnosis of Breast Cancer by Modular Neural Network.," in Proceedings 3rd IEEE International Conference on Computer Science and Information Technology, Chengdu, 9th-11th July IEEE, 2010, pp. 115-119.

[14] http://www.wcrf.org/, "Cancer_statistics/world_cancer_statistics.php," in World Health Organization, 2018.

[15] I.K. Maitra, "Technique forpreprocessingof digital mammogram," in Computer methods and programs in biomedicine, 2012, pp. 175-188.

[16] J. A. Jaleel and S. Salim, "Mammogram mass classification based on discrete wavelet transform textural features," in Advances in Computing, Communications and Informatics IEEE International Conference on ICACCI, 2014, pp. 718-722.

[17] J. Du and L.Wang,"Differentiating benign from malignant solid breast lesions: combined utility of conventional ultrasound and contrast enhanced ultrasound in comparison with magnetic resonance imaging.," European journal of radiology, pp. 3890-3899, 2012.

[18] K.Ganesan, "Automated diagnosis of mammogram images of breast cancer using discrete wavelet transform and spherical wavelet transform features: a comparative study," 3, 2014, pp. 605-615.

[19] K. Ganesan, "Computer-aided breast cancer detection using mammograms: a review.," in IEEE Reviews in biomedical engineering , 6, 2013.

[20] L. d. O. Martins and A. M. d. Santos, "Classification of normal, benign and malignant tissues using co-occurrence matrix and Bayesian neural network in mammographic images," in Neural Networks, IEEE Proceedings of the Ninth Brazilian Symposium on SBRN, 6, 2006, pp. 24-29.

[21] M. Ashraf, L. Kim and H. Xu, "Information Gain and Adaptive Neuro-Fuzzy Inference System for Breast Cancer Diagnoses.," in Proceedings Computer Sciences Convergence Information Technology , Seoul, 2nd edition, 2010, pp. 911-915.

[22] M. M. Eltoukhy and I. Faye, "An Optimized Feature Selection Method For Breast Cancer Diagnosis in Digital Mammogram using Multiresolution Representation," Applied Mathematics & Information Sciences, pp. 2921-2928, 2014.

[23] M. S. Salve, "Classification of Mammographic images using Gabor Wavelet and Discrete Wavelet Transform," International Journal of advanced research inECE ISSN, pp. 573-578, 2013.

[24] N. Vállez and G. Bueno, "Breast density classification to reduce false positives in CADe systems," in Computer methods and programs in biomedicine, 2014, pp. 569-584.

[25] Neeta Jog, Arvind Pandey, "Implementation of Segmentation and Classification Techniques for Mammogram Images," IOSR Journal of Engineering (IOSRJEN), vol. 05, no. 02, February. 2015.

[26] Online,Top 10 Female Cancer in Addis Ababa," Membership/membership-list/100-addisababa. [Online]. [Accessed 21 Apr 2017].

[27] P.K.Dash, M.R.Senapati, “Intelligent Systems Based on Local Linear Wavelet Neural Network and Recursive Least Square Approach for Breast Cancer Classification”, Artificial Intelligence and Review, Springer, ISSN 0269-2821. vol 39, issue 2, pp 151-163, February 2013, DOI: 10.1007/s10462-011-9263-5.

[28] P.K.Dash, M.R.Senapati and I.Vijaya “Rule Extraction by Training Radial Basis Functional Neural Network with Particle Swarm Optimization” published in American Journal of Science, Science Publication, ISSN: 1549-3636, vol 3, issue 8, pp.592-599,2007

[29] S. A. N. Hazlina H., "Back Propagation Neural Network for the Prognosis of Breast Cancer: Comparison on Different Training Algorithms," in Proceedings Second International Conference on Artificial Intelligence in Engineering & Technology , Sabah, 3rd edition, 2004, pp. 445-449.

[30] S.B. Shanthi, A novel approach for classification of abnormalitiesin digitized mammograms., Sadhana: part 5, 2014.

[31] S. Deepa, Dr.V.Subbiah Bharathi, "Textural Feature Extraction and Classification of Mammogram Images using CCCM and PNN," IOSR Journal of Computer Engineering (IOSR-JCE), vol. Volume 10, no. 6, May. -Jun. 2013.

[32] S. Mojarad, S. Dlay, W. Woo and G. Sherbet, "Breast Cancer prediction and cross validation using multilayer perceptron neural networks.,"in Proceedings 7th Communication Systems Networks and Digital Signal Processing, Newcastle, 21st-23rd July IEEE , 2010, pp. 760-674.

[33] S. Muralaand and J. Wu, Local Mesh Patterns Versus Local Binary Patterns: Biomedical Image Indexing and Retrieval, 2014.

[34] S. N. Mishra, A. Patra, S. Das, M. R. Senapati , "An adaptive local linear optimized radial basis functional neural network model for financial time series prediction" Neural Computing and Applications, vol.28, Issue 1, January 2017,Pages101-110, doi:10.1007/s00521-015-2039-0.

[35] T. Kiyan & T. Yildirim, "Breast Cancer Diagnosis Using Statistical Neural Networks," Journal of Electrical & Electronics Engineering, vol. 4, no. 2, pp. 1149-1153, 2004.
Tomasi, C., Manduchi, R, "Bilateral filtering for gray and color images," in Proceedings of the ICCV, India, 1998, pp. 839-846.

[36] Varela C., Timp S., and Karssemeijer N,"Use of border information in the classification of mammographic masses," in Med. Biol, 2006, pp. 31-51/9155/.

[37] V. Chakkarwar and M. S. Salve, "Classification of Mammographic images using Gabor Wavelet and Discrete Wavelet Transform," International Journal of advanced research in ECE ISSN, pp. 573-578, 2013.

[38] W. Bernard "Thinking about Thinking: The Discovery of the LMS Algorithm", IEEE Signal Processing Magazine, pp.100-103, 2005.

[39] W.C. Chang, L. Jiebo and K. Parker, "Image segmentation via adaptive Kmean clustering and knowledge based morphological operations with biomedical applications," in IEEE transaction on image processing, 1998.

[40] Williams Street NW, Atlanta, Georgia, Quick facts breast cancer, 2011, pp. 44-66.

[41] Wolberg,~W.~H., \& Mangasarian,~O.~L, "Multisurface method of pattern separation for medical diagnosis applied to breast cytology," in In {\it Proceedings of the National Academy of Sciences}, {\it 87}, 1990 , pp. 9193--9196.

[42] W. V. M. Schwarzer, "On the Misuses of Artificial Neural Networks for Prognostic and Diagnostic Classification in Oncology," Statistics in Medicine, vol. 19, pp. 541-561, 2005.

[43] Y.Ireaneus Anna Rejani, Dr.S.Thamarai Selvi Noorul 'Early Detection Of Breast Cancer Using SVM Classifier Technique', International Journalon Computer Science and Engineering Vol.1(3), 2009, 127-130

[44] Y. J. Oyang, S. C. Hwang and Y. Y. Ou, "Data classification with radial basis function networks based on novel kernel density estimation algorithm," IEEE Transaction on Neural networks, vol. 16, no. 1, pp. 225-236, 2005.

[45] W.S. Tamil Selvi, J. Dheeba, N. Albert Singh, 'Computer aided detection of breast cancer on mammograms: A swarm intelligence optimized wavelet neural network approach', Journal of Biomedical Informatics 49 (2014) 45–52, 2014 Elsevier Inc.

[46] www.kaggle.com/overratedgman/mammographic-mass-data-set

[47] www.nature.com/articles/sdata2017.177

[48] Zhang, ~J, "Selecting typical instances in instance-based learning," inIn {\it Proceedings of the Ninth International Machine Learning Conference}, Aberdeen, Scotland: Morgan Kaufmann, (1992), pp. (pp. 470--479)

[49] Zhang, ~J, "Selecting typical instances in instance-based learning," inIn {\it Proceedings of the Ninth International Machine Learning Conference}, Aberdeen, Scotland: Morgan Kaufmann, (1992), pp. (pp. 470--479).

50 Zheng B., Chang Y.-H., and Gur D, " Computerized detection of masses in digitized mammograms using single-image segmentation and a multilayer topographic feature analysis," in Acad. Radiol , 1995, p. 959–966 .

[51] Zineb. B, Omar .B , G. C. Daniel, and C. J. Aida, "A Comparative Study of Machine Learning Algorithms for Financial Data Prediction," International Symposium on Advanced Electrical and Communication Technologies (ISAECT), pp. 1-5, 2018.

Appendix

Appendix 1: Medical input mammogram image analysis

To identifying potential abnormalities with a mammogram, classifying color and regions of mammogram as positive or negative. The systems use image processing algorithms to analyze mammograms for possible.

```
clc;
clear all;
close all;
[fname path] = uigetfile('*.*','Enter an Image');
fname = strcat(path,fname);% Read image from file RGB
standard truecolor composite.To specifies which bands to
read.And it can construct a RGB composite in a single step.
Truecolor =
multibandread('paris.lan',[512,512,7],'uint8=>uint8',...
                              128,'bil','ieee-
le',{'Band','Direct',[3 2 1]});% The truecolor composite has
very litle contrast and the colors are unbalanced
i = imread(fname);
B = imresize(i,[100 100]); % resize the images
figure
hold on
subplot(1,2,1);
image(i);
title('Original mammogram image','Fontsize',12)
xlabel('a length(cm)','Fontsize',12);
ylabel('width(cm)','Fontsize',12);
text(size(B,8),size(B,1)+15,...
'a',...
'Fontsize',14)
 subplot(1,2,2);
im = mean(B,3);
image(im);
title('RGB intensity image','Fontsize',12)
colormap(hot(256))
xlabel('b length(cm)','Fontsize',12);
ylabel('width(cm)','Fontsize',12);
text(size(im,8),size(im,1)+15,...
'c',...
```

```
'Fontsize',14)
hold on
i = B;
 i = truecolor;
 Bd = imresize(i1,[100 100]) % Use correlation to explore
unbalanced truecolor composite. The visible bands are highly
correlated with each other. The two andthree bands
scatterplots are an excellent way to gauge the degree of
thecorrelation among spectral bands.
r = Bd(:,:,1);
g = Bd(:,:,2);
b = Bd(:,:,3);  %To apply a linear contrast stretch to the
truecolor composite image, thesurface features are easier to
recognize by using image adjust.
stretched_truc = imadjust(i1,stretchlim(i1));% An enhanced
the truecolor composite in case of de-
correlationstretch,whichis separation across highly
correlated channels.This performed byadjusting parameters
value('Tol') of a linear contrast stretch.
decort_t =(decorrstretch(i1,'Tol',0.01));% The decorrelation
stretch extremely decrease in correlation. Hence the surface
features have become much more clearly visible.
r1 =(decort_t(:,:,1));
g1 = decort_t(:,:,2);
b1 = decort_t(:,:,3);
iGray = rgb2gray(B);
dec = (decorrstretch(iGray,'Tol',0.01));
dec1 = imadjust(dec,stretchlim(dec));
figure;
subplot(2,2,1);imshow(Bd);
title('Grayscale image after correlation(un-enhanced
image)','Fontsize',12);
text(size(Bd,8),size(Bd,1)+15,...
'a',...
'Fontsize',14)
 axis off
 axis image
subplot(2,2,2);
Bd = imresize(decort_t,[100 100]);
imshow(Bd)
title('Grayscale after decorrrralation(enhanced image)
stretch ','Fontsize',12)
 axis off
 axis image
text(size(Bd,8),size(Bd,1)+15,...
'b',...
'Fontsize',14)
subplot(2,2,3);
plot3(r(:),g(:),b(:),'.')
grid ('on')
hold on
```

```
xlabel('Red(band 3)','Fontsize',12)
ylabel('Green(band 2)','Fontsize',12)
zlabel('Blue(band 1)','Fontsize',12)
title('scatterplot of the not visible image after correlation
image stretch','Fontsize',12)
 axis off
 axis image
text(size(im,8),size(im,1)+15,...
'c',...
'Fontsize',14)
subplot(2,2,4);
plot3(r1(:),g1(:),b1(:),'.')
grid ('on')
hold on
xlabel('Red(band 3)','Fontsize',12)
ylabel('Green(band 2)','Fontsize',12)
zlabel('Blue(band 1)','Fontsize',12)
title('scatterplot of the visible band after de-correlation
stretch','Fontsize',12)
 axis off
 axis image
text(size(im,8),size(im,1)+1,...
'd',...
'Fontsize',12)%separation color images(RGB)
iR= B;
iR(:,:,2:3) = 0;
figure;
subplot(2,2,1);
imshow(iR);
title('Read Image','Fontsize',12);
axis off
axis image
text(size(im,8),size(im,1)+15,...
'a',...
'Fontsize',14)
iG= B;
iG(:,:,1:2:3) = 0;
subplot(2,2,2);
imshow(iG);
title('Green Image','Fontsize',12);
axis off
axis image
text(size(im,8),size(im,1)+15,...
'b',...
'Fontsize',14)
iB= B;
iB(:,:,1:2) = 0;
subplot(2,2,3);
imshow(iB);
title('Blue Image','Fontsize',12);
axis off
```

```
axis image

text(size(im,8),size(im,1)+15,...
'c',...
'Fontsize',14)
iR1 = B(:,:,1);%Rather than making other 0 let's as select1

iG1 = B(:,:,2);
iB1= B(:,:,3);
numBins = 100;
iGray = rgb2gray(B);%Gray Scale Images
iGray2 = uint8(0.299*double(iR1) + 0.587*double(iG1) +
0.114*double(iB1));
iGray2 = imadjust(iGray2);
xlimits = [0 150]; ylimits = [0 2500];
gy = histeq(iGray2);
dec2 =(decorrstretch(gy,'Tol',0.01));%de-correlated grayscale
subplot(2,2,4),imshow(iGray2); title('Grayscale
image','Fontsize',12);
% axis off
% axis image
text(size(im,8),size(im,1)+15,...
'd',...
'Fontsize',14)%to analysis the contrast
Grayscale image by histogram
figure;
subplot(2,2,1);imhist(r1,100);title('True color after
decorrelated image','Fontsize',12)
xlabel('x  = Intensity Level(in Grayscale)','FontSize',12,...
'FontWeight','bold','Color','b','LineWidth',10)
ylabel('y = Count frequency data','FontSize',12,...
'FontWeight','bold','Color','b','LineWidth',10);
text(size(im,8),size(im,1)+15,...
'a',...
'Fontsize',14)
subplot(2,2,2);imhist(gy,100);title('Gray scale after
decorrelated images ','Fontsize',12);
xlabel('x  = Intensity Level(in Grayscale)','FontSize',12,...
'FontWeight','bold','Color','b','LineWidth',10)
ylabel('y = Count frequency data','FontSize',12,...
'FontWeight','bold','Color','b','LineWidth',10);
text(size(im,8),size(im,1)+15,...
'b',...
'Fontsize',14 )
subplot(2,2,3),imshow(dec1); imhist(dec1,100);title('After
assembled grayscale with truecolor de-correlated images
','Fontsize',12);
xlabel('x  = Intensity Level(in Grayscale)','FontSize',12,...
'FontWeight','bold','Color','b','LineWidth',10)
ylabel('y = Count frequency data','FontSize',12,...
'FontWeight','bold','Color','b','LineWidth',10);
```

```
text(size(im,8),size(im,1)+15,...
'c',...
'Fontsize',14 )
subplot(2,2,4);imshow(dec2); imhist(dec2,100);title('After
assembled grayscale with truecolor decorrelated adjust images
','Fontsize',12);
xlabel('x  = Intensity Level(in Grayscale)','FontSize',12,...
'FontWeight','bold','Color','b','LineWidth',10)
ylabel('y = Count frequency data','FontSize',12,...
'FontWeight','bold','Color','b','LineWidth',10);
text(size(im,8),size(im,1)+15,...
'd',...
'Fontsize',14 )
```

Appendix 2: Removing noise and edge detection

```
% Filter and edge detection,converts the truecolor image
i1 = rgb2gray(i);% RGB to the grayscale intensity image i
i2 = imadjust(i1);% Adjust image intensity values
ie =edge(i1,'prewitt');% Egde detection
imr = bwmorph(ie,'dilate',2);% specific morphological
operation to the binary image ie
numBins =200;
% Remove noise from images using mean filter
noise = imnoise(i,'gaussian',0.03); % add noise to image.The
default is zero mean noisewith 0.03 variance.
cnf = ones(9,9)/40; % convolutional corner
noise_filt= imfilter(noise,cnf);%Filters the multidimensional
imagesSet Handle Graphics object properties.
[m,n] = size(i1);
output = zeros(m,n);
for i=1:m
for j=1:n% set the neighborhold bounderiers
       rmin=max(1,i-1);
       rmax=min(m,i+1);
       cmin=max(1,j-1);
       cmax=min(n,j+1);
%the the neighborhold matrix,denoting by temp
       temp = i1(rmin:rmax,cmin:cmax);
% the mean pixel of the output for neighborhold is
       output(i,j)= mean(temp(:));
end
end
%the output convert to uint8
output = uint8(output);
figure,
subplot(2,2,1), imshow(ie), title('Edge detection image using
prewitt method','Fontsize',12);
text(size(ie,8),size(ie,1)+15,...
'a',...
'Fontsize',14);
```

```
subplot(2,2,2), imshow(imr),title('Edge detection Image using
morphological method','Fontsize',12);
text(size(imr,8),size(imr,1)+15,...
'b',...
'Fontsize',14);
subplot(2,2,3),imshow(output),title('Remove noise by mean
filter','Fontsize',12);
text(size(output,8),size(output,1)+15,...
'c',...
'Fontsize',14);
subplot(2,2,4),imshow(noise_filt), title('Remove noise by
smoothing mean filter','Fontsize',12);
text(size(noise_filt,8),size(noise_filt,1)+15,...
'b',...
'Fontsize',14);
```

Appendix 3: Segmentation code

```
 Auto-generated by colorThresholder app on 01-May-2019

function [BW,maskedRGBImage] = createMask(RGB)
% Convert RGB image to chosen color space
RGB = im2double(RGB);
cform = makecform('srgb2lab', 'AdaptedWhitePoint',
whitepoint('D65'));
I = applycform(RGB,cform);
% Define thresholds for channel 1 based on histogram settings
channel1Min = 0.000;
channel1Max = 96.557;
% Define thresholds for channel 2 based on histogram settings
channel2Min = -17.105;
channel2Max = 46.247;
% Define thresholds for channel 3 based on histogram settings
channel3Min = -4.199;
channel3Max = 6.779;
% Create mask based on chosen histogram thresholds
BW = (I(:,:,1) >= channel1Min ) & (I(:,:,1) <= channel1Max)
&...
    (I(:,:,2) >= channel2Min ) & (I(:,:,2) <= channel2Max)
&...    (I(:,:,3) >= channel3Min ) & (I(:,:,3) <=
channel3Max);
% Initialize output masked image based on input image.
maskedRGBImage = RGB;
% Set background pixels where BW is false to zero.
maskedRGBImage(repmat(~BW,[1 1 3])) = 0;
% to segment colors in an automated fashion using the L*a*b*
color space and K-means clustering
II = uint8(I);
i1 = rgb2gray(I);
i2 = imadjust(i1);
ie =edge(i1,'prewitt');
```

```
imr = bwmorph(ie,'dilate',5);
 [bw,rgb] = remove_backgroundIm(II);
subplot(2,2,1),imshow(I),title('Original
image','Fontsize',12);
text(size(I,2),size(I,1)+15,...
'Breast Image , Mammogram', ...
'FontSize',10,'HorizontalAlignment','right');
 text(size(I,8),size(I,1)+15,...
'a',...
'Fontsize',14)
subplot(2,2,2),imshow(bw),title('Binary
image','Fontsize',12);
text(size(bw,8),size(bw,1)+15,...
'b',...
'Fontsize',14)
subplot(2,2,3), imshow(imr),title('Edge segmented
image','Fontsize',12);
text(size(imr,8),size(imr,1)+15,...
'c',...
'Fontsize',14)
subplot(2,2,4),imshow(rgb),title('Remove background
image','Fontsize',12);
text(size(rgb,8),size(rgb,1)+15,...
'd',...
'Fontsize',14)
```

Appendix 5: features extraction code

```
% Reading the reference Image
I = imread('0r11.jpg');
%Reading the target image
I1 = imread('reff5.jpg');
% Convert Original Image to Grayscale
I = rgb2gray(I);
I1 = rgb2gray(I1);
%Scale and rotate the original image to create the distorted
image
scale = 1.6;
J = imresize(I1, scale);
theta = 0.03918;
distorted = imrotate(J,theta);
index = 0.4;
distorted = imrotate(distorted,index);
% Detect Feature Points and Visualize the strongest feature
points found in the reference image, SURF features method
bPts = detectSURFFeatures(I);%Speeded-Up Robust Features
(SURF) algorithm to findshapeless features.
scenePts = detectSURFFeatures(distorted);
%Extract feature descriptors at the interest points in both
images.Extract features
[bFeatures, bpts] = extractFeatures(I, bPts);
```

```
[partFeatures, partpts] = extractFeatures(distorted,
scenePts);% Find Putative Point Matches, Match features
bPairs = matchFeatures(bFeatures, partFeatures,'MaxRatio',
1);%Display putatively matched features.
matchedBoxPts = bPts(bPairs(:, 1), :);
matchedPartPts = scenePts(bPairs(:, 2), :);
% Locate the Object in the Scene Using Putative Matches
% estimateGeometricTransform calculates the transformation
relating the matched points,while eliminating outliers.
 [tform, inlierBoxPts, inlierPartPts] = ...
     estimateGeometricTransform(matchedBoxPts,
matchedPartPts, 'affine');
%Get the bounding polygon of the reference image
bPolygon = [115, 133;...   % top-left
        size(I, 2), 2;... % top-right
        size(I, 206), size(I, 206);... % bottom-right
        4, size(I, 1);... % bottom-left
    195, 160]; % top-left again to close the polygon
% Transform the polygon into the coordinate system of the
target image. The transformed polygon indicates the location
of the object in the scene.
newBPolygon = transformPointsForward(tform, bPolygon);
% Display the matching point pairs with the outliers removed
and Display the detected object.Visualize putative matches.
figure;
subplot(2,2,1), imshow(I); title('Reference
image','Fontsize',12);
text(size(I,8),size(I,1)+15,...
'a',...
'Fontsize',14)
subplot(2,2,2),imshow(distorted); title('Target
image','Fontsize',12);
text(size(distorted,8),size(distorted,1)+15,...
'b',...
'Fontsize',14)
subplot(2,2,3),imshow(I),title('100 strongest feature tumor
scene from image reference','Fontsize',12);
text(size(I,8),size(I,1)+15,...
'c',...
'Fontsize',14)
hold on; plot(selectStrongest(bpts, 100));
subplot(2,2,4),imshow(distorted),title('175 image of a
cluttered tumor scene target','Fontsize',12);
text(size(distorted,8),size(distorted,1)+15,...
'd',...
'Fontsize',14)
hold on; plot(selectStrongest(scenePts, 175));
 figure;
 subplot(2,2,1),showMatchedFeatures(I, distorted,
matchedBoxPts, ...
```

```
     matchedPartPts, 'montage'); %Show  with a color-coded
plot of corresponding points connected by a line
corresponding feature points
 title('Putatively matched features tumor scene (including
spurious matches)','Fontsize',12);
 legend('Reference image','Target tumor
scene','Location','NorthOutside')
subplot(2,2,2),showMatchedFeatures(I, distorted,
inlierBoxPts,...
    inlierPartPts, 'montage');
title('Matched features tumor scene','Fontsize',12);
legend('Reference image','Target tumor
scene','Location','NorthOutside')
subplot(2,2,3),imshow(distorted);
hold on;
line(newBPolygon(:, 1), newBPolygon(:, 2),
'Marker','o','Color','black','LineWidth',0.001);
title('The exact tumor scene was detected from normal body
image','Fontsize',12);
text(120,163,'o','color','yellow','FontSize',40);
```

Appendix 6: features selection code

```
% features selection. Calculate parameters using the 2D-DWT

[cA1,cH1,cV1,cD1] = dwt2(signal1,'db4');
[cA2,cH2,cV2,cD2] = dwt2(cA1,'db4');
[cA3,cH3,cV3,cD3] = dwt2(cA2,'db4');
DWT_feat = [cA3,cH3,cV3,cD3];
G = pca(DWT_feat);
g = graycomatrix(G);
stats = graycoprops(g,'Contrast Correlation Energy
Homogeneity');
Contrast = stats.Contrast;
Correlation = stats.Correlation;
Homogeneity = stats.Homogeneity;
Mean = mean2(G);
Standard_Deviation = std2(G);
Entropy = entropy(G);
RMS = mean2(rms(G));
Variance = mean2(var(double(G)));
a = sum(double(G(:)));
Smoothness = 1-(1/(1+a));
Kurtosis = kurtosis(double(G(:)));
Skewness = skewness(double(G(:)));
% InverseDifference Movement
m = size(G,1);
n = size(G,2);
in_diff = 0;
for i = 1:m
for j = 1:n
        temp = G(i,j)./(1+(i-j).^2);
```

```
        in_diff = in_diff+temp;
end
end
IDM = double(in_diff);
performanceParameter = [Contrast,Correlation,Homogeneity,
Mean, Standard_Deviation, Entropy, RMS, Variance, Smoothness,
Kurtosis, Skewness, IDM]
```